Cooperative mechanism of diffusion in metal glass

L. N. Davydov

National Science Center ''Kharkov Physicotechnical Institute,'' 310108 Kharkov, Ukraine
(Submitted May 27, 1997; revised July 3, 1997)
Fiz. Nizk. Temp. **23**, 1331–1336 (December 1997)

General relations for diffusion coefficients for the cooperative mechanism of diffusion are obtained on the basis of the proposed model of metal–metalloid glass. The thermodynamics of Bernal–Polk complexes is developed by using the Ising–Nakano Hamiltonian and the theory of frozen-in fluctuations. The temperature dependence of diffusivity is analyzed in the cases of large and small variance of pair interatomic correlations. © *1997 American Institute of Physics.* [S1063-777X(97)01112-2]

Diffusion in frozen-in metastable metals known as metallic glasses (MG) was investigated by many authors (see, for example, Refs. 1–3). A universal mechanism of diffusion in MG has not been established so far. Both individual mechanisms of diffusion, e.g., the pseudovacancion mechanism[4–6] and the cooperative mechanism[7,8] in which several neighboring atoms participate simultaneously in an individual act of lattice rearrangement are being worked out. The possibility of a cooperative mechanism of diffusion in MG was confirmed by an analysis of experimental data.[3] It cannot be ruled out, however, that diffusion mechanisms in different MG are different. The indeterminacy in this problem is primarily due to the lack of clear ideas on the structure of MG, including point defects in these materials.

In this paper, we propose a model description of MG of the metal–metalloid type on the basis of a Hamiltonian including the one-particle energy of metal atoms determined by all atoms of MG (both atoms of the metal and the metalloid) as well as the correlation between metal atoms. The role of the metalloid in this case is formally reduced to the overdetermination of the parameters of the Hamiltonian as compared to the case of pure metal; naturally, such an overdetermination is significant from the physical point of view, which follows from the role of metalloids as amorphizer in vitrification and MG stability. This description can be used for determining the cooperative diffusion coefficient.

DESCRIPTION OF THE MODEL

We consider each metal atom in a corresponding spatial cell (coordination polyhedron). As regards metalloid atoms, they occupy positions in the voids of Bernal polyhedrons[9] (analogous to interstitial positions in a crystal). In the absence of an amorphizing metalloid, the potential relief is determined by metallic bonds and is therefore smooth (blurred). (Such a form of the relief formed by metallic bonds is confirmed by well-known facts such as very weak temperature dependences of diffusivity and viscosity in liquid metals.[10]) This relief is superimposed by relatively sharp additional wells due to metal–metalloid covalent bonds.

Disregarding the details in the form of the potential, we ascribe the Ising spin $\sigma=+1(\sigma=-1)$ to metal atoms with one-particle energy larger (smaller) than a certain critical energy. We assume that p is the fraction of the phase volume corresponding to $\sigma=+1$ and introduce the parameter

$$\Lambda=\frac{p}{1-p}\equiv\exp(-2L). \tag{1}$$

We also assume that atoms with $\sigma=+1$ cannot participate in lattice rearrangements (fixed atoms), while atoms with $\sigma=-1$ can take part in such rearrangements (excited atoms).

Introducing pair interatomic interaction and neglecting an insignificant constant term in the expression for energy, we can write the Hamiltonian of the system in the form

$$H=-\frac{1}{2z}\sum_{i,j}J_{ij}\sigma_i\sigma_j-w\sum_i\sigma_i, \tag{2}$$

where z is the coordination number and $w>0$ (the summation over j is carried out for nearest neighbors of the ith atom).

From the point of view of Gibbs distribution (and hence all thermodynamic relations), Hamiltonian (2) with the additional condition (1) is equivalent to the temperature-dependent effective Hamiltonian

$$\widetilde{H}=H+LT\sum_i\sigma_i. \tag{3}$$

Hamiltonian (3) has the form of the well-known Ising–Nakano Hamiltonian which was analyzed in detail for the case of the ''exchange integral'' J_{ij} which does not change as we go over from one cell to another.[11,12] In the case of MG under investigation, the quantity J_{ij} must have a variance. We assume that the variance is of Gaussian form:

$$P(J_{ij})\sim\exp\left(-\frac{(J_{ij}-J_0)^2}{2V^2}\right), \tag{4}$$

where $V=\langle(J_{ij}-J_0)^2\rangle^{1/2}$. As regards the one-particle parameters w and Λ, their variance will be neglected for simplicity.

The Hamiltonian (3) with the additional condition of freezing-in (nonthermodynamic type) of fluctuations (4) forms the basis of the theory of spin glass.[13] The only difference is the emergence of the temperature-dependent ''effective magnetic field''

$$h=w-LT. \tag{5}$$

In view of the absence of a consistent theory of spin glass, we put aside, among other things, the determination of the state of MG (either a metastable configuration or one of energetically equivalent configurations that are not separated from each other by a potential barrier) (see Refs. 14 and 15 in this connection). We shall use the well-known results of the theory of spin glass, namely, introduce an analog of magnetization $\sigma(T)\equiv\langle\sigma\rangle$ (angle brackets indicate averaging). (It should be recalled that, in the case of frozen-in fluctuations under investigation, we average not the partition function, but free energy, i.e., the logarithm of partition function, over these fluctuations; the quantities $\sigma(T)$ are determined by differentiating the averaged free energy with respect to w.) For $\sigma(T)=+1(\sigma(T)=-1)$, all the atoms of the metal are fixed (free); therefore, $\sigma(T)$ will be called the fixation parameter.

We have

$$\sigma(T)=(2\pi)^{-1/2}\int_{-\infty}^{\infty}dt\ \exp\left(-\frac{t^2}{2}\right)\tanh\frac{\Theta}{T}, \tag{6}$$

$$\Theta=Vq^{1/2}t+J_0\sigma+w-LT, \tag{7}$$

where $q\equiv q(T)$ is the memory parameter defined by the equation

$$q(T)=(2\pi)^{-1/2}\int_{-\infty}^{\infty}dt\ \exp\left(\frac{-t^2}{2}\right)\tanh^2\frac{\Theta}{T}. \tag{8}$$

It is known from the theory of spin glass that solutions of Eqs. (6)–(8) are different depending on whether or not the inequality $J_0>V$ is satisfied. If this inequality holds, we have solutions of the ferromagnetic type; if $w/L<J_0$ in this case, a first-order phase transition occurs at $T=w/L$. We will be interested in the case when $J_0<V$ and solutions of the spin-glass type are realized. In order to simplify formulas to the maximum possible extent, we assume that $V\gg J_0$.

Relations (6) and (8) are simplified considerably in two special cases that will be considered here: $V\sim w, L\gg 1$ (a) and $V\ll w$ (b) (although $V\gg J_0$ in all cases). It will be proved below that $T_c\propto wL^{-1}$ in the case (a), and hence we are interested only in the temperature range $T\ll w,V$. Using the asymptotic form of hyperbolic tangent

$$\tanh x=\mathrm{sgn}[1-2\exp(-2|x|)], \tag{9}$$

we obtain

$$\sigma(T)=\mathrm{erf}\,\frac{w-LT}{\sqrt{2}V}-O\left(\frac{T^2}{V^2}\right), \tag{10}$$

$$q(T)=1-O\left(\frac{T}{V}\right), \tag{11}$$

where erf is the error integral defined as

$$\mathrm{erf}\,x=\frac{2}{\sqrt{\pi}}\int_0^x\exp(-t^2)dt, \tag{12}$$

($O(x)$ denotes a positive correction of the order of x).

It should be noted that for $LT/V\to 0$ (it will be proved below that this corresponds to $T/T_c\to 0$), the functions $\sigma(T)$ and $q(T)$ approach the values $\sigma(0)$ and 1, respectively, following not the exponential, but the power law.

In case (b), relations (6) and (8) assume the form

$$\sigma(T)=\tanh\left(\frac{w}{T}-L\right);\quad q(T)=\tanh^2\left(\frac{w}{T}-L\right). \tag{13}$$

In this case, both parameters σ and q approach unity as $T\to 0$ according to the exponential law.

Concluding the section, let us formulate the main assumptions from which we are proceeding in fact.

1. In the condensed state, the motion of an atom can be approximately regarded as finite (confined to a certain cell of the order of atomic size). A cell rearrangement or a transition of the atom from one cell to another occurs over a time much longer than the period of vibrations in the cell.
2. In the solid as well as in the liquid state at a temperature slightly higher than the melting point T_m, there exists an hierarchy of energies: the binding energy, and hence the characteristic energy parameters of a cell (which are of the order of eV) are larger than the temperatures under investigation. Consequently, if we describe the motion of atoms in cells by the Hamiltonian $H(q_1,p_1,\ldots,q_N,p_N)$ (q_i,p_i are canonical variables and N is the number of atoms), we can assume that the parameters of this Hamiltonian are independent of temperature.
3. The phase volume of each atom of a metal can be divided into two regions: the states corresponding to fixed ($\sigma=+1$) and excited ($\sigma=-1$) atoms. Averaging over the phase volume within each region leads to the Ising–Nakano equivalent Hamiltonian (3) in the problem on calculation of the partition of function.
4. Frozen-in fluctuations of the parameters of the Hamiltonian (to be more precise, ''exchange integral'' J_{ij} describing the correlation of atoms) are characterized by the Gaussian distribution with a large variance.

COOPERATIVE MECHANISM OF DIFFUSION

In order to find the diffusion coefficient, we supplement the above four assumptions with a fifth assumption.

5. Excited atoms (those with $\sigma_i=-1$) can move almost freely under the action of mechanical stresses of concentration gradients. It should be emphasized that we are speaking not so much of diffusion as the freedom of movement in the sense of a rheological flow as in the case of liquids. Then MG corresponds to the concentration $y<y_c$ of these atoms, where y_c is a certain threshold concentration.

In terms of the parameter characterizing the preservation of complexes for the temperature T_c (the upper temperature boundary for the existence of MG), we obtain the following equation:

$$\sigma(T_c)=1-2y_c. \tag{14}$$

Naturally, in the case of (relatively slow) heating, MG goes over to the crystalline and not to the liquid state at the point T_c since the short-range order rearrangement after

which crystallization becomes possible has already occurred (e.g., segregation of a metal and a metal–metalloid stoichiometric compound).

Going over to diffusion in the sense of the last (fifth) assumption, we assume that the small ($\delta a \ll a$, δa is the characteristic displacement of atoms and a the atomic spacing) local cooperative rearrangement of the lattice becomes possible if n adjacent atoms of the metal become excited. In this case, for $n \ll z$, we obtain the following expression for y_c:

$$y_c = [\nu(n)]^{-1/n}, \tag{15}$$

where $\nu(n)$ is the number of possible realizations of states with n excited neighbors (per lattice site). Considering that $z=12$ for most sites in MG (the coordination polyhedron is icosahedron), we find from simple combinatorial and geometrical considerations that

$$y_c(3) = 30^{-1/3} \approx 0.322;$$

$$y_c(4) = 20^{-1/4} \approx 0.473;$$

$$y_c(5) = 30^{-1/5} \approx 0.506. \tag{16}$$

Since such a local rearrangement of the lattice is an elementary act of diffusion, the diffusion coefficient of the metal can be naturally represented in the form

$$D(T) = D_g(T)\left[\frac{1-\sigma(T)}{2y_c}\right]^n. \tag{17}$$

The second cofactor in this relation gives the probability of atomic excitation (both thermal and frozen-in) required for an elementary act of diffusion; the quantity D_g can be connected with the diffusion coefficient D_l in a liquid solution of the same composition as MG. Indeed, we assume that an elementary act of lattice rearrangement is the same for the liquid and glass-like phases. Taking into account the fact that almost all complexes in the liquid are dissociated ($\sigma(T) \simeq -1$), we have

$$D_g(T) = \frac{z_0}{z_l} D_l(T), \tag{18}$$

where z_l is the total number of diffusion paths for a given atom and z_0 the number of paths that are open in MG.

Naturally, in an accurate analysis we must take into account elementary acts of diffusion of n atoms. Such an analysis requires the knowledge of the distribution function for groups being rearranged over the number of atoms contained in them and probably the temperature dependence of this distribution. However, bearing in mind that the simultaneous participation of a large number of atoms in the rearrangement has a low probability, we confine our analysis to the case of groups with the same number of atoms and assume for estimates that $n=3$; then it follows from geometrical considerations that $z_l = 20$. Since only one diffusion channel can be open in MG (the probability of opening of each next path is proportional to $[1-\lambda(T)]/2$ for values of T not very close to T_c, and hence is small), we obtain

$$D(T) = z_l^{-1} D_l(T)\left[\frac{1-\sigma(T)}{2y_c}\right]^n. \tag{19}$$

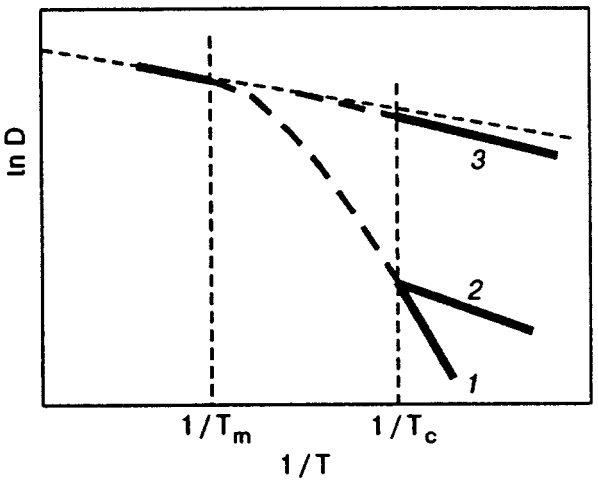

FIG. 1. Dependence of diffusion coefficient on reciprocal temperature in a perfect sample (curve *1*), insufficiently quenched sample (curve *2*) for large dispersion of paired correlations (curve *3*) (the instability region is shown by dashed line; T_m is the melting point).

Let us consider the form of the function $D_l(T)$. If we were dealing with a simple liquid (liquefied inert gas or melt of a nontransition metal), the diffusion would be an activationless process, and function $D_l(T)$ would follow the Swalin quadratic law.[16] In the case under consideration, the quantity D_l must depend on temperature according to the Arrhenius law owing to covalent bonds, and hence

$$D(T) = z_l^{-1} D_0 \exp\left(-\frac{E_l}{T}\right)\left[\frac{1-\sigma(T)}{2y_c}\right]^n, \tag{20}$$

where D_0 and E_l are the same preexponential factor and the diffusion activation energy as in a melt of the same composition as the MG.

THE CASE OF LOW DISPERSION

We first consider the case of small variance of the parameter J_{ij}, $V \ll w$ (naturally, $J_0 \ll V$). Substituting (13) into (20), we obtain the temperature dependence of the diffusion coefficient for MG:

$$D(T) = z_l^{-1} y_c^{-n} D_0\left[N_F\left(\frac{2w}{T} - 2L\right)\right]^n \exp\left(\frac{-E_l}{T}\right), \tag{21}$$

where $N_F(x) = (e^x+1)^{-1}$ is the Fermi distribution function. It can be seen that at low temperatures [$T \ll w(L-1/2)^{-1}$ for $L>0$ and $T \ll 2w$ for $L<0$], the diffusion coefficient obeys the Arrhenius law with the activation energy

$$E_0 = 2nw + E_l = 2n(L + \text{Arth}\ \ \sigma_c)T_c + E_l \tag{22}$$

and the pre-exponential factor

$$D_A = z_l^{-1} y_c^{-n} D_0 \exp 2nL. \tag{23}$$

Curve *1* in Fig. 1 shows schematically the dependence of D on T.

Generally speaking, diffusion over macroscopic distances should be described by taking into account the correlation factor whose magnitude is of the order of unity and which strongly depends on the mechanism of diffusion. We

can assume that the larger the number of atoms participating in a cooperative act of diffusion, the lower the probability of the step which is exactly opposite to the given step, and the closer the correlation factor to unity. We shall assume that it is equal to unity.

It should be noted that the preexponential factors D_0 for different liquid metals[17] differ insignificantly, having the same order of magnitude as $D_0 \simeq (3-30)\cdot 10^{-8}$ m^2/s. If the diffusion activation energy in the liquid phase is relatively small ($E_l \ll 2nw$), the diffusion activation energy in different MG will be proportional to the corresponding T_c in accordance with (22). Consequently, the diffusion coefficients in different MG as functions of the reduced temperature T/T_c can often nearly coincide. Such an approximate similitude law has apparently been observed in experiments.[18]

Unfortunately, an exact comparison of obtained relations with experimental results is hardly possible at the moment in spite of the rich available information on diffusion in MG.[1–3,18] This is due to the following two circumstances: there are no data on the temperature dependence of the diffusion coefficients in melts in MG of the same composition, and a considerable fraction of available data on diffusion in MG corresponds to insufficiently annealed samples that are far from being perfect. But the diffusion coefficients in defective MG can be much larger than in perfect samples (see in this connection the experiments described in Ref. 19) as a result of diffusion over extended defects, i.e., regions with weakened atomic bonds of the type of planes or channels formed by atoms with $z<12$.

Nevertheless, we can draw several qualitative conclusions.

(1) The diffusion activation energy (defined as the slope of the curve $\ln D$ to the $1/T$ axis) in a perfect MG is higher than in the corresponding melt (curve *1* in Fig. 1).
(2) If we assume that $D_A \sim 10^{19}$ m^2/s in a perfect MG (as in the case[19] of Au in $Pd_{77.5}Cu_6Si_{16.5}$ at $T \approx T_g$ (T_g is the glass-formation temperature) and substitute for D_0 the value $D_0 \simeq (3-30)\cdot 10^{-8}$ m^2/s typical of the preexponential factor for liquids,[17] we obtain $L \sim 10$.
(3) In insufficiently annealed MG samples, the dependence of $\ln D$ on $1/T$ has the form shown by curve *2*. The increase in the steepness of the curve observed as we approach T_c from the side of smaller values of T is associated with partial annealing of defects, as a result of which the samples become close to a perfect MG. The effective preexponential factor D_A' becomes smaller than D_A.

It should be emphasized in this connection that it would be interesting to measure the diffusion coefficient both in perfectly annealed MG samples, and in melts of the same compositions.

Here we analyzed the possibility of a description of cooperative diffusion by using the proposed approach and its intrinsic noncontradictory nature. A comparison with experimental results shows that the values of the parameter L are within reasonable limits.

We confined our analysis to the diffusion of metal atoms in alloys and disregarded diffusion of an impurity. An analysis of experimental results on diffusion in annealed metal–metalloid alloys[3] shows that the diffusion coefficients strongly (although ambiguously) depend on the diffusate. The activation energy is in linear correlation with the preexponential factor. In the proposed model, this correlation can apparently be explained by the presence of the factor nL in the activation energy (22) as well as in the pre-exponential factor (23). Naturally, this product is different for different atoms of the diffusate.

THE CASE OF LARGE DISPERSION

Let us now consider the case of a large variance of the quantity J_{ij}, $V \sim w$, and $V \gg T_c$.

Substituting (10) into (20), we can present diffusion coefficient in the form

$$D(T) = D_A(T)\exp\left(-\frac{E_l}{T}\right), \tag{24}$$

$$D_A(T) = D_0\left[\Phi\left(\frac{w-LT}{V}\right)\right]^n, \tag{25}$$

where

$$\Phi(x) = (2\pi)^{1/2}\int_x^\infty \exp\left(-\frac{t^2}{2}\right)dt. \tag{26}$$

Pay attention to the fact that the expression in the brackets in (25) has no exponential asymptotic form for $T \to 0$ (and tends to a finite limit $\Phi(w/V)$). For this reason, formulas (24)–(26) correspond to the Arrhenius law with the same activation energy E_l as for a liquid melt and with a preexponential factor $D_A(T)$, decreasing slowly upon cooling (curve *3* in Fig. 1).

[1] B. Cantor, in *Rapidly Quenched Metals*, vol. 1 (ed. by S. Steeb and H. Warlimont) North-Holland Publ. Co., Amsterdam (1985).
[2] B. S. Bokshtein, I. V. Karpov, and L. M. Klinger, Izv. Vuzov, Ser. Chern. Met. **11**, 87 (1985).
[3] S. K. Sharma, M.-P. Macht, and V. Naundorf, J. Non-Cryst. Solids **156–158, pt. 1**, 437 (1993).
[4] D. K. Belashchenko, Fiz. Met. Metalloved. **53**, 1076 (1982).
[5] D. K. Belashchenko and Fam Khak Hung, Fiz. Met. Metalloved. **57**, 1050 (1984).
[6] L. N. Davydov and Z. A. Spolnik, Phys. Status Solidi B **191**, 57 (1995).
[7] D. Gupta, K. N. Tu, and K. W. Asai, Phys. Rev. Lett. **35**, 796 (1975).
[8] B. S. Bokhshtein, L. M. Klinger, I. M. Razumovskii, and E. N. Uvarova, Fiz. Met. Metalloved. **51**, 561 (1981).
[9] D. E. Polk, Acta Metall. **20**, 485 (1972).
[10] P. Gray, in *Physics of Simple Liquids* (ed. by H. Temperley, J. Rowlinson, and G. Rushbrroke), North Holland, Amsterdam (1968).
[11] H. Nakano, Prog. Theor. Phys. **50**, 1510 (1973).
[12] K. Honda and Y. Kato, Phys. Lett. **44A**, 497 (1973).
[13] S. F. Edwards and P. W. Anderson, J. Phys. F **5**, 965 (1975).
[14] K. H. Fisher, Phys. Status Solidi B **130**, 13 (1985).
[15] D. Chowdhury and A. Mookerjee, Phys. Rept. **114**, 1 (1984).
[16] R. A. Swalin, Acta Metall. **7**, 736 (1959).
[17] P. P. Arsent'ev and L. A. Koledov, *Metallic Melts and Their Properties* [in Russian], Metallurgiya, Moscow (1976).
[18] B. Cantor and R. W. Cahn, in *Amorphous Metallic Alloys* (ed. by P. E. Luborsky), Butterworths, London (1983).
[19] H. S. Chen, L. C. Kimerling, J. M. Poate, and W. L. Brown , Appl. Phys. Lett. **32**, 461 (1978).

Translated by R. S. Wadhwa

Microscopic mechanism of the effect of composition and topological orders of metal glasses on plastic shear resistance

A. S. Bakai

National Science Center ''Kharkov Physicotechnical Institute,'' 310108 Kharkov, Ukraine

V. Z. Bengus and E. D. Tabachnikova

*B. Verkin Institute for Low Temperature Physics and Engineering, National Academy of Sciences of the Ukraine, 310164 Kharkov, Ukraine**

P. Duhaj

Institute of Physics of Slovakia Academy of Sciences, 84228 Bratislava, Slovakia
(Submitted May 30, 1997)
Fiz. Nizk. Temp. **23**, 1337–1344 (December 1997)

Singularities (minima) in the critical stress of catastrophic plastic shear are observed in the course of variation of composition and topological orders in metal glasses $Fe_{85-x}Co_xB_{15}$ ($x=15$, 17, 19, 21, 25, 30, 40, 50, 64 at. %) due to a change in the chemical composition. The minima are observed for $x=21$ and 40 at. %, which is close to the rational ratios 3:1 and 1:1 of atomic concentrations of Fe and Co, that are regarded as stoichiometric ratios for the formation of nanoclusters with a high average binding energy. The change in the atomic structure of cluster boundaries is considered as a microscopic mechanism of the effect of composition and topological orders on the resistance to plastic shear. The difference in the concentrations of coinciding sites at cluster boundaries is estimated for metal glasses of stoichiometric and nonstoichiometric compositions. © *1997 American Institute of Physics.*
[S1063-777X(97)01212-7]

1. INTRODUCTION

The atomic structure of a solid determines its mechanical properties. However, the establishment of the relation between mechanical properties and atomic structure for structurally disordered amorphous systems such as metal glasses remain a complicated problem since the atomic structure of composition and topological orders in metal glasses has not been studied sufficiently. High-resolution electron microscopy of various metal glasses[1–4] revealed regions of average order of 1–3 nm in size, while experiments involving ionic-field microscopy proved[5,6] that metal glasses have a polycluster structure. Polyclusters formed by noncrystalline ordered nanoclusters (having a size up to 10 nm) are separated by boundaries, but the detailed atomic structure of nanoclusters and cluster boundaries has not been established yet. Since mechanical properties of solids are very sensitive to details of atomic structure (type of local ordering and density of point and extended defects), an analysis of these properties can be an effective tool for studying the defects of atomic structure.

It was assumed earlier that metal glasses are homogeneous noncrystalline solid solutions in the form of chaotic atomic mixtures. If this is true, the properties of metal glasses must change monotonically with the composition. If, however, metal glasses possess a nanocluster substructure with a short-range and intermediate ordering, a nonmonotonic change in the ordering of nanoclusters and the structure of cluster boundaries upon a monotonic change in chemical composition can result in a nonmonotonic change in the macroscopic properties of a metal glass. In particular, for compositions close to stoichiometric compositions of crystalline analogs, we can expect an increase in the local composition and topological ordering, and hence in the average binding energy of atoms in nanoclusters. The structural relaxation of boundaries is inhibited in this case, and the concentration of noncoinciding sites at cluster boundaries must increase.[1)] Thus, the formation of ''strong'' clusters (with quasi-stoichiometric compositions) is accompanied by the formation of ''weak'' boundaries.

First steps in the establishment of correlation between the atomic structure (composition and topological orders) and properties of metal glasses were made by comparing the macroscopic properties of metal glasses of certain ''stoichiometric'' composition and glasses whose compositions are far from ''stoichiometric'' ones.[9–11]

No attempts have yet been made to calculate these stoichiometric compositions. A qualitative analysis proved that, in the case of binary metal glasses, glasses with eutectic compositions must contain ''strong'' nanoclusters.[9] This hypothesis was confirmed for metal glasses of the Fe–B system, for which singularities on concentration dependences of some physical parameters were observed for the glass with the eutectic composition $Fe_{83}B_{17}$. Among other things, narrow (in concentration) and deep minima of strength were observed and explained by a high average binding energy of

atoms in nanoclusters and a strong disorder of cluster boundaries.[9,10]

In view of the high volume energy of cluster boundaries (approximately 5% of atoms of the material belong to boundary layers when the size of nanoclusters is ~ 10 nm), it is these boundaries, their structure and resistance to plastic shear that plays a decisive role in the mechanical properties of metal glasses. The minimum of the critical stress σ_{fp} corresponding to catastrophic plastic shear and observed for ''weak'' cluster boundaries in a eutectic metal glass was found to be manifested most clearly as compared to peculiarities in other properties.[9,10] Similar singularities in physical properties must also be observed for other metal glasses formed by ''strong'' nanoclusters.

In order to establish the relation between the microscopic structure and mechanical properties of metal glasses on the basis of the above concepts and to find new metal glasses in which the composition and topological orders lead to the formation of ''strong'' nanoclusters, we analyzed systematically the concentration dependence of σ_{fp} in metal glasses of the $Fe_{85-x}Co_xB_{15}$ system by varying the composition of the metallic subsystem. It was found that at least two compounds in this system, i.e., $Fe_{64}Co_{21}B_{15}$ and $Fe_{45}Co_{40}B_{15}$, exhibit singularities (minima of σ_{fp}) typical of metal glasses with such composition and topological orders, leading to the formation of ''strong'' nanoclusters. This publication is devoted to the description of these results.

2. MATERIALS AND METHODS

Metal glasses of the system $Fe_{85-x}Co_xB_{15}$ ($x=15$, 17, 19, 21, 25, 30, 40, 50, 64 at. %) were prepared by rapid tempering of the melt in a rotating drum (planar flow casting) at the Institute of Physics of the Slovak Academy of Sciences (Bratislava) in the form of strips of 10 mm width and 30 μm thickness. The amorphous state of the strips was tested by using x-ray diffractometry. The critical stress σ_{fp} of catastrophic shear was measured at 300 K during extension of samples with a working length of 20 mm at a strain rate 8.3×10^{-5} s^{-1} on a deformation test machine with a rigidity of 10 kN/mm. Required separate measurements were made at 4.2 K. Each experimental point for σ_{fp} was obtained by averaging the results of measurements on five samples. The morphology of fracture surfaces was observed by using a scanning electron microscope TESLA BS-300.

3. EXPERIMENTAL RESULTS

3.1. Concentration dependence of critical stress of catastrophic shear

The dependence of the critical stress σ_{fp} of catastrophic shear of metal glasses $Fe_{85-x}Co_xB_{15}$ on the cobalt concentration at 300 K is shown in Fig. 1. It can be seen that σ_{fp} has two minima at $x=21$ and 40 at. % Co. These concentrations almost coincide with the points corresponding to the ratios 3:1 and 1:1 of atomic concentrations of Fe and Co. The point $x=64$ at. % Co, which is close to the concentration ratio 1:3 of Fe and Co atoms, also gives a small value of σ_{fp}, but we cannot state that it corresponds to a minimum since no data for higher concentrations are available.

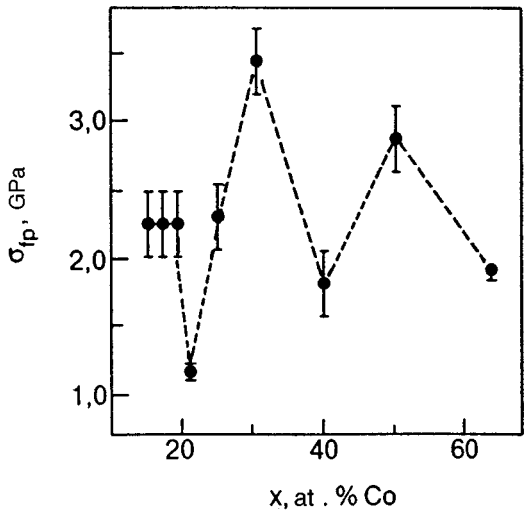

FIG. 1. Concentration dependence of critical stress σ_{fp} of catastrophic shear in metal glasses $Fe_{85-x}Co_xB_{15}$ at 300 K.

Figure 1 also shows a spread $\delta\sigma_{fp}$ of the experimentally measured values of σ_{fp} for metal glasses with all concentrations under investigation. It was found that the values of $\delta\sigma_{fp}$ for concentrations 21 and 64 at. % Co, which approximately correspond to the ratios 3:1 and 1:3 of Fe and Co concentrations, amount to only $\pm(60-100)$MPa (approximately of the size of symbols in the figure), while for other Co concentrations the values of $\delta\sigma_{fp}$ are $\pm(350-400)$MPa, i.e., are several times larger than for the two special concentrations mentioned above.

3.2. Plastic (viscous) fracture of metal glasses of all studied compositions

Metal glasses of all studied compositions (including those corresponding to 21, 40, and 64 at. % Co mentioned above) experienced viscous shear fracture, which was confirmed by fractographic observations: the surface morphology for catastrophic plastic shear and fracture had the appearance of a ''vein-type'' ornament formed due to meniscus instability as a result of rupture of ''quasiliquid''[12] (superplastic)[13] layer appearing on the surface of catastrophic plastic shear as a result of local adiabatic heating.[14,15] Such observations are especially important for compositions corresponding to minima of σ_{fp} (Fig. 2) since they indicate that these minima are not consequences of brittle fracture which leads to small breaking stresses,[16,17] but are due to low resistance to plastic shear and viscous fracture.

3.3. Change in critical stress of catastrophic shear upon cooling

Table I contains values of critical stress of catastrophic shear at 300 and 4.2 K for metal glasses $Fe_{64}Co_{21}B_{15}$ and $Fe_{66}Co_{19}B_{15}$. It can be seen that in the course of cooling from 300 to 4.2 K, the value of this quantity for the first composition corresponding to a minimum of σ_{fp} increases

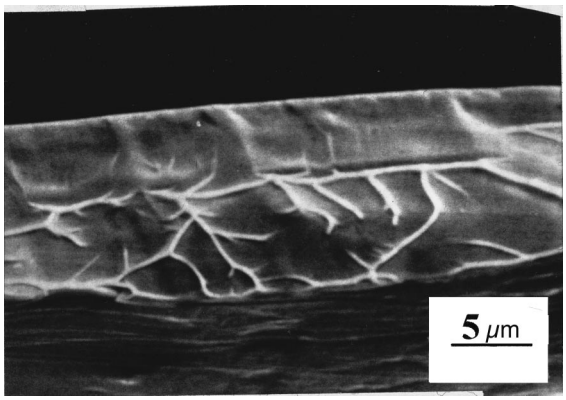

FIG. 2. Photograph of the surface of catastrophic plastic shear surface and fracture in axial extension of a strip of metal glass $Fe_{64}Co_{21}B_{15}$ at 300 K, obtained by using a scanning electron microscope.

insignificantly (by 8%), while for the second composition which does not coincide with a minimum of σ_{fp} this increase is much stronger (by 32%).

4. DISCUSSION OF RESULTS

4.1. Peculiarities of concentration dependences of mechanical parameters of metal glasses

It is well known that composition ordering, the formation of superstructures or intermetallic compounds of a certain stoichiometric composition, determine nonmonotonic dependences of the structure and parameters of crystalline alloys on their composition.[18,19]

The existence of singularities on concentration dependences of parameters for metal glasses is not obvious *a priori* (see above). It indicates that metallic glasses cannot be regarded as a disordered homogeneous atomic mixture of the components and that their atomic structure contains ordered atomic configurations whose properties are determined by the concentrations of the components. This is confirmed, for example, by singularities of the concentration dependences of critical stress of catastrophic plastic shear in metal glasses, which were observed from an analysis of the systems $Fe_{100-x}B_x$[9,10] and $Fe_{85-x}Co_xB_{15}$, namely, minima of σ_{fp} for some special concentrations x as well as maxima of the shear modulus in $Ni_{100-x}Zr_x$ metal glasses for compositions corresponding to intermetallides in the crystalline state.[20] This is in accord with the above-mentioned composition and topological orders observed in metal glasses and with the nanocluster type of their atomic structure established earlier.[1–7]

The presence of ''strong'' nanoclusters in a eutectic alloy (such as $Fe_{83}B_{17}$) appears as natural since crystallization in a eutectic melt is limited to the minimum possible (eutectic) temperature just by noncrystalline clusters with a high average binding energy. Such ideas are in agreement with the stoichiometries of binary eutectics, which were established long ago by Hume-Rothery and Anderson.[21]

The reasons behind the formation of ''strong'' nanoclusters in ternary metal glasses $Fe_{85-x}Co_xB_{15}$ with rational ratios of atomic concentrations of Fe and Co are apparently the same as for composition ordering in binary crystalline Fe–Co alloys with the stoichiometric ratios 3:1, 1:1, and 1:3 of atomic concentrations of Fe and Co.[22] The gain in binding energy in this case exceeds the increase in free energy due to a decrease in the entropy of mixing and configurational entropy.

All these results taken together show that the short-range composition ordering occurs during the formation of glasses in the absence of a long-range ordering. The composition ordering and the topological ordering accompanying it decrease the configuration entropy and increase the average binding energy of atoms in clusters. The decrease in configuration entropy diminishes the number of possible atomic configurations in the cluster boundary layer, while the increase in the binding energy of atoms in clusters increases the cluster rigidity. Both these effects suppress structural relaxation of boundary layers. Besides, the composition order is inevitably violated at cluster boundaries. This leads to a loss of strength, i.e., to ''weakening'' of boundaries.

TABLE I. Critical stresses σ_{fp} of catastrophic shear at 300 and 4.2 K for metal glasses $Fe_{64}Co_{21}B_{15}$ and $Fe_{66}Co_{19}B_{15}$.

	σ_{fp}, GPa	
T, K	$Fe_{64}Co_{21}B_{15}$	$Fe_{66}Co_{19}B_{15}$
300	1.2	2.2
4.2	1.3	2.9

4.2. Microscopic mechanism of the effect of composition and topological orders on the critical stress of plastic shear

Boundaries play a decisive role in mechanical properties of metal glasses with a polycluster structure. At high temperatures (close to the glass-formation point T_g) and low stresses, a diffusive-viscous flow of polyclusters takes place, which is similar to a flow of polycrystals according to the Coble mechanism.[23] According to Lifshits,[24] both the boundary diffusion of atoms and the slip along the boundaries are important in this case. At low temperatures, when diffusion is suppressed, slip is the main mechanism of plastic deformation.

Internal interfaces in metal glasses are the boundaries between clusters[7] forming the structure of a metal glass. During low-temperature (nonuniform) deformation, the slip originating along cluster boundaries acquires features of an unstable catastrophic process due to local thermal softening in the band of adiabatic plastic shear,[14,15] leading to shear fracture of the metal glass.

According to the polycluster model of amorphous bodies, cluster boundaries offer a lower resistance to plastic shear as compared to that in the bulk of the clusters.[8] This resistance to plastic shear is mainly determined by the atomic structure of cluster boundaries, namely, the concentration c_c of coinciding sites at these boundaries and by the distribution of local critical shear stresses σ_c at these sites due to internal stresses. The smaller the number of coinciding sites at the boundary between clusters, the smaller the resistance offered by the boundary to plastic shear along it. Figure 3 shows schematically a two-dimensional polycluster with a cluster boundary containing coinciding and noncoinciding sites of

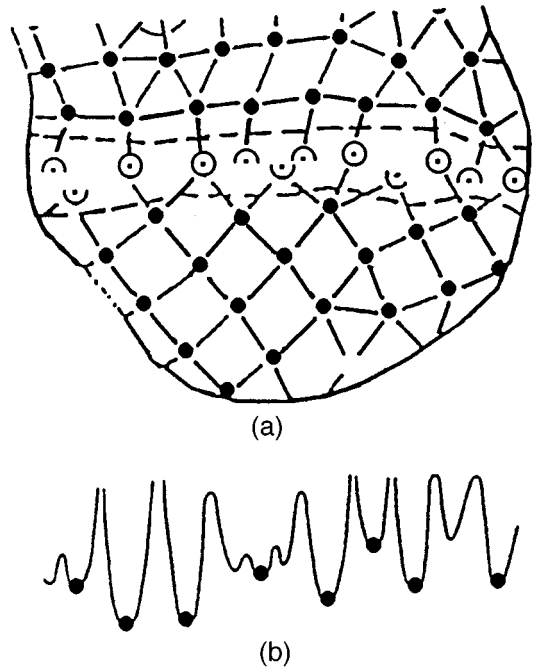

FIG. 3. (a) Schematic diagram of a two-dimensional polycluster with a cluster boundary (dashed lines): coinciding sites (circles) and noncoinciding sites (semicircles) at the cluster boundary, and regular sites of neighboring locally regular clusters (●). (b) Corresponding potential relief along the cluster boundary.[25]

two neighboring locally regular clusters as well as the corresponding potential relief along the cluster boundary.[25]

The critical stress σ_p of plastic shear along the cluster boundary in the absence of thermally activated rearrangements is defined as follows [see (14.46) in Ref. 8]:

$$\sigma_p=(\langle\sigma_c\rangle-\delta_c/2)c_c\equiv\sigma_{0c}c_c, \tag{1}$$

where $\langle\sigma_c\rangle$ is the average local critical shear stress at coinciding sites on the cluster boundary, $\delta_c/2$ the half-width of the distribution of the values of σ_c, and c_c the concentration of coinciding sites at the cluster boundary.

Expression (1) is valid for $\delta_c\leqslant 2\langle\sigma_c\rangle/3$ and $c_c=1-c_{nc}$, where c_{nc} is the concentration of noncoinciding sites at the cluster boundary. For $\delta_c>2\langle\sigma_c\rangle/3$, we can used the following estimate[8] for the value of σ_{0c}: $\sigma_{0c}\approx\langle\sigma_c\rangle/2$. Thus, we can write

$$\langle\sigma_c\rangle/2<\sigma_{0c}\leqslant\langle\sigma_c\rangle. \tag{2}$$

In the general case, the value of σ_p is close to the critical stress σ_{fp} of catastrophic shear at which shear fracture of the polycluster takes place.[8] For this reason, we shall assume in estimates that $\sigma_p\approx\sigma_{fp}$ and has the same concentration dependence (see Fig. 1).

It follows from formula (1) that the observed concentration dependence of σ_p is due to the dependences of σ_{0c} and c_c on the composition of the metal glass, and the value of $\langle\sigma_c\rangle$ must increase upon composition ordering in the metallic subsystem. The increment of this quantity can be roughly estimated as

$$\Delta\langle\sigma_c\rangle/\langle\sigma_c\rangle\sim\varepsilon_0/\varepsilon_b, \tag{3}$$

where ε_0 is the ordering energy and ε_b the binding energy per atom. Usually, the value of ε_b for metals amounts to 1.5–2 eV, while $\varepsilon_0\approx k_BT_0$, where T_0 is the temperature of ordering and k_B Boltzmann's constant. For the crystalline alloy $Fe_{50}Co_{50}$, $T_0\approx 1000$ K,[26] and hence $\varepsilon_0\approx 0.1$ eV, while for the alloy $Fe_{75}Co_{25}$, $T_0\approx 840$ K[26] and $\varepsilon_0\approx 0.08$ eV. Consequently, the increment $\Delta\langle\sigma_c\rangle$ appearing as a result of composition ordering of Fe and Co in $Fe_{85-x}Co_xB_{15}$ does not exceed $0.1\langle\sigma_c\rangle$.

As regards the quantities δ_c and c_c, their values can change not only as a result of composition ordering in clusters themselves, but mainly due to the change in the structure of cluster boundaries accompanying this ordering. It can be seen from Fig. 1 that the values of critical stress σ_{fp} of catastrophic shear for stoichiometric compositions are approximately half the values for close nonstoichiometric compositions. This decrease should be attributed completely to the change in the values of δ_c and c_c as a result of a change in the structure of cluster boundaries due to composition ordering.

The values of c_c cannot be measured experimentally by direct methods of high-resolution electron microscopy or ionic-field microscopy so far. For this reason, it would be interesting to compare the values of c_c determined by formula (1) for metal glasses of stoichiometric and nonstoichiometric compositions.

4.3. Estimation of the ratio of concentrations of coinciding sites at cluster boundaries of metal glasses of stoichiometric and nonstoichiometric compositions

We denote by $\sigma_p^{\min}$, $\sigma_{0c}^{\min}$, and $c_c^{\min}$ the quantities appearing in (1) for a stoichiometric composition and by $\sigma_p^{\max}$, $\sigma_{0c}^{\max}$, and $c_c^{\max}$ the same quantities for the nearest nonstoichiometric composition. Then we can write

$$c_c^{\min}/c_c^{\max}=(\sigma_p^{\min}/\sigma_p^{\max})(\langle\sigma_c^{\max}\rangle-\delta_c^{\max}/2)/(\langle\sigma_c\rangle^{\min}-\delta_c^{\min}/2). \tag{4}$$

For small ($\delta_c^{\min,\max}\ll 2\langle\sigma_c\rangle$) and large ($\delta_c^{\min,\max}>2\langle\sigma_c\rangle/3$) width of the spread in local critical stresses, the second factor on the right-hand side of (4) is close to unity. In these cases, we have the following estimate for the ratio of concentrations for coinciding sites:

$$c_c^{\min}/c_c^{\max}=(\sigma_p^{\min}/\sigma_p^{\max})\approx 0.5. \tag{5}$$

This corresponds to disordering of cluster boundaries due to an increase in the concentration of noncoinciding sites for a stoichiometric composition.

The ratio $c_c^{\min}/c_c^{\max}$ can become smaller if composition ordering is accompanied by an increase in the average value of internal stresses in the boundary layer, and hence by an increase in δ_c if $\delta_c^{\max}\ll\langle\sigma_c^{\max}\rangle/3$. In this case, the softening of cluster boundaries is due to an increase in the concentration of noncoinciding sites as well as due to an increase in local internal stresses at cluster boundaries.

TABLE II. Estimated values of $c_c^{\min}/c_c^{\max}$ for different types of stoichiometric structures in metal glasses.

Compositions			Type of Stoichiometry	$c_c^{\min}/c_c^{\max}$
$Fe_{85-x}Co_xB_{15}$:	$x^{\min}=21$;	$x^{\max}=19$	Ordering in metallic subsystem of nanocluster	0.52
$Fe_{85-x}Co_xB_{15}$:	$x^{\min}=40$;	$x^{\max}=30$	Same	0.53
$Fe_{100-x}B_x$:	$x^{\min}=17$;	$x^{\max}=16$	Binary eutectic	0.90

The relation (5) obviously gives an upper estimate of the relative decrease in the fraction of coinciding sites as a result of composition ordering and the formation of ''strong'' clusters.

It should be noted that the values of σ_p appearing in formulas (1)–(3) correspond to the temperature 0 K, while experimental measurements of concentration dependences of σ_{fp} were made at a nonzero temperature (300 K). The temperature dependence of σ_{fp} is determined by the joint effect of thermal activation, which decreases the value of σ_{fp} upon heating, and a decrease of internal stresses at coinciding sites upon heating, which reduce the value of σ_{fp}. In order to take into account the difference in the values of σ_{fp} at 0 and 300 K, we shall use the data from Table I for 4.2 and 300 K, which gives

$$\sigma_{fp}^{\min}(4.2\ \mathrm{K})/\sigma_{fp}^{\max}(4.2\ \mathrm{K})<\sigma_{fp}^{\min}(300\ \mathrm{K})/\sigma_{fp}^{\max}(300\ \mathrm{K}). \tag{6}$$

It follows readily from (3) and (4) that

$$c_c^{\min}/c_c^{\max}<(\sigma_p^{\min}/\sigma_p^{\max})<\sigma_{fp}^{\min}(300\ \mathrm{K})/\sigma_{fp}^{\max}(300\ \mathrm{K}). \tag{7}$$

Then the ratios of concentrations of coinciding sites in metal glasses $Fe_{85-x}Co_xB_{15}$ of stoichiometric and nonstoichiometric compositions determined from Fig. 1 are 0.52 (for $x=21$ and 19 at. %) and 0.53 (for $x=40$ and 30 at. %). Consequently, cluster boundaries in metal glasses of indicated stoichiometric compositions contain approximately half the number of coinciding sites at the boundaries in metal glasses of close nonstoichiometric compositions. This difference in atomic structure of cluster boundaries determines the microscopic mechanism of the effect of composition and topological orders on mechanical properties of metal glasses.

The observed small values of the spread in experimental values of σ_{fp} for compositions of metal glasses corresponding to the ratios 3:1 and 1:3 of atomic concentrations of Fe and Co can be regarded as an indication of a more standard atomic structure of cluster boundaries in metal glasses of these compositions.

The difference in the values of σ_{fp} for stoichiometric (eutectic) and nonstoichiometric compositions in the system $Fe_{100-x}B_x$ is not so large.[9,10] In the framework of the proposed model, this is due to the fact that $c_c^{\min}/c_c^{\max}<0.9$.

A comparison of the obtained estimates of the ratio $c_c^{\min}/c_c^{\max}$ for the determined stoichiometric compositions of various types enables us to estimate qualitatively the difference in the average binding energies for stoichiometric and nonstoichiometric clusters caused by different factors. Table II contains all the estimates obtained for the ratios of concentrations of coinciding sites at cluster boundaries in metal glasses of stoichiometric and nonstoichiometric compositions.

It can be seen that the difference is considerably stronger in the case of the $Fe_{85-x}Co_xB_{15}$ system than in the $Fe_{100-x}B_x$ system, which can be the subject of a subsequent experimental verification.

5. CONCLUSIONS

(1) Critical stresses σ_{fp} of catastrophic plastic shear is measured experimentally during extension of strips of metal glasses $Fe_{85-x}Co_xB_{15}$ ($15<x<64$) at 300 K as a function of the composition by varying the ratio of atomic concentrations of metallic components Fe and Co. The *minima* of σ_{fp} are observed for compositions with $x=21$ and 40 at. %, which are close to the rational ratios 3:1 and 1:1 of atomic concentrations of Fe and Co.

(2) These compositions are interpreted as *stoichiometric* compositions for the formation of composition ordering in nanoclusters of metal glasses, which correspond to the maximum average binding energy for atoms in nanoclusters, and accordingly, to cluster boundaries with reduced concentration of coinciding sites and lower critical stress of plastic shear.

(3) The *main microscopic mechanism of the effect* of variation of composition of metal glasses on the resistance to plastic shear lies in the change in concentration of coinciding sites at cluster boundaries upon a change in *composition and topological orders*.

(4) The ratio of *concentrations of coinciding sites* at cluster boundaries in stoichiometric and nonstoichiometric metal glasses for the systems $Fe_{85-x}Co_xB_{15}$ and $Fe_{100-x}B_x$ is estimated (taking into account the results of measurements of σ_{fp} at 4.2 K) on the basis of the polycluster model of the structure of an amorphous solid. Thus, the hypothesis concerning the decisive role of internal interfaces in the plasticity of solids is used for *predicting differences in the atomic structure of cluster boundaries* in metal glasses of stoichiometric and nonstoichiometric compositions.

The authors are grateful to Dr. K. Csach, J. Miskuf, and V. Ocelik (Institute of Experimental Physics, Slovak Academy of Sciences, Kosice) for their help in fractographic observations of the catastrophic shear surfaces in metal glasses under investigation and to Prof. V. D. Natsik for valuable critical remarks.

*E-mail: bengus@ilt.kharkov.ua

[1)]Noncoinciding sites as well as point defects are typical of crystalline and cluster boundaries.[7,8]

[1] Y. Hirotsu and R. Akada, Jpn. J. Appl. Phys. **23**, L479 (1984).
[2] K. Anazawa, Y. Hirotsu, and Y. Ichinose, J. Non-Cryst. Solids **156–158**, 196 (1993).
[3] Y. Hirotsu, Mater. Sci. Eng. A **179/180**, 97 (1994).
[4] M. Matsushita, Y. Hirotsu, T. Ohkubo, and T. Oikawa, J. Electron Microsc. **45**, 105 (1996).
[5] A. S. Bakai, V. B. Kulko, I. M. Mikhailovskij, and O. A. Velikodnaya, J. Non-Cryst. Solids **182**, 315 (1995).
[6] L. I. Fedorova, I. M. Mikhailovskij, V. A. Ksenofontov, and P. Ya. Poltinin, Zh. Tekhn. Fiz. **64**, 177 (1994) [Tech. Phys. **39**, 327 (1994)].
[7] A. S. Bakai, in *Topics in Applied Physics*, **72**, *Glassy Metals III* (ed. by H. Beck and H.-J. Gunterodt), Springer, Berlin (1994).
[8] A. S. Bakai, *Polycluster Amorphous Solids* [in Russian], Gosenergoatomizdat, Moscow (1987).
[9] V. Z. Bengus, P. Duhaj, E. B. Korolkova *et al.*, Low Temp. Phys. **20**, 853 (1994).
[10] V. Z. Bengus, P. Duhaj, E. D. Tabachnikova *et al.*, Mater. Sci. Forum **225–227**, 21 (1996).
[11] W. Weiss and H. Alexander, J. Phys. F **17**, 1983 (1987).
[12] A. S. Argon, in *Glass Science and Technology*, vol. 5, Academic Press, New York (1980).
[13] V. Bengus, E. Tabachnikova, K. Csach *et al.*, Scr. Metall. Mater. **35**, 781 (1996).
[14] V. Z. Bengus, E. D. Tabachnikova, S. E. Shumilin *et al.*, Int. J. Rapid Solidif. **8**, 21 (1993).
[15] E. D. Tabachnikova, V. Z. Bengus, and V. V. Molokanov, Mater. Sci. Forum **225–227**, Part 1,107 (1996).
[16] V. Z. Bengus, E. D. Tabachnikova, and V. I. Startsev, Phys. Status Solidi A **81**, K11 (1984).
[17] E. D. Tabachnikova, Fiz. Met. Metalloved. **64**, 1205 (1987)
[18] R. M. White and T. H. Geball, *Long Range Order in Solids*, Academic Press, New York (1979).
[19] N. S. Kurnakov, S. Zhemchuzhnyi, and M. Zasedatelev, Izv. St. Petersburg Politekhn. Inst. **22**, 487 (1914).
[20] J. B. Rubin and R. B. Schwarz, Phys. Rev. B **50**, 795 (1994).
[21] W. Hume-Rothery and E. Anderson, Philos. Mag. **5**, 383 (1960).
[22] M. A. Krivoglaz and A. A. Smirnov, *Theory of Order-Disorder Alloys*, Macdonald, London, 1964.
[23] R. Coble, J. Appl. Phys. **34**, 1679 (1963).
[24] I. M. Lifshits, Zh. Éksp. Teor. Fiz. **44**, 1349 (1963) [Sov. Phys. JETP **17**, 909 (1963)].
[25] A. S. Bakai, Mater. Sci. Forum **123–125**, 145 (1993).
[26] A. E. Vol, *Structure and Properties of Binary Metallic Systems* [in Russian], vol. 2, Fizmatgiz, Moscow (1962).

Translated by R. S. Wadhwa

Oscillations of the spectrum of acoustic phonons interacting with composite fermions

A. L. Zazunov and D. V. Fil

*Institute of Single Crystals, National Academy of Sciences of the Ukraine, 310001 Kharkov, Ukraine**
(Submitted July 7, 1997)
Fiz. Nizk. Temp. **23**, 1345–1348 (December 1997)

The interaction of collective excitations in a composite fermion system with phonon modes is considered. It is shown that for parameters corresponding to real systems in which the fractional quantum Hall effect is observed, the phase velocity of acoustic phonons has an oscillating dependence on the wave vector. The obtained oscillating structure of the phonon spectrum is determined to a considerable extent by the external magnetic field and electron concentration. © *1997 American Institute of Physics.* [S1063-777X(97)01312-1]

The model of composite fermions was proposed by Jain[1] as a possible mechanism of the hierarchy of fractional filling factors, which is observed in experiments on fractional quantum Hall effect. Filling factors correspond to Hall plateaus and, accordingly, to the minima of the longitudinal component of resistivity tensor. The idea of the approach formulated in Ref. 1 is based on the assumption that elementary excitations in such a system are composite quasiparticles. These quasiparticles are fermions carrying an even number $(2m)$ of flux quanta of a statistical gauge field and a statistical charge corresponding to this field. In the mean-field approximation, we can reduce the statistical interaction to an additional magnetic field $\mathbf{B}_{\rm st}$ (acting on statistical charges) antiparallel to the applied field $\mathbf{B}$. The filling factors ν corresponding to the integral number p of filled Landau levels in the field $\Delta B=|B-B_{\rm st}|$ correspond to the experimentally observed hierarchy $\nu=p/(2mp\pm1)$. Jain's publication[1] initiated a large number of theoretical and experimental works devoted to composite fermions. The mathematical apparatus of the model of composite fermions based on the description of statistical interaction involving the introduction of an auxiliary Chern–Simons gauge field was developed in Refs. 2 and 3 (see also Ref. 4). Similar models were analyzed in detail earlier for systems with a fractional statistics (see, for example, Refs. 5–8). The idea of composite fermions was confirmed experimentally in a number publications devoted to the temperature and field dependence of conductivity,[9–13] the observation of a magnetic focussing effect,[14,15] and the study of propagation of surface acoustic waves.[16–18] These experiments proved that thermodynamic and transport properties of the system near $\nu=1/2$ (for which $\Delta B=0$) are similar to the properties of a two-dimensional electron gas in a weak magnetic field.

Another possible confirmation of the composite fermion model is associated with the study of the effects due to collective modes in such a system, which correspond to gauge field fluctuations relative to the value determined by $B_{\rm st}$ (if we use the formalism developed in Refs. 2, 3). The role of such fluctuations is significant in anyon systems: such fluctuations are responsible for the emergence of an anyonic acoustic mode, and hence superfluid properties of the anyon gas for certain values of the statistical parameter. The spectrum of collective modes in the system of composite fermions and the dynamic form factors were calculated by Simon and Halperin[19] who proved that the variance of collective excitations is characterized by the oscillatory dependence on the wave vector, while the scale and the number of oscillations are determined by the filling factor. The oscillatory structure of the spectrum of collective modes can be confirmed, among other things, by their interaction with lattice vibrations. This interaction can result in a rearrangement of the phonon spectrum, which strongly depends on the filling factor. The present communication is devoted to an analysis of this problem. Similar effects as applied to anyon systems were considered earlier in Ref. 20.

Let us consider a two-dimensional system of completely polarized composite fermions interacting with phonons. The Hamiltonian of the system has the form

$$H=H_{CF}+H_{\rm ph}+H_{\rm int}, \tag{1}$$

where

$$H_{CF}=\int d^2r\Psi^+(\mathbf{r})\,\frac{1}{2m_{CF}}\,[-i\nabla+eA_\Delta(\mathbf{r})-\mathbf{a}(\mathbf{r})]^2\Psi(\mathbf{r})+\frac{1}{2}\int d^2r\int d^2r'[\Psi^+(\mathbf{r})\Psi(\mathbf{r})-n_0]V(|\mathbf{r}-\mathbf{r}'|)[\Psi^+(\mathbf{r}')\Psi(\mathbf{r}')-n_0], \tag{2}$$

$$H_{\rm ph}=\sum_{\lambda\mathbf{q}}\ \omega_{\lambda\mathbf{q}}\left(b^+_{\lambda\mathbf{q}}b_{\lambda\mathbf{q}}+\frac{1}{2}\right), \tag{3}$$

$$H_{\rm int}=\frac{1}{\sqrt{S}}\sum_{\lambda\mathbf{q}}\ \int d^2r\mathrm{e}^{i\mathbf{qr}}\Psi^+(\mathbf{r})\Psi(\mathbf{r})g_{\lambda\mathbf{q}}(b_{\lambda\mathbf{q}}+b^+_{\lambda(-\mathbf{q})}), \tag{4}$$

Ψ is the fermion field, m_{CF} the mass of composite fermions, n_0 their average concentration,

$$\mathbf{a}(\mathbf{r})=\varphi\int d^2r'[\Psi^+(\mathbf{r}')\Psi(\mathbf{r}')-n_0]\,\frac{\hat{\mathbf{z}}\times(\mathbf{r}-\mathbf{r}')}{|\mathbf{r}-\mathbf{r}'|^2} \tag{5}$$

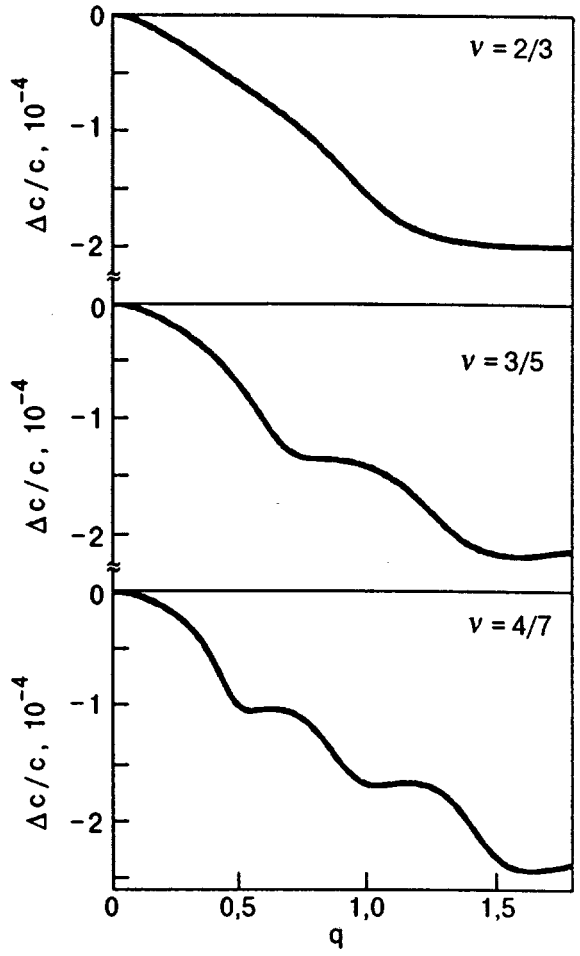

FIG. 1. Relative change in the velocity of acoustic phonons as a function of wave vector (q is measured in the units of $q_0=(4\pi n_0)^{1/2}$).

the vector potential of the Chern–Simons statistical field, $\varphi=2m$ the field flux carried by a composite particle, $\hat{\mathbf{z}}$ the unit vector along the field $\mathbf{B}$, $\mathbf{A}_\Delta$ the vector potential of the effective field $\Delta B=|1-\varphi\nu|B$, $V(\mathbf{r})=e^2/\varepsilon r$ the Coulomb interaction potential, ε the permittivity, $b^+(b)$ are the creation (annihilation) operators for phonons, $\omega_{\lambda\mathbf{q}}$ the phonon frequencies, $g_{\lambda\mathbf{q}}$ the matrix elements of interaction of phonons with composite fermions, and S is the area of the system. For the sake of definiteness, we assume that $g_{\lambda\mathbf{q}}\neq 0$ only for a certain polarization λ. Then the renormalization of the phonon spectrum is determined by a pole of the phonon Green's function $G_\lambda(\mathbf{q},\omega)$ satisfying the equation

$$G_\lambda^{-1}(\mathbf{q},\omega)=[G_\lambda^0(\mathbf{q},\omega)]^{-1}-g_{\lambda\mathbf{q}}^2K^{00}(\mathbf{q},\omega), \tag{6}$$

where $G_\lambda^{(0)}(\mathbf{q},\omega)$ is the Green's function for free electrons and $K^{00}(\mathbf{q},\omega)$ the polarization Green's function for composite fermions, which is defined (in the random-phase approximation) by the matrix equation

$$\hat{K}^{-1}(\mathbf{q},\omega)=[\hat{K}^{(0)}(\mathbf{q},\omega)]^{-1}-\hat{V}(\mathbf{q}), \tag{7}$$

in which the matrix indices assume the values 0,y if the x-axis is chosen along the vector $\mathbf{q}$. In Eq. (7), we have

$$\hat{V}(\mathbf{q})=\frac{2\pi}{q}\begin{pmatrix} e^2\varepsilon^{-1} & -i\varphi \\ i\varphi & 0\end{pmatrix}, \tag{8}$$

$$K_{\mu\nu}^{(0)}(\mathbf{q},\omega)=D_{\mu\nu}^{(0)}(\mathbf{q},\omega)+\frac{n_0}{m_{CF}}\,\delta^{\mu\nu}(1-\delta^{\mu 0}), \tag{9}$$

where $D_{\mu\nu}^{(0)}(\mathbf{q},\omega)$ is the Fourier component of the current–current Green's function for free fermions in the field ΔB:

$$D_{\mu\nu}^{(0)}(\mathbf{r},t;\mathbf{r}',t')=-i\langle T\{j^\mu(\mathbf{r},t)j^\nu(\mathbf{r}',t')\}\rangle_0$$

with the zero current component defined as $j^0(\mathbf{r})=\Psi^+(\mathbf{r})\Psi(\mathbf{r})-n_0$.

The calculation of $K_{\mu\nu}^0$ at $T=0$ for an arbitrary ν gives

$$K_{\mu\nu}^{(0)}(\mathbf{q},\omega)=\frac{1}{2\pi\Delta\omega_c}\begin{pmatrix} q^2\Sigma_0 & \mp iq\Delta\omega_c\Sigma_1 \\ \pm iq\Delta\omega_c\Sigma_1 & (\Delta\omega_c)^2(\Sigma_2+\nu_\Delta)\end{pmatrix}. \tag{10}$$

Here and below, the upper sign corresponds to $\nu<1/2m$ and the lower sign to $\nu>1/2m$ (for a given m). In formula (10), $\Delta\omega_c=e\Delta B/m_{CF}$ is the effective cyclotron frequency, $\nu_\Delta=\pm\nu/(1-\varphi\nu)$ the effective filling factor,

$$\Sigma_j=e^{-x}\sum_{nm=0}^{\infty} f_n(1-f_m)\,\frac{n!}{m!}\,\frac{x^{m-n-1}(m-n)}{(\omega/\Delta\omega_c)^2-(m-n)^2}$$
$$\times[L_n^{m-n}(x)]^{2-j}\left((m-n-x)L_n^{m-n}(x)+2x\,\frac{dL_n^{m-n}(x)}{dx}\right)^j,$$

where $x=(ql_\Delta)^2/2$, $l_\Delta=(e\Delta B)^{-1/2}$ is the effective magnetic length, $L_n^{m-n}(x)$ the generalized Laguerre polynomial,

$$f_n=\begin{cases}1, & n\leqslant p-1,\\ \eta, & n=p,\\ 0, & n\geqslant p+1,\end{cases}$$

and p and η are the integral and fractional parts of ν_Δ. While deriving formula (10), we assumed that the time τ of composite fermion relaxation is infinitely long. Taking into account the finiteness of τ, we obtain corrections $\sim(\Delta\omega_c\tau)^{-2}$ to the phonon frequency renormalization, which can be neglected if we assume that the condition $\Delta\omega_c\tau\gg 1$ is observed for all ν_Δ.

Substituting (7), (8), and (10) into (6), we obtain the dispersion equation in the form

$$(\omega^2-\omega_{\lambda\mathbf{q}}^2)\left[\left(\Sigma_1\mp\frac{1}{\varphi}\right)^2-\Sigma_0\left(\nu_\Delta+\Sigma_2+\frac{e^2q}{\varphi^2\varepsilon\Delta\omega_c}\right)\right]$$
$$-\frac{g_{\lambda\mathbf{q}}^2\omega_{\lambda\mathbf{q}}q^2}{\pi\varphi^2\Delta\omega_c}\,\Sigma_0=0. \tag{11}$$

Proceeding from Eq. (11), we consider the renormalization of the acoustic phonon spectrum ($\omega_{\lambda\mathbf{q}}=cq$). The solutions of Eq. (11) corresponding to the phonon mode for $\nu=2/3$, 3/5, and 4/7 (filling factors corresponding to the fractional quantum Hall effect) are shown in Fig. 1 as functions of q. The relative change $\Delta c/c$ in the phase velocity is laid along the ordinate axis and q in the units of $q_0=(4\pi n_0)^{1/2}$ along the abscissa axis. The matrix element of interaction is chosen in the form $g_{\lambda\mathbf{q}}=\Lambda q(2\rho d\omega_{\lambda\mathbf{q}})^{-1/2}$, where Λ is the deformation potential, ρ the density of the

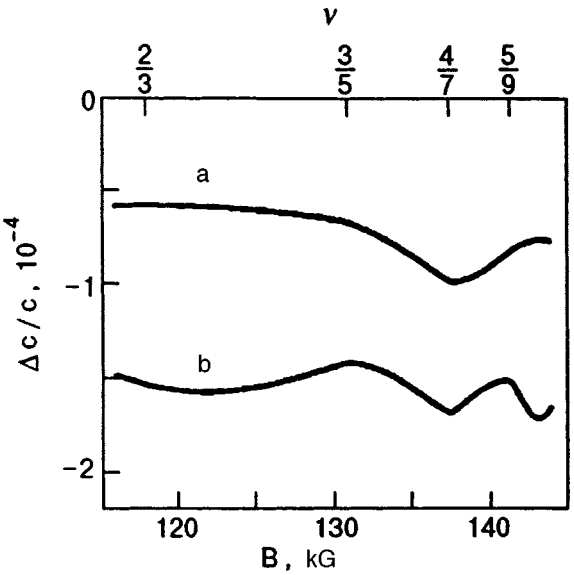

FIG. 2. Magnetic-field dependences of the change in the velocity of acoustic phonons for $q=0.5q_0(a)$ and $q=q_0(b)$.

elastic medium, and d the thickness of the layer in which the lattice mode propagates. We used the parameters $n_0=2\times10^{11}$ cm^{-2}, $m_{CF}=0.25m_e$, $\varepsilon=12.6$, $c=4\cdot10^5$ cm/s, $\Lambda=7.4$ eV, $\rho=5.3$ g/cm^3, and $d=500$ Å. For the chosen parameters and for the range of q under investigation, the phonon frequency lies below the frequencies of collective modes for composite fermions. It can be seen from Fig. 1 that the renormalized velocity of phonons has an oscillatory dependence on the wave vector, the number and scale (in q) of oscillations depending significantly on the filling factor. It should be noted that if we disregard the quantity (5) in Hamiltonian (1), the dependence $\Delta c(q)$ is transformed into a dependence close to linear for $q<q_0$, i.e., the effect under investigation is mainly determined by the interaction of phonons with collective modes. In our opinion, the sensitivity of the oscillatory structure of the spectrum to the parameters B and n_0 which can be easily varied in the course of experiment differs significantly from the case of the anyon–phonon interaction[20] (the role of such a parameter in Ref. 20 was played by the anyon statistics which is an intrinsic parameter of the system). Figure 2 shows the dependence of $\Delta c/c$ on B for two values of q. The dependences $\Delta c(B)$ has a number of kinks for the values of B corresponding to integral ν_Δ. The jump in the derivative is associated with the beginning of filling of a new Landau level in the system of composite fermions as the field decreases by ΔB. The inclusion of the localized states between Landau levels must lead to the formation of horizontal segments on the $\Delta c(B)$ dependence in the regions of kinks.

Thus, the interaction of composite fermions with the lattice for parameters corresponding to real samples in which the fractional quantum Hall effect is observed can lead to an oscillatory dependence of the phase velocity of acoustic phonons on the wave vector. The emerging oscillatory structure of the phonon spectrum will be modified upon a change of the applied magnetic field or electron concentration.

*E-mail: fil@isc.kharkov.ua

[1] J. K. Jain, Phys. Rev. Lett. **63**, 199 (1989).
[2] A. Lopez and E. Fradkin, Phys. Rev. B **44**, 5246 (1991).
[3] B. I. Halperin, P. A. Lee, and N. Read, Phys. Rev. B **47**, 7312 (1993).
[4] E. Fradkin, *Field Theories of Condensed Matter Systems*, Addison-Wesley Publ. Comp. (1991).
[5] F. Wilczek, *Fractional Statistics and Anyon Superconductivity*, World Scientific, Singapore (1989).
[6] Y. H. Chen, F. Wilczek, E. Witten, and B. I. Halperin, Int. J. Mod. Phys. B **3**, 1001 (1989).
[7] A. L. Fetter, C. B. Hanna, and R. B. Laughlin, Phys. Rev. B **39**, 9679 (1989).
[8] A. Zee, in *High Temperature Superconductivity* (ed. by K. Bedell, D. Coffey, D. Pines, and J. R. Schrieffer), Addison-Wesley Publ. Comp. (1991).
[9] R. R. Du, H. L. Stormer, D. C. Tsui *et al.*, Phys. Rev. Lett. **70**, 2944 (1993).
[10] D. R. Leadey, R. J. Nicholas, C. T. Foxon, and J. J. Harris, Phys. Rev. Lett. **72**, 1906 (1994).
[11] R. R. Du, H. L. Stormer, D. C. Tsui *et al.*, Phys. Rev. Lett. **73**, 3274 (1994).
[12] H. C. Manoharan, M. Shayegan, and S. J. Klepper, Phys. Rev. Lett. **73**, 3270 (1994).
[13] W. Kang, H. L. Stormer, L. N. Pfeiffer *et al.*, Phys. Rev. Lett. **71**, 3850 (1993).
[14] J. H. Smet, D. Weiss, R. H. Blick *et al.*, Phys. Rev. Lett. **77**, 2272 (1996).
[15] V. J. Goldman, B. Su, and J. K. Jain, Phys. Rev. Lett. **72**, 2065 (1994).
[16] R. L. Willett, M. A. Paalanen, R. R. Ruel *et al.*, Phys. Rev. Lett. **65**, 112 (1990).
[17] R. L. Willett, R. R. Ruel, K. W. West *et al.*, Phys. Rev. Lett. **71**, 3846 (1993).
[18] R. L. Willett, R. R. Ruel, M. A. Paalanen *et al.*, Phys. Rev. B **47**, 7344 (1993).
[19] H. Simon and B. I. Halperin, Phys. Rev. B **47**, 17368 (1993).
[20] D. V. Fil and O. I. Tokar, Physica C **230**, 207 (1994).

Translated by R. S. Wadhwa

On paired nature of superfluid condensate in helium-II

S. I. Vil'chinsky

*Taras Shevchenko University, 252022 Kiev, Ukraine**

E. A. Pashitsky

Institute of Physics, National Academy of Sciences of the Ukraine, 252650 Kiev, Ukraine

P. I. Fomin

*Institute of Applied Physics and Institute of Theoretical Physics, National Academy of Sciences of the Ukraine, 252142 Kiev, Ukraine***

(Submitted June 2, 1997)
Fiz. Nizk. Temp. **23**, 1267–1271 (December 1997)

A hypothesis on pairing of helium atoms below the λ-point is put forth on the basis of empirical data on the dynamics of ^{3}He impurity atoms in superfluid ^{4}He, that suggest an abnormally large effective mass of ^{3}He. The role of paired condensate in superfluidity of ^{4}He is considered as well as the possibility of additional experimental proofs of the pairing of ^{4}He atoms, including the observation of vortices with a half-integral velocity circulation quantum. © *1997 American Institute of Physics.* [S1063-777X(97)00112-6]

The existence of a coherent condensate of pairs of ^{4}He atoms in liquid helium below the λ-point and its role in the microscopic structure of the superfluid component ρ_s were discussed repeatedly in the literature.[1–9] However, this question remains disputable in view of the lack of a microscopic theory of a superfluid Bose liquid and the scarceness of experimental data in this field. The possibility of coexistence of a one-particle Bose condensate ($\langle\hat{\Psi}_0\rangle\neq 0$) and the condensate of weakly couples boson pairs ($\langle\hat{\Psi}_p\cdot\Psi_{-p}\rangle\neq 0$), which are similar to Cooper pairs in a superconductor[10] to a certain extent, was discussed earlier.[1–7]

It was proved in Ref. 8, however, that such a coexistence of two condensates, viz., the one-particle condensate (OC) with a small number of particles ($n_0\ll n$), which is ''depleted'' due to interaction between bosons, and the intense paired condensate (PC) formed in the case of a strong attraction in a wide range of momenta $p\neq 0$, leads to instability of the superfluid Bose system, while the ground state containing only PC without any traces of OC at $T=0$ is stable.

Here we pay attention to significant empirical evidence confirming the formation of coupled pairs of ^{4}He atoms in superfluid helium and consider some consequences of this circumstance. We are speaking of the interpretation of the origin of the anomalously large effective mass m_3^* of ^{3}He atoms in ^{3}He–^{4}He solutions:[11] $m_3^*=(2.38\pm 0.04)m_3$ according to heat-capacity measurements with a ^{3}He concentration of the order of 1%,[12] and $m_3^*\approx 2.35m_3$ according to impurity excitation spectra[13] (where m_3 is the mass of a ^{3}He atom). The reason behind such a strong increase in the mass of ^{3}He impurity atoms in superfluid ^{4}He requires a serious theoretical substantiation and cannot be explained (in our opinion) by only the interaction of elementary excitations (at any rate, in the first order perturbation theory).[14]

It is worth noting that the value of m_3^* is close (from above) to the total mass of ^{3}He and ^{4}He atoms:

$$m_3+m_4=\frac{7}{3}\,m_3=2.33(3)m_3,$$

indicating (in our opinion) the existence of coupled states of ^{3}He and ^{4}He atoms in superfluid helium.

The fact that m_3^* is slightly larger than $(7/3)m_3$ in a dilute solution ($\sim 1\%$) ^{3}He in ^{4}He can be due to the interaction with quasiparticles (phonons) considered by Slyusarev and Struminskii,[14] while an increase in the mass to $m_3^*=(2.38\pm 0.04)m_3$ in a 5% ^{3}He–^{4}He solution[12] can apparently be due to direct interaction between ^{3}He atoms.[12]

But if ^{3}He–^{4}He solutions contain coupled pairs of ^{3}He and ^{4}He atoms, the ever pure ^{4}He below T_λ must contain coupled pairs of ^{4}He atoms since the paired interaction potential for them is virtually the same as the potential of interaction between ^{3}He and ^{4}He, and the energy of zero-point vibrations is lower in view of the larger reduced mass ($\mu_{4-4}=m_4/2$ instead of $\mu_{3-4}=(3/4)m_4$, where m_4 is the mass of ^{4}He atoms). Moreover, the exchange interaction of two identical Bose particles must also facilitate their pairing. Hence it follows that the superfluid component ρ_s in ^{4}He can be a condensate of coupled pairs of ^{4}He atoms.

It should be emphasized that such a condensate is not completely identical to the ''Cooper'' PC[1–9] with strongly overlapping wave functions of boson pairs. This can be proved by using the approach developed in Rev. 8 for Bose systems with a ''depleted'' OC and an intense PC, in which the number of particles in the Bose condensate $n_0\ll n$ (n is the total number of particles), and the system of Dyson–Belyaev equations[15] for the normal Σ_{11} and anomalous Σ_{12} eigenenergy components assumes the following form to within principal terms in the small parameter $n_0/n\ll 1[p=\mathbf{p},\omega)]$:

$$\Sigma_{11}=n'V_0+n_0\Lambda(p)\tilde{V}(p)+\varphi(p), \tag{1}$$

$$\Sigma_{12}(p)=n_0\Lambda(p)\tilde{V}(p)+\psi(p), \tag{2}$$

where

$$\varphi(p)=i\int \frac{d^4p'}{(2\pi)^4}\,G_{11}(p')\tilde{V}(p-p')\Gamma(p,p'), \tag{3}$$

$$\psi(p)=i\int \frac{d^4p'}{(2\pi)^4}\,G_{12}(p')\tilde{V}(p-p')\Gamma(p,p'). \tag{4}$$

Here n' is the number of bosons in overcondensate (excited) states, $V_0\equiv V(0)$ the zeroth Fourier component of the initial potential $V(p)$ of paired interaction between particles, $G_{11}(p)$ and $G_{12}(p)$ are the normal and anomalous Green's functions for bosons, $\Gamma(p,p')$ is the vertex component of interaction taking into account many-particle effects, $\Lambda(p)=\Gamma(p,0)=\Gamma(0,p)$, and $\tilde{V}(p)$ is the renormalized (''screening'') Fourier component of the interaction potential:

$$\tilde{V}(\mathbf{p},\omega)=V(\mathbf{p})[1-V(\mathbf{p})\Pi(\mathbf{p},\omega)]^{-1}, \tag{5}$$

where $\Pi(p)$ is the polarization operator for bosons:

$$\Pi(p)=i\int \frac{d^4p'}{(2\pi)^4}\,[G_{11}(p')G_{11}(p'-p) + G_{12}(p')G_{12}(p'-p)]\Gamma(p',p). \tag{6}$$

It should be noted that the approximation used in Ref. 8 ($n_0\ll n,n'\approx n$), which makes it possible to write ''truncated'' equations (1) and (2) for Σ_{11} and Σ_{12}, is diametrically opposite to the Bogoliubov approximation[16] for a nearly ideal Bose gas, in which $n_0\approx n$ and $n'\ll n$.

In the absence of OC ($n_0\equiv 0$), the order parameter $\Psi(p)$ of a coherent PC is degenerate in phase and is defined for $T\to 0$ by a homogeneous nonlinear integral equation:[8]

$$\Psi(p)=-\int \frac{d^3p'}{(2\pi)^3}\,\Gamma(p,p')\tilde{V}(p-p')\,\frac{\Psi(p')}{2\varepsilon(p')}, \tag{7}$$

where

$$\varepsilon(p)=\left\{\left[\frac{p^2}{2m}-\mu+nV_0+\varphi(p)\right]^2-\left|\Psi(p)\right|^2\right\}^{1/2}, \tag{8}$$

and μ is the chemical potential for bosons, which, according to the Hugenholtz–Pines theory,[17] taking into account (1) and (2) for $n_0=0$ and $n'\approx n$, has the form

$$\mu=\Sigma_{11}(0)-\Sigma_{12}(0)=nV_0+\varphi(0)-\Psi(0). \tag{9}$$

It should be noted that in Refs. 1–8 it was assumed that the one-particle spectrum $\varepsilon(p)$ contains a finite gap $\Delta\neq 0$ for $p=0$. According to Refs. 7 and 8, for $n_0=0$ this automatically leads to violation of relation (9) as well as the Reatto–Chester asymptotic form[18] for the paired correlation function $\langle\hat{\Psi}(\mathbf{r})\hat{\Psi}(\mathbf{r}')\rangle$, which is transformed from the power dependence $\sim|\mathbf{r}-\mathbf{r}'|^{-2}$ into the exponential dependence $\sim\exp(-\kappa|\mathbf{r}-\mathbf{r}'|)$, where $\kappa\sim\Delta$. However, the presence of the gap Δ in a boson spectrum with an intense PC is not essential (in contrast to the case of fermions).[10] For this reason, the quasiparticle spectrum remains acoustic with $\varepsilon\approx pu$ for $p\to 0$, where $n=\sqrt{\Psi(0)/m^*}$ (m^* is the effective mass of bosons taking the interaction into account), and relation (9) and the hydrodynamic asymptotic form

$$\langle\Psi(\mathbf{r})\cdot\hat{\Psi}(\mathbf{r}')\rangle>\sim|\mathbf{r}-\mathbf{r}'|^{-2}$$

are preserved in the absence of OC.

A nontrivial solution $\Psi(p)\neq 0$ of the integral equation (7), corresponding to the formation of a coherent PC without a OC, exists only when the effective interaction $\Gamma\tilde{V}$ in a wide range of momenta corresponds to attraction ($\Gamma\tilde{V}<0$) which must be stronger than the repulsion between pairs for $p\to 0$, required for macroscopic stability of the system to spontaneous compression.

It should be noted that effective attraction in a certain region of the momentum space ($p\neq 0$) emerges even in a Bose system with repulsion between particles. If we consider ^{4}He atoms to be rigid spheres with an infinitely strong repulsion at distances $r<a$ (where a is the diameter of a ^{4}He atom), the self-consistent potential of interaction, according to Ref. 19, has the form

$$V(p)=V_0\,\frac{\sin pa}{pa} \tag{10}$$

and is negative due to diffraction effects (i.e., corresponds to attraction) in the region $(\pi/a)<p<(2\pi/a)$. Here we mean only the first region of negative values of $V(p)$ since the value of $p=2\pi/a$ for $a\simeq 2.5$ Å virtually coincides with the finite allowed value of quasimomentum $p_{\max}\approx 2.5$ Å^{-1} of elementary excitations in superfluid ^{4}He. It should be noted that the Bogoliubov spectrum of one-particle excitations in an almost ideal Bose gas[16]

$$E(p)=\left[p^2u^2(p)+\frac{p^4}{4m^2}\right]^{1/2},$$

$$u(p)=\sqrt{\frac{nV(p)}{m}} \tag{11}$$

with the interaction potential (10) is similar to the spectrum of quasiparticles in superfluid helium[19,20] for certain values of parameters (see Ref. 19), although the main criterion of applicability of the Bogoliubov theory,[16] according to which the number n' of overcondensate excitations is smaller than the number n_0 of particles in the Bose condensate, does not hold for the quantum Bose liquid ^{4}He. At the same time, attraction between particles in a Bose liquid can be enhanced significantly in the region $p>(\pi/a)$, while repulsion can be suppressed in the region $p<(\pi/a)$ due to collective many-particle effects described by renormalized (''effective'') potentials $\tilde{V}(p)$ in the vertex part of $\Gamma(p,p')$. Indeed, an estimation of the polarization operator $\Pi(p)$ of a normal Bose gas in the random-phase approximation gives

$$\Pi_0(p,\Omega)=\frac{1}{2\pi^2}\int_0^{k_{\max}}\frac{k^2dk}{\Omega^2-(p^2/4m)+2\mu-(k^2/m)} \approx-\frac{m}{\pi a}<0 \tag{12}$$

for large values of

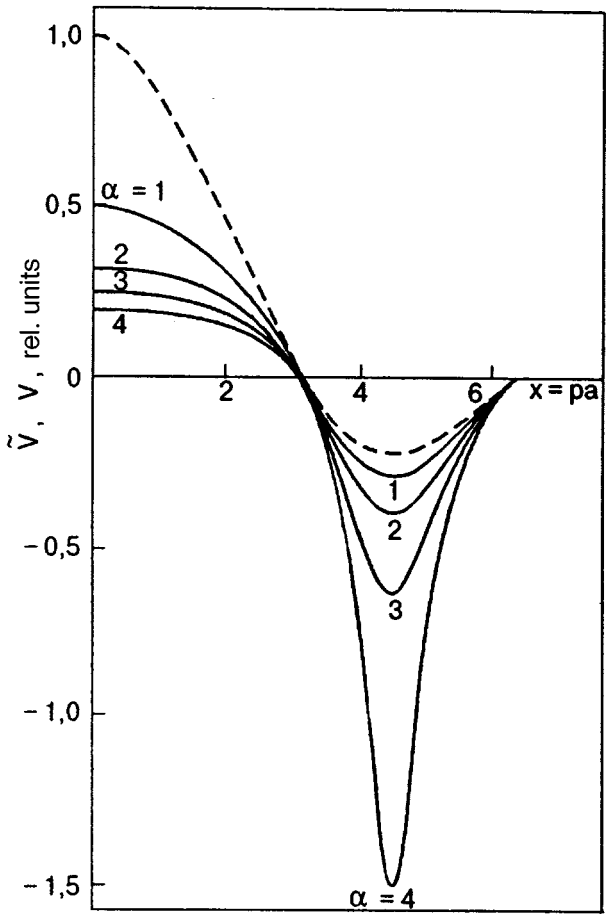

FIG. 1. Initial (dashed curve) (10) and renormalized (solid curves) (5) potentials as functions of $x=pa$ for different values of α.

$$k_{\max}\approx m\sqrt{\Omega-(p^2/4m)+2\mu},$$

where Ω and $\mathbf{p}$ are the total energy and momentum of two particles. Obviously, the negative sign of $\Pi(p)$ in the effective potential (5) corresponds to a suppression of the repulsion $V(p)>0$ and to an enhancement of attraction $V(p)<0$. The dashed curve in Fig. 1 describes the initial potential (10) as a function of $x=pa$, while solid curves correspond to similar dependences of the renormalized potential (5) for different values of the dimensionless interaction parameter $\alpha=mV_0/a\pi$. It can be seen that the integral contribution from the region of attraction $(\pi/a)\leqslant p\leqslant(2\pi/a)$ can become larger than the contribution from suppressed repulsion for $p\leqslant(\pi/a)$ in Eq. (7) for large values of α. Naturally, the inclusion of Van der Waals forces acting between ^{4}He atoms leads to still stronger enhancement of attraction and can facilitate the formation of an intense PC in HeII or coupled pairs of ^{4}He atoms.

It should be noted that the existence of a PC with an order parameter $\Psi(p)\neq 0$ does not imply the formation of coupled boson pairs in a superfluid Bose liquid since Eq. (7) is similar to the integral equation for the wave function of interacting particles in vacuum:

$$\Psi_0(p)=\int \frac{d^3p'}{(2\pi)^3}\,V(\mathbf{p}-\mathbf{p}')\,\frac{\varphi_0(p')}{\omega_0-2\varepsilon_0(p')+i\delta};$$

$$(\delta\to 0) \tag{13}$$

with the zero binding energy

$$\omega_0\equiv\Omega-p^2/2m=0.$$

A coherent PC contains only strongly overlapping pairs of bosons of the type of Cooper pairs.[8]

At the same time, the astonishing closeness of the value of the effective mass m_3^* of an impurity ^{3}He atom in HeII to the total mass (m_3+m_4) of ^{3}He and ^{4}He atoms indicates the possibility of formation of coupled states of He atoms, i.e., the formation of weakly overlapping (local) pairs of atoms owing to strong attraction in the momentum range $p>(\pi/a)$ (see Fig. 1). Indeed, it is well known that the interaction of atoms in identical or close energy states is characterized by the potential V determined by the mutual arrangement of atoms (especially by the separation r between their nuclei). For a certain equilibrium distance r_0 and for not very high kinetic energies of free atoms, a more or less stable chemical bond can be formed between atoms as a result of atomic interaction, whose strength can be judged from the lifetime of the molecule or from the chemical bond energy. The possibility of formation of bound states of helium atoms follows from the data presented in Ref. 22: the equilibrium distance for the He–He bond is 2.965 Å, which is in accord with the atomic spacing $r_0\simeq 3$ Å calculated for the observed ^{4}He density $\rho\approx 0.16$ g/cm^3 (we assume that the radius of a ^{4}He atom is ~ 0.5 Å), while the depth of the potential well corresponding to a stable state of He–He is 0.93 meV, which corresponds to a temperature of the order of 9 K. In the case when the superfluid component is mainly formed by a condensate of coupled pairs of atoms, Gastrow's wave function[23] in the real space should be used instead of the function $\varphi(p)$ in the momentum space:

$$\Phi_j=\prod_{i<j} f(|\mathbf{r}_i-\mathbf{r}_j|)=\exp\left(-\frac{1}{2}\sum_{i<j} V(|\mathbf{r}_i-\mathbf{r}_j|)\right). \tag{14}$$

This function takes into account many-particle correlations and is a good approximation for describing the state of liquid ^{4}He.[24,25]

Thus, we cannot rule out the fact that the superfluid component in HeII is mainly formed by a condensate of coupled pairs of ^{4}He atoms with doubled mass $2m_4$. A direct proof of this fact could be the experimental observation of quantized vortices with a half-integral velocity circulation quantum $\varkappa=h/2m_4$. The available experimental data[26–29] do not allow us to determine unambiguously the circulation of the superfluid velocity $\mathbf{v}_s$ around Onsager vortex filaments. For example, Whitmore and Zimmermann[28] measured the effective circulation Γ normalized to the density ρ_s of the superfluid component, which changes upon a transition from the Bose condensate to a condensate of coupled pairs of ^{4}He atoms with the doubled mass $2m_4$ of quasiparticles, but with half the concentration $n/2$.

In conclusion, the authors express their gratitude to A. F. Andreev and V. I. Pentegov for fruitful discussions.

*E-mail: sivil@popper1.isf.kiev.ua
**E-mail: pfomin@gluk.apc.org

[1] T. G. Valatin and D. Butler, Nuovo Cimento **10**, 37 (1958).
[2] V. Girardenu and R. Arnowitt, Phys. Rev. **113**, 755 (1959).
[3] A. Coniglio and M. Maricov, Nuovo Cimento **48**, 249 (1967).
[4] W. A. B. Evans and Y. Impry, Nuovo Cimento **63**, 155 (1969).
[5] A. Coniglio and F. Mancini, Nuovo Cimento **63**, 227 (1969).
[6] R. Hasting and T. W. Hally, Phys. Rev. B **12**, 267 (1975).
[7] P. S. Kondratenko, Teor. Mekh. Fiz. **22**, 278 (1975).
[8] Yu. A. Nepomnyashchii and E. A. Pashitsky, Zh. Éksp. Teor. Fiz. **98**, 178 (1990) [Sov. Phys. JETP **71**, 98 (1990)].
[9] S. I. Shevchenko, Fiz. Nizk. Temp. **11**, 339 (1985) [Sov. J. Low Temp. Phys. **11**, 183 (1985)].
[10] J. Schrieffer, *Theory of Superconductivity*, Benjamin, NY, 1964.
[11] B. N. Esel'son, V. N. Grigor'ev, V. G. Ivanov *et al.*, *Solutions of* ^{3}He–^{4}He *Quantum Liquids* [in Russian], Nauka, Moscow (1973).
[12] A. C. Anderson, W. R. Roach, R. E. Sarwinski, and P. C, Wheatly, Phys. Rev. Lett. **16**, 263 (1968).
[13] V. I. Sobolev and B. N. Esel'son, Zh. Éksp. Teor. Fiz. **60**, 240 (1971) [Sov. Phys. JETP **33**, 132 (1971)].
[14] V. N. Slyusarev and M. A. Struminskii, Ukr. Fiz. Zh. **14**, 453 (1969).
[15] S. T. Belyaev, Zh. Éksp. Teor. Fiz. **34**, 417 (1958) [Sov. Phys. JETP **7**, 289 (1958)].
[16] N. N. Bogoliubov, Izv. Akad. Nauk SSSR, Ser. Fiz. **11**, 77 (1947).
[17] N. Hugenholtz and D. Pines, Phys. Rev. **116**, 489 (1959).
[18] L. Reatto and C. V. Chester, Phys. Rev. **155**, 88 (1967)
[19] K. Brueckner, *Theory of Nuclear Structure*, London (1959).
[20] J. L. Yarnell, G. P. Arnold, P. J. Bendt, and E. C. Kerr, Phys. Rev. **113**, 1379 (1959).
[21] D. Hashaw and A. Woods, Phys. Rev. **121**, 1266 (1961).
[22] *Encyclopedia of Physics* [in Russian], vol. 3, Bol'shaya Rossiiskaya Entsiklopediya, Moscow (1992).
[23] R. Gastrow, Phys. Rev. **98**, 1478 (1955).
[24] M. L. Ristig, P. Hecking, P. M. Lam, and T. W. Clark, Phys. Lett. **A63**, 94 (1977).
[25] M. L. Ristig, Phys. Rev. B **B18**, 1207 (1978).
[26] W. F. Vinen, Proc. Roy. Soc. **F260**, 218 (1961).
[27] G. W. Rayfield and F. Reif, Phys. Rev. Lett. **11**, 305 (1963).
[28] S. C. Whitmore and W. Zimmermann, Phys. Rev. **166**, 181 (1968).
[29] S. Putterman, *Superfluid Hydrodynamics*, North-Holland, Amsterdam (1974).

Translated by R. S. Wadhwa

On Hamiltonian formulation of hydrodynamic equations for superfluid ^{3}He–A

A. A. Isayev and S. V. Peletminsky

*National Science Center ''Kharkov Physicotechnical Institute,'' 310108 Kharkov, Ukraine**
(Submitted June 18, 1997)
Fiz. Nizk. Temp. **23**, 1272–1280 (December 1997)

The Poisson brackets for the dynamic variables describing the spin and orbital dynamics of superfluid ^{3}He–A are obtained by using a consistent Hamiltonian formalism. The analysis is based on the derivation of the kinematic component of the system Lagrangian and on the consideration of variations of dynamic variables, which leave the kinematic component of the Lagrangian invariant. Equations of motion for the dynamic variables are derived, and Galilean invariance of the obtained equations is considered by proceeding from the invariance of the system Lagrangian to Galilean transformations. © *1997 American Institute of Physics.* [S1063-777X(97)00212-0]

1. INTRODUCTION

This research is devoted to the derivation of the hydrodynamic equations for superfluid ^{3}He–A by using the Hamiltonian approach. The construction of hydrodynamics of the superfluid A-phase of ^{3}He has formed the subject of a large number of publications (see, for example, Refs. 1 and 2 and the references cited therein). Several approaches can be singled out in this case. Some authors[3–6] based their analysis on the microscopic approach, which is model-dependent as a rule. This is important for obtaining quantitative estimates of various coefficients appearing in hydrodynamic equations. However, the most general form of hydrodynamic equations permitted by symmetry conditions can be established only phenomenologically[7–9] by using the method of conservation laws. An attempt at constructing nonlinear hydrodynamic equations by using the Lagrangian formalism was also made by Khalatnokov and Lebedev.[10] Here we proceed from the Hamilton approach.[11,12] It should be noted that the concept of intrinsic orbital angular momentum[13] associated with the angular momentum of Cooper pairs plays an important role in all approaches. We introduce the intrinsic orbital angular momentum as a generator of spatial rotations of the variables describing liquid-crystal degrees of freedom.

The determination of Poisson brackets (PB) of dynamic variables plays a fundamental role in the Hamiltonian approach. In contrast to ordinary mechanical systems, the PB of dynamic variables for condensed media have a nontrivial structure. In the case of normal physical systems, the description on the hydrodynamic stage of evolution is constructed on the basis of densities of additive integrals of motion whose, PB are well known. A description of a system with spontaneously broken symmetry involves the introduction of additional hydrodynamic parameters that are not associated with conservation laws, but are due to the broken symmetry. Since these additional variables have no operator expressions in the secondary quantization representation, the PB for these variables can be obtained by simple computation of commutators as usual in a quantum-mechanical derivation of PB. The construction of PB for dynamic variables associated with symmetry breaking (both with the densities of additive integrals of motion and with one another) constitutes the main problem. In the case of superfluid ^{3}He–A, such variables are the spin and spatial anisotropy vectors $d_\alpha(x)$ and $l_i(x)$ as well as the superfluid momentum $p_i(x)$.

The Hamiltonian formulation of hydrodynamic equations for superfluid ^{3}He–A at $T=0$ was proposed by Volovik and Balatskii[14] who assumed that the motion of the normal component is frozen and did not write the PB corresponding to the momentum density. We also include the entropy density in the complete system of PB, which allows us to formulate the adiabaticity condition for processes occurring in the A-phase. For this purpose, we introduce in the theory the dynamic variables conjugate to the momentum- and entropy densities, i.e., the displacement vector $u_i(x)$ and the formally introduced variable $\psi(x)$ (see Sec. 2), which are cyclic (the Hamiltonian H of the system is independent of these variables). In order to obtain a complete system of PB, we follow the variational principle described in Ref. 12, according to which the structure of the Poisson brackets of the dynamic variables $\varphi_\alpha(x)$ is essentially determined by the form of the kinematic component $L_k(\varphi,\dot{\varphi})$ of the Lagrangian, which can be found from the relation

$$L=L_k(\varphi,\dot{\varphi})-H(\varphi)\equiv\int d^3xF_\alpha(x;\varphi)\dot{\varphi}_\alpha(x)-H(\varphi)$$

[L is the Lagrangian, $H(\varphi)$ the Hamiltonian, and $F_\alpha(x;\varphi(x',t))$ a certain functional of the dynamic variables $\varphi_\alpha(x)$], and by the variations of dynamic variables $\delta\varphi_\alpha(x,t)=\delta\varphi_\alpha[x;\varphi(x',t)]$, which leave the kinematic component invariant. The latter can be represented in the form

$$\delta\varphi_\alpha(x)=\{\varphi_\alpha(x),G\}, \tag{1}$$

where G is the generator of infinitely small canonical transformations, which is defined, in accordance with the general theory,[12] as

$$G=\int d^3xF_\alpha(x,\varphi)\,\delta\varphi_\alpha(x). \tag{2}$$

This class of variations can be extended by supplementing the Lagrangian with the total time derivative of an arbitrary functional $\gamma(\varphi)$, which leads to a new definition of the functional $F_\alpha(x,\varphi)$:

$$F_\alpha[x,\varphi(x')]\to F'_\alpha[x,\varphi(x')]=F_\alpha(x,\varphi(x'))+\frac{\delta\gamma(\varphi(x'))}{\delta\varphi_\alpha(x)}.$$

An advantage of the approach developed here is that it allows us to obtain PB by considering the most general canonical transformations of dynamic variables, which are determined from the requirement of invariance of the kinematic component of the Lagrangian constructed on the basis of the functional $F'_\alpha[x,\varphi(x')]$. These transformations not necessarily belong to a group with broken symmetry. Moreover, the application of dynamic variables allows us to write the Lagrangian (as well as its kinematic component) in a simpler form than in the case when the Lagrangian is written in terms of physical dynamic variables through which the state of the system under investigation is described. The complete PB algebra obtained on the basis of such a kinematic component permits subsequent separation of subalgebras corresponding to physical variables. It should also be noted that the variational principle used by us leads to PB automatically satisfying the Jacobi identity. Since the structure of kinematic component of the Lagrangian plays the basic role in our analysis, our next step is the obtaining of the functional $L_k=\int d^3x\mathscr{L}_k(x)$ for superfluid ^{3}He–A.

2. KINEMATIC COMPONENT OF LAGRANGIAN AND PB FOR SUPERFLUID ^{3}He–A

Let us first consider for illustration the construction of the kinematic component of the Lagrangian for classical continuous media. If we disregard in this case the processes associated with entropy transfer, the functional $\mathscr{L}_k(x)$ has the form[15]

$$\mathscr{L}_k(x)=\pi_i(x)b_{ij}^{-1}(x)\dot{u}_j(x),\quad b_{ij}(x)=\delta_{ij}-\nabla_j u_i(x), \tag{3}$$

where $\pi_i(x)$ is the momentum density, $u_i(x)$ the displacement vector, and x_i the Euler coordinate of an element of a continuous medium. Using the kinematic component (3), we can obtain PB for the variables $u_i(x)$ and $\pi_i(x)$. Besides, in order to derive the adiabaticity equation, we must know the PB of the entropy density $\sigma(x)$ with the remaining dynamic variables. For this purpose, we write the kinematic component of the Lagrangian (3) in the form

$$\mathscr{L}_k(x)=\underline{\pi}_i(x)b_{ij}^{-1}(x)\dot{u}_j(x)-\sigma(x)\dot{\psi}(x), \tag{4}$$

where

$$\underline{\pi}_i(x)=\pi_i(x)-\sigma(x)\nabla_i\psi(x). \tag{5}$$

The variable $\psi(x)$ which is conjugate to the variable $\sigma(x)$ has been introduced in the kinematic component formally and should be regarded as cyclic in the derivation of the equations of motion. The origin of the second term in formula (4) is evident, while the structure of the quantity $\underline{\pi}_i(x)$ requires clarification. Note that the momentum density $\pi_i(x)$ in (3) is associated with translations in the space of the variables $u_i(x)$ and $\pi_i(x)$. When we introduce the new variables $\sigma(x)$ and $\psi(x)$, the momentum density $\pi_i(x)$ is determined by translations in the space of all the variables $u_i(x)$, $\pi_i(x)$, $\sigma(x)$, and $\psi(x)$ and can be written in the form

$$\pi_i(x)=\underline{\pi}_i(x)+\pi_i^\sigma(x),$$

where $\underline{\pi}_i(x)$ is the momentum density associated with translations in the space of variables $u_i(x)$ and $\pi_i(x)$ only, while $\pi_i^\sigma(x)$ is associated with translations in the space of $\sigma(x)$ and $\psi(x)$. Since the quantities $\psi(x)$ and $\sigma(x)$ are generalized coordinates and momenta, the quantity $\pi_i^\sigma(x)$ is defined as

$$\pi_i^\sigma(x)=\sigma(x)\nabla_i\psi(x).$$

For this reason, the momentum density $\underline{\pi}_i(x)$ associated with translations in the space of the variables $u_i(x)$ and $\pi_i(x)$ has the form (5), which leads to the structure of the functional $\mathscr{L}_k(x)$ in (4).

Using $\mathscr{L}_k(x)$, we can obtain the following PB (the examples of corresponding canonical transformations are given in Ref. 12; here and below, we shall write only nontrivial PB):

$$\begin{aligned}
&\{\pi_i(x),\sigma(x')\}=-\sigma(x)\nabla_i\delta(x-x'),\\
&\{\pi_i(x),\psi(x')\}=\delta(x-x')\nabla_i\psi(x),\\
&\{\sigma(x),\psi(x')\}=\delta(x-x'),\\
&\{u_i(x),\pi_k(x')\}=b_{ik}(x)\delta(x-x'),\\
&\{\pi_i(x),\pi_k(x')\}=\pi_k(x)\nabla'_i\delta(x-x')-\pi_i(x')\nabla_k\delta(x-x').
\end{aligned} \tag{6}$$

The obtained density of the kinematic component (4) of the Lagrangian corresponds to continuous media. We can easily generalize this functional to the case of magnetoelastic media. For this purpose, we write the density of the kinematic component for a magnet characterized by complete spontaneous breaking of symmetry relative to spin rotations (broken $SO(3)$ symmetry):[16]

$$\mathscr{L}_k(x)=-s_\alpha(x)\omega_\alpha(x),\quad \omega_\alpha\equiv\frac{1}{2}\varepsilon_{\alpha\beta\gamma}(\tilde{a}\dot{a})_{\gamma\beta}. \tag{7}$$

Here $s_\alpha(x)$ is the spin density and $a_{\alpha\beta}(x)$ the rotation matrix which is an additional dynamic variable describing the breaking of symmetry to spin rotations (the three angles θ_α parametrizing the rotational matrix $a_{\alpha\beta}$ are conjugate to the three spin components s_α). Using the functional $\mathscr{L}_k(x)$ in (7), we can obtain PB:[16]

$$\begin{aligned}
&\{s_\alpha(x),s_\beta(x')\}=\varepsilon_{\alpha\beta\gamma}s_\gamma(x)\delta(x-x'),\\
&\{a_{\alpha\beta}(x),s_\gamma(x')\}=a_{\alpha\rho}(x)\varepsilon_{\rho\beta\gamma}\delta(x-x').
\end{aligned} \tag{8}$$

It was proved in Ref. 12 that the momentum density associated with translations in the space of variables $s_\alpha(x)$ and $a_{\alpha\beta}(x)$ is defined as

$$\pi_i^s\equiv s_\alpha\omega_{\alpha i},\quad \omega_{\alpha i}\equiv\frac{1}{2}\varepsilon_{\alpha\beta\gamma}(\tilde{\alpha}\nabla_i a)_{\gamma\beta}.$$

Consequently, the density of the kinematic component of the Lagrangian for magnetoelastic media can be written in the form

$$\mathscr{L}_k(x)=\underline{\pi}_i(x)b_{ij}^{-1}(x)\dot{u}_j(x)-\sigma(x)\dot{\psi}(x)-s_\alpha(x)\omega_\alpha(x). \tag{9}$$

where

$$\underline{\pi}_i=\pi_i-\sigma\nabla_i\psi-s_\alpha\omega_{\alpha i}. \tag{10}$$

The last term in formula (9) is the density of the kinematic component of the Lagrangian for magnetic systems. Accordingly, the momentum density π_i is a generator of spatial translations in the space of variables u_i, π_i, σ, ψ, s_α, and $a_{\alpha\beta}$, the momentum density $\pi_i^\sigma=\sigma\nabla_i\psi$ is a generator in the space of variables σ and ψ, and the momentum density $\pi_i^s=s_\alpha\omega_{\alpha i}$ is a generator in the space of variables s_α and $a_{\alpha\beta}$. Consequently, the momentum density associated with translations in the space of variables u_i and π_i has the form (10), which determines the structure of the density of the kinematic component (9) of the Lagrangian. The application of the functional $\mathscr{L}_k(x)$ in the form (9) leads to two more PB in addition to (6) and (8):

$$\{\pi_i(x),s_\alpha(x')\}=-s_\alpha(x)\nabla_i\delta(x-x'),$$
$$\{\pi_i(x),a_{\alpha\beta}(x')\}=\delta(x-x')\nabla_i a_{\alpha\beta}(x). \tag{11}$$

After these preliminary remarks, we are ready to write the kinematic component of the Lagrangian for superfluid ^{3}He–A. It follows from the above analysis that the construction of translation operators and their densities for various physical fields appearing in the Lagrangian plays an important role in determining the structure of the kinematic component. The dynamic variables for superfluid ^{3}He–A are the number density of particles $n(x)$, the densities of the momentum $\pi_i(x)$, spin $s_\alpha(x)$ and entropy $\sigma(x)$, and the vectors of spin $d_\alpha(x)$ and spatial $l_i(x)$ anisotropy as well as the superfluid momentum $p_i(x)$. We also include in dynamic variables the density of intrinsic orbital angular momentum $\underline{l}_i(x)$ associated with the angular momentum of Cooper pairs. We write the density of the kinematic component of the Lagrangian, which will be used for obtaining PB of dynamic variables of the A-phase:

$$\mathscr{L}_k(x)=\underline{\pi}_i(x)b_{ij}^{-1}(x)\dot{u}_j(x)-\sigma(x)\dot{\psi}(x)-s_\alpha(x)\omega_\alpha(x)$$
$$-\xi_i(x)\dot{g}_i(x)-\xi_i^*(x)\dot{g}_i^*(x), \tag{12}$$

where

$$\underline{\pi}_i=\pi_i-\sigma\nabla_i\psi-s_\alpha\omega_{\alpha i}-\xi_k\nabla_i g_k-\xi_k^*\nabla_i g_k^*. \tag{13}$$

Here $\xi_i(x)$ and $g_i(x)$ are certain generalized complex coordinates and momenta through which the physical dynamic variables $n(x)$, $l_i(x)$, $p_i(x)$, and $\underline{l}_i(x)$ will be expressed. Since the part of the functional $\mathscr{L}_k(x)$ containing the variables ξ_i and g_i has the standard form known from classical mechanics, the following formulas are valid:

$$\{\xi_i(x),g_k(x')\}=\{\xi_i^*(x),g_k^*(x')\}=\delta_{ik}\delta(x-x'). \tag{14}$$

The momentum density $\underline{\pi}_i(x)$ in (12) is associated, as before, with translations in the space of the variables $u_i(x)$ and $\pi_i(x)$ and is constructed in analogy with the previous cases.

Henceforth, we shall need the PB $\{\pi_i(x),\xi_h(x')\}$, $\{\pi_i(x),g_k(x')\}$. In order to derive these PB, we consider, along with the variations

$$\delta\pi_i(x)=-\nabla_j[\delta x_j(x)\pi_i(x)]-\pi_j(x)\nabla_i\delta x_j(x),$$
$$\delta u_i(x)=b_{ij}(x)\delta x_j(x),\quad \delta\psi(x)=-\delta x_i(x)\nabla_i\psi(x),$$
$$\delta\sigma(x)=-\nabla_i[\delta x_i(x)\sigma(x)],$$
$$\delta s_\alpha(x)=-\nabla_i[s_\alpha(x)\delta x_i(x)],$$
$$\delta a_{\alpha\beta}(x)=-\delta x_i(x)\nabla_i a_{\alpha\beta}(x) \tag{15}$$

also the variation

$$\delta\xi_i(x)=-\nabla_k(\xi_i(x)\delta x_k(x)),$$
$$\delta g_i(x)=-\delta x_k(x)\nabla_k g_i(x), \tag{16}$$

which leave the kinematic component of the Lagrangian invariant. On the other hand, variations (16) can be represented, in accordance with (1) and (2), in the form

$$\delta\xi_i(x)=\{\xi_i(x),G\},\quad \delta g_i(x)=\{g_i(x),G\},$$

where G is the generator of transformations (15) and (16), which is defined as

$$G=\int d^3x\Big(\underline{\pi}_i(x)b_{ij}^{-1}(x)\delta u_j(x)-\sigma(x)\delta\psi(x)$$
$$-\frac{1}{2}\varepsilon_{\alpha\beta\gamma}s_\alpha(x)a_{\mu\gamma}(x)\delta a_{\mu\beta}(x)-\xi_i(x)\delta g_i(x)$$
$$-\xi_i^*(x)\delta g_i^*(x)\Big)=\int d^3x\,\pi_i(x)\delta x_i(x).$$

This leads to the PB

$$\{\pi_i(x),\xi_k(x')\}=-\xi_k(x)\nabla_i\delta(x-x').$$
$$\{\pi_i(x),g_k(x')\}=\nabla_i g_k(x)\delta(x-x') \tag{17}$$

(similar expressions can be obtained for complex conjugate quantities ξ_k^* and g_k^*).

Let us first consider the spin dynamics of the A-phase, which is described by the spin density $s_\alpha(x)$ with the unit spin anisotropy vector $d_\alpha(x)$. We define the vector d_α through the formula

$$d_\alpha=\underline{d}_\beta a_{\beta\alpha}, \tag{18}$$

where $\underline{d}_\beta$ is an arbitrary constant unit vector and $a_{\alpha\beta}$ the rotational matrix introduced by us in the analysis of a magnet with broken $SO(3)$ symmetry. Carrying out the convolution of the vector $\underline{d}_\alpha$ with the rotational matrix $a_{\alpha\beta}$ in formulas (8) and (11), we obtain the algebra of PB for the variables $s_\alpha(x)$ and $d_\alpha(x)$:

$$\{s_\alpha(x),s_\beta(x')\}=\varepsilon_{\alpha\beta\gamma}s_\gamma(x)\delta(x-x'),$$
$$\{s_\alpha(x),d_\beta(x')\}=\varepsilon_{\alpha\beta\gamma}d_\gamma(x)\delta(x-x'), \tag{19}$$

as well as PB with the momentum density $\pi_i(x)$:

$$\{\pi_i(x),s_\alpha(x')\}=-s_\alpha(x)\nabla_i\delta(x-x'),$$
$$\{\pi_i(x),d_\alpha(x')\}=\delta(x-x')\nabla_i d_\alpha(x). \tag{20}$$

The Poisson brackets (19) and (20) form the basis of the derivation of equations in spin dynamics of the superfluid A-phase. Equations of motion in the Hamiltonian approach have the form

$$\dot{\varphi}_\alpha(x)=\{\varphi_\alpha(x),H\}$$

[$\varphi_\alpha(x)$ are dynamic variables]. This gives

$$\dot{s}_\alpha+\nabla_k(v_k^n s_\alpha)=\varepsilon_{\alpha\beta\gamma}\left(\frac{\delta H}{\delta s_\beta}\,s_\gamma+\frac{\delta H}{\delta d_\beta}\,d_\gamma\right),$$

$$\dot{d}_\alpha+(v_k^n\nabla_k)d_\alpha=\varepsilon_{\alpha\beta\gamma}\frac{\delta H}{\delta s_\beta}\,d_\gamma,\quad v_k^n\equiv\frac{\delta H}{\delta\pi_k}. \tag{21}$$

These equations are a generalization of the Leggett equations[17] taking into account the motion of the normal component.

Let us go over to an analysis of orbital dynamics. It is characterized by the variables $\sigma(x)$, $n(x)$, $\pi_i(x)$, $l_i(x)$, $p_i(x)$, and $\underline{l}_i(x)$. We introduce physical dynamic variables $n(x)$, $l_i(x)$, $p_i(x)$, and $\underline{l}_i(x)$ connecting them with the generalized coordinates and momenta $g_i(x)$ and $\xi_i(x)$. Let us consider infinitely small phase transformations with the phase $2\delta\varphi(x)$:

$$\delta\xi_i(x)=2i\delta\varphi(x)\xi_i(x),\quad \delta g_i(x)=-2i\delta\varphi(x)g_i(x),$$

$$\delta\xi_i^*(x)=-2i\delta\varphi(x)\xi_i^*(x),\quad \delta g_i^*(x)=2i\delta\varphi(x)g_i^*(x). \tag{22}$$

The density of the kinematic component (12) remains invariant if we also consider the transformations of the momentum density along with transformations (22):

$$\delta\pi_k(x)=-2i(\xi_i(x)g_i(x)-\xi_i^*(x)g_i^*(x))\nabla_k\delta\varphi(x). \tag{23}$$

According to (2), the generator of transformations (22) and (23) is given by

$$G=\int d^3x n(x)\,\delta\varphi(x),$$

$$n(x)\equiv 2i[\xi_i(x)g_i(x)-\xi_i^*(x)g_i^*(x)]. \tag{24}$$

The quantity $n(x)$ defining the generator of local phase transformations has the meaning of the number density of particles. Then it follows from (23) that

$$\delta\pi_k(x)=-n(x)\nabla_k\delta\varphi(x).$$

On the other hand, presenting the variation $\delta\pi_k(x)$ in the form

$$\delta\pi_k(x)=\{\pi_k(x),G\},\quad G=\int d^3x n(x)\,\delta\varphi(x),$$

and considering that the function $\delta\varphi(x)$ is arbitrary, we obtain the PB

$$\{\pi_k(x),n(x')\}=-n(x)\nabla_k\delta(x-x'). \tag{25}$$

Let us now consider infinitely small rotations of the vectors ξ_i and g_i:

$$\delta\xi_i(x)=\varepsilon_{ijk}\delta\varphi_j(x)\xi_k(x),\quad \delta g_i(x)=\varepsilon_{ijk}\delta\varphi_j(x)g_k(x). \tag{26}$$

($\delta\varphi_j$ are rotational angles) and similar expressions for complex conjugate quantities ξ_i^* and g_i^*. Along with transformations (26), we also consider transformations of the momentum density

$$\delta\pi_l(x)=\varepsilon_{ijk}[\xi_i(x)g_k(x)+\xi_i^*(x)g_k^*(x)]\nabla_l\delta\varphi_j(x), \tag{27}$$

which leave the kinematic component (12) invariant. According to (2), the generator of transformations (26) and (27) has the form

$$G=\int d^3x\underline{l}_i(x)\,\delta\varphi_i(x),$$

$$\underline{l}_i(x)\equiv\varepsilon_{ijk}[\xi_j(x)g_k(x)+\xi_j^*(x)g_k^*(x)]. \tag{28}$$

The quantity $\underline{l}_i(x)$ defines the generator of local rotations (26) and will be interpreted by us as the intrinsic orbital angular momentum of Cooper pairs in the A-phase (see below). Taking (28) into consideration, we obtain the following expression for variations $\delta\pi_i(x)$:

$$\delta\pi_i(x)=-\underline{l}_j(x)\nabla_i\delta\varphi_j(x).$$

On the other hand, we have

$$\delta\pi_i(x)=\{\pi_i(x),G\},\quad G=\int d^3x\underline{l}_i(x)\,\delta\varphi_i(x).$$

This gives the PB

$$\{\pi_i(x),\underline{l}_j(x')\}=\underline{l}_j(x)\nabla_i'\delta(x-x'). \tag{29}$$

Let us now define the spatial anisotropy vector l_i and the superfluid momentum p_i through the formulas

$$l_i=i\varepsilon_{ijk}g_jg_k^*,\quad p_i=\frac{i}{4g_lg_l^*}(g_k\nabla_ig_k^*-g_k^*\nabla_ig_k). \tag{30}$$

Under the local phase transformations (22), the vector l_k does not change, and the superfluid momentum is transformed according to the law

$$p_i\to p_i'=p_i+\nabla_i\varphi.$$

Suppose that we are treating the quantities $g_ig_i^*$, g_i^2, and g_i^{*2} as dynamic variables. Considering that

$$H=\int d^3x\varepsilon(x),$$

$$\varepsilon(x)=\varepsilon[x;\sigma(x'),n(x'),\pi_i(x'),l_i(x'),p_i(x'),\underline{l}_i(x')] \tag{31}$$

(we write here the energy density as a function of only those variables that describe orbital dynamics) as well as representations (24), (28), (30) and the PB (14) and (16), we obtain the following equations of motion for these variables:

$$\left(\frac{\partial}{\partial t}+v_i^n\nabla_i\right)g_kg_k^*=0,$$

$$\left(\frac{\partial}{\partial t}+v_i^n\nabla_i+4i\mu\right)g_k^2=0,$$

$$\left(\frac{\partial}{\partial t}+v_i^n\nabla_i-4i\mu\right)g_k^{*2}=0;\quad \mu\equiv\frac{\delta H}{\delta n}, \tag{32}$$

which have trivial solutions

$$g_k^2=g_k^{*2}=0 \tag{33}$$

and $g_k g_k^* = C$ (C is a constant independent of coordinates and time). Henceforth, we assume that $C=1$ everywhere, i.e.,

$$g_k g_k^* = 1. \tag{34}$$

Thus, the vector g_k is a normalized complex vector whose square is equal to zero, which permits the following representation:

$$g = \frac{1}{\sqrt{2}} (\Delta_1 + i\Delta_2); \quad \Delta_1^2 = \Delta_2^2 = 1, \quad \Delta_1 \Delta_2 = 0. \tag{35}$$

Taking relations (33) and (34) into account, we find that the spatial anisotropy vector l_i is a unit vector ($l_i^2 = 1$), while the superfluid momentum p_i is finally determined by the expression

$$p_i = \frac{i}{4} (g_k \nabla_i g_k^* - g_k^* \nabla_i g_k). \tag{36}$$

The vectors Δ_1, Δ_2, and $\mathbf{1} = [\Delta_1 \Delta_2]$ form local quantization axes in the microscopic theory. It follows from definitions (30), (36), and the representation (35) that the vectors p_i and l_i are connected through the Mermin–Ho identity

$$\nabla_i p_k - \nabla_k p_i = \frac{1}{2} 1 \cdot (\nabla_i 1 \times 1)[\nabla_i 1, \nabla_k 1]. \tag{37}$$

It can easily be seen that the superfluid momentum p_i does not change upon simultaneous fulfillment of the phase transformation (22) and rotation around the direction $\mathbf{l}$ through the angle $2\delta\varphi$, for which $\delta\varphi_j = 2 l_j \delta\varphi$ (combined phase–rotation invariance).

Formulas (24), (28), (30), and (36) solve the above problem on the relation between the dynamic variables $n(x)$, $\underline{l}_i(x)$, $l_i(x)$, $p_i(x)$ and the generalized coordinates and momenta $g_i(x)$ and $\xi_i(x)$. Using the above representations and PB (14) and (16), we can easily find the following algebra of PB for variables describing orbital dynamics of superfluid ^{3}He–A:

$$\begin{aligned}
&\{\pi_i(x), \pi_k(x')\} = \pi_k(x) \nabla_i' \delta(x-x') \\
&\qquad - \pi_i(x') \nabla_k \delta(x-x'), \\
&\{\pi_i(x), n(x')\} = -n(x) \nabla_i \delta(x-x'), \\
&\{\pi_i(x), \sigma(x')\} = -\sigma(x) \nabla_i \delta(x-x'), \\
&\{\pi_i(x), l_j(x')\} = \delta(x-x') \nabla_i l_j(x), \\
&\{\pi_i(x), \underline{l}_j(x')\} = -\underline{l}_j(x) \nabla_i \delta(x-x'), \\
&\{\pi_i(x), p_j(x')\} = (\nabla_i p_j - \nabla_j p_i) \delta(x-x') \\
&\qquad - p_i(x) \nabla_j \delta(x-x'), \\
&\{n(x), p_i(x')\} = \nabla_i' \delta(x-x'), \\
&\{\underline{l}_i(x), p_j(x')\} = \frac{1}{2} l_i(x') \nabla_j' \delta(x-x'), \\
&\{\underline{l}_i(x), \underline{l}_j(x')\} = \varepsilon_{ijk} \underline{l}_k \delta(x-x'), \\
&\{\underline{l}_i(x), l_j(x')\} = \varepsilon_{ijk} l_k \delta(x-x').
\end{aligned} \tag{38}$$

Having obtained this algebra, we consider the interpretation of the quantity $\underline{L}_i = \int d^3x \underline{l}_i(x)$ as intrinsic orbital angular momentum. For this purpose, we also introduce the orbital angular momentum $L_i^0 = \int d^3x \varepsilon_{ikl} x_k \pi_l$ constructed with the help of momentum density $\pi_l(x)$. In accordance with (6), the quantities L_i^0, $P_i \equiv \int d^3x \pi_i(x)$ satisfy the well-known PB

$$\{P_i, L_j^0\} = \varepsilon_{ijl} P_l, \quad \{L_i^0, L_j^0\} = \varepsilon_{ijk} L_k^0.$$

It follows from (38) that the quantities $\underline{L}_i$ and P_i satisfy the relations

$$\{P_i, \underline{L}_j\} = 0, \quad \{\underline{L}_i, \underline{L}_j\} = \varepsilon_{ijk} \underline{L}_k.$$

Noting that $\{L_i^0, \underline{L}_j\} = 0$, we obtain the following relations for the total angular momentum $L_i = L_i^0 + \underline{L}_i$:

$$\{P_i, L_j\} = \varepsilon_{ijk} P_k, \quad \{L_i, L_j\} = \varepsilon_{ijk} L_k.$$

In addition, it follows from relations (38) that under transformations with the generator L_i^0, the quantities $n(x)$ and $l_i(x)$ are transformed as scalars:

$$\{n(x), L_j^0\} = -\varepsilon_{jkl} x_k \nabla_l n(x),$$

$$\{l_i(x), L_j^0\} = -\varepsilon_{jkl} x_k \nabla_l l_i(x),$$

while the quantities $\pi_i(x)$ and $p_i(x)$ are transformed as vectors:

$$\{\pi_i(x), L_j^0\} = \varepsilon_{ijl} \pi_l(x) - \varepsilon_{jkl} x_k \nabla_l \pi_i(x),$$

$$\{p_i(x), L_j^0\} = \varepsilon_{ijl} p_l(x) - \varepsilon_{jkl} x_k \nabla_l p_i(x).$$

On the other hand, under transformations with the generator $\underline{L}_j$, the quantities $n(x)$, $\pi_i(x)$, and $p_i(x)$ are not transformed:

$$\{n(x), \underline{L}_j\} = \{\pi_i(x), \underline{L}_j\} = \{p_i(x), \underline{L}_j\} = 0,$$

while the spatial anisotropy vector $l_i(x)$, which is similar to the director vector in liquid crystals, is transformed according to the law

$$\{l_i(x), \underline{L}_j\} = \varepsilon_{ijk} l_k(x).$$

Thus, the intrinsic orbital angular momentum $\underline{L}_i = \int d^3x \underline{l}_i(x)$ is introduced by us as a generator of spatial rotations of variables of the liquid-crystal type and possesses properties similar to the spin angular momentum S_α. It follows from PB with the quantities L_i^0 and $\underline{L}_i$ that, under transformations with the total orbital angular momentum L_i, the number density of particles $n(x)$ is transformed as a scalar: $\{n(x), L_j\} = -\varepsilon_{jkl} x_k \nabla_l n(x)$, while the quantities $\pi_i(x)$, $p_i(x)$, and $l_i(x)$ are transformed as vectors:

$$\{w_i(x), L_j\} = \varepsilon_{ijl} w_l(x) - \varepsilon_{jkl} x_k \nabla_l w_i(x),$$

$$w_i(x) = \{\pi_i(x), p_i(x), l_i(x)\}.$$

The condition of rotational invariance of the energy density of the system is formulated with the help of the total orbital angular momentum L_i and has the form

$$\{L_i, \varepsilon(x)\} = \varepsilon_{ikl} x_k \nabla_l \varepsilon(x). \tag{39}$$

3. EQUATIONS OF ORBITAL DYNAMICS

Before we write equations of orbital dynamics, the following circumstance is worth noting. Since Cooper pairs possess an orbital angular momentum and an intrinsic orbital angular momentum of density $\underline{l}_i$, the quantity $\underline{l}_i$ makes a contribution to the total momentum density j_i

$$j_i = \pi_i + \frac{1}{2}\,\mathrm{curl}_i \underline{1} \tag{40}$$

(upon such a redefinition, the total momentum remains unchanged, $\int d^3x j_i(x) = \int d^3x \pi_i(x)$). Accordingly, the energy density (31) is a function of variables π_i and $\underline{l}_i$ only through the momentum density j_i:

$$\begin{aligned}\varepsilon[x;\sigma(x'),n(x'),\pi_i(x'),l_i(x'),p_i(x'),\underline{l}_i(x')] \\ = \varepsilon[x;\sigma(x'),n(x'),j_i(x'),p_i(x')].\end{aligned} \tag{41}$$

It follows immediately from this equation that

$$\omega = \frac{1}{2}\,\mathrm{curl}\ \mathbf{v}^n; \quad \omega \equiv \frac{\delta H}{\delta \underline{1}}, \quad \mathrm{v}^n \equiv \frac{\Delta H}{\delta \pi} = \frac{\Delta H}{\delta \mathrm{j}}, \tag{42}$$

i.e., local rotation of the normal component is of the rigid-body type. The orbital angular momentum L_i constructed from the quantity $L_i \equiv \int d^3x \varepsilon_{ikl} x_k j_l$, is the sum of the orbital angular momentum $L_i^0 \equiv \int d^3x \varepsilon_{ikl} x_k \pi_l$ and the intrinsic angular momentum $\underline{L}_i = \int d^3x \underline{l}_i(x)$ and coincides with the total orbital angular momentum $L_i = L_i^0 + \underline{L}_i$. Thus, we include just for the momentum density j_i in the system of hydrodynamic equations the equation of motion.

The system of PB (38) forms the basis for deriving hydrodynamic equations for superfluid ^{3}He–A. In the local limit, when the energy density $\varepsilon(x)$ has the form

$$\begin{aligned}\varepsilon(x) = \varepsilon[\sigma(x), n(x), j_i(x), s_a(x), l_i(x), \\ \nabla_k l_i(x), p_i(x), d_\alpha(x)],\end{aligned}$$

taking into account the Mermin–Ho identity (37), we obtain the following hydrodynamic equations for the A-phase:

$$\dot{n} + \nabla_i\left(v_i^n n + \frac{\partial \varepsilon}{\partial p_i}\right) = 0, \quad \dot{\sigma} + \nabla_i(v_i^n \sigma) = 0,$$

$$\dot{p}_i + \nabla_i\left(v_k^n p_k + \mu + \frac{1}{4}\, l_k\, \mathrm{curl}_k \mathbf{v}^n\right) + \frac{1}{2}\, 1 \cdot (\nabla_i 1 \times \dot{1}] = 0, \tag{43}$$

$$\dot{l}_i + (v_k^n \nabla_k) l_i + \frac{1}{2}\,[1\ \mathrm{curl}\ \mathbf{v}^n]_i = 0, \quad \dot{j}_i = -\nabla_k t_{ik},$$

$$\dot{\underline{l}}_i + \nabla_k(v_k^n \underline{l}_i) + \frac{1}{2}\,[\underline{1}\ \mathrm{curl}\ \mathbf{v}^n]_i + [1 \cdot \mathbf{h}]_i + \frac{1}{2}\,\nabla_k\left(l_i \frac{\partial \varepsilon}{\partial p_k}\right) = 0.$$

Here t_{ik} is the tensile stress tensor

$$t_{ik} = t_{ik}^s + t_{ik}^a, \tag{44}$$

$$\begin{aligned}t_{ik}^s = p\,\delta_{ik} + \frac{1}{2}\left(j_i v_k^n + p_i \frac{\partial \varepsilon}{\partial p_k} + \nabla_i l_r \frac{\partial \varepsilon}{\partial \nabla_k l_r} + (i \leftrightarrow k)\right) \\ + \frac{1}{2}\,\underline{l}_s\left(\varepsilon_{irs}\nabla_r v_k^n + \varepsilon_{krs}\nabla_r v_i^n\right) - \frac{1}{4}\left(\underline{l}_i\ \mathrm{curl}_k \mathbf{v}^n\right. \\ \left. + \underline{l}_k\ \mathrm{curl}_i \mathbf{v}^n\right),\end{aligned}$$

$$t_{ik}^a = \frac{1}{2}\,\varepsilon_{ikm}\nabla_j\left(\frac{1}{2}\, l_m \frac{\partial \varepsilon}{\partial p_j} + \tau_{mj}\right), \quad \tau_{mj} = \varepsilon_{ikm} l_k \frac{\partial \varepsilon}{\partial \nabla_j l_i};$$

and p is the pressure,

$$p = -\varepsilon + T\sigma + \mu n + j_k v_k^n + s_\alpha \frac{\partial \varepsilon}{\partial s_\alpha} + \frac{1}{2}\,\underline{l}_k\,\mathrm{curl}_k \mathbf{v}^n;$$

$$T \equiv \frac{\partial \varepsilon}{\partial \sigma}, \quad h_i \equiv \frac{\partial \varepsilon}{\partial l_i} - \nabla_k \frac{\partial \varepsilon}{\partial \nabla_k l_i}.$$

We denote the symmetric and antisymmetric components of stress tensor in (44) by t_{ik}^s and t_{ik}^a, respectively. While separating the symmetric component of tensor t_{ik}, we have used of the rotational invariance condition (39), which can be written, after the evaluation of PB, in the form

$$\varepsilon_{ikl}\left(\frac{\partial \varepsilon}{\partial l_k}\, l_l + \frac{\partial \varepsilon}{\partial \nabla_k l_r}\,\nabla_l l_r + \frac{\partial \varepsilon}{\partial \nabla_r l_k}\,\nabla_r l_l + \frac{\partial \varepsilon}{\partial p_k}\, p_l + v_k^n j_l\right) = 0.$$

Although the stress tensor has the antisymmetric component (that has the form of spatial derivative), the following differential conservation law is valid for the density $[\mathbf{r}\cdot\mathbf{j}]$ of the total orbital angular momentum:

$$\frac{\partial}{\partial t}\,(\varepsilon_{ikl} x_k j_l) = -\nabla_s\left(\varepsilon_{ikl} x_k t_{ls} + \frac{1}{2}\, l_i \frac{\partial \varepsilon}{\partial p_s} + \tau_{is}\right).$$

It can be easily seen that equations (43) are compatible with the Mermin–Ho identity:

$$\frac{\partial}{\partial t}\left(\nabla_i p_k - \nabla_k p_i - \frac{1}{2}\,\mathbf{1}\cdot[\nabla_i 1 \times \nabla_k 1]\right) = 0.$$

The dynamic equations (43) obtained by using the Hamiltonian approach are generalizations of corresponding equations from Ref. 1 to the case of Galilean-noninvariant systems[1)] and also include the equation for intrinsic orbital angular momentum. The last equation in (43) is not written as a rule while formulating equations of orbital dynamics since intrinsic orbital angular momentum is small in view of strong overlapping of Cooper pairs $l_i \sim \rho(\Delta_0/\varepsilon_F)^2$, in the weak-coupling approximation and at $T=0$; see Ref. 13). It follows from Eq. (43) that the inclusion of the motion of the normal component cannot be reduced only to the emergence of convective terms; the terms proportional to curl $\mathbf{v}^n$ and associated with vortex motion of the normal component also appear. This can lead, for example, to the drag effect, i.e., the generation of translational motion of the superfluid component by rotational motion of the normal component with $\nabla(l_k \mathrm{curl}_k \mathbf{v}^n) \neq 0$ (see the equation for the superfluid momentum p_i).[18]

If a system possesses Galilean invariance, the energy density $\varepsilon(\mathbf{x})$ under Galilean transformations with the parameter $\mathbf{v}$ obeys the law

$$\varepsilon'(\mathbf{x})=\varepsilon(\mathbf{x}-\mathbf{v}t)+j_i(\mathbf{x}-\mathbf{v}t)v_i+\frac{1}{2}\rho(\mathbf{x}-\mathbf{v}t)v^2,$$

$$\rho(\mathbf{x})\equiv mn(\mathbf{x}) \tag{45}$$

(m is the mass of a ^{3}He atom). The application of the energy functional satisfying the property (45) leads to a system of hydrodynamic equations, which also possesses Galilean invariance. In order to verify this, let us first prove the Galilean invariance of the system Lagrangian that corresponds to the kinematic component (12). Then the variational principle will also lead to Galilean invariance of Eqs. (43). In accordance with (12), the density of the system Lagrangian has the form

$$\mathscr{L}(\mathbf{x})=\underline{\pi}_i(\mathbf{x})b_{ij}^{-1}(\mathbf{x})\dot{u}_j(\mathbf{x})-\sigma(\mathbf{x})\dot{\psi}(\mathbf{x})-s_\alpha(\mathbf{x})\omega_\alpha(\mathbf{x})$$
$$-\xi_i(\mathbf{x})\dot{g}_i(\mathbf{x})-\xi_i^*(\mathbf{x})g_i^*(\mathbf{x})-\varepsilon(\mathbf{x}). \tag{46}$$

The transformation properties of the variables appearing in (46) to Galilean transformations are determined by the formulas

$$\pi_i'(\mathbf{x})=\pi_i(\mathbf{x}-\mathbf{v}t)+\rho(\mathbf{x}-\mathbf{v}t)v_i,$$

$$u_i'=u_i(\mathbf{x}-\mathbf{v}t)+v_it,\quad \sigma'(\mathbf{x})=\sigma(\mathbf{x}-\mathbf{v}t),$$

$$\psi'(\mathbf{x})=\psi(\mathbf{x}-\mathbf{v}t),\quad s_\alpha'(\mathbf{x})=s_\alpha(\mathbf{x}-\mathbf{v}t),$$

$$a_{\alpha\beta}'(\mathbf{x})=a_{\alpha\beta}(\mathbf{x}-\mathbf{v}t),$$

$$\xi_i'(\mathbf{x})=\xi_i(\mathbf{x}-\mathbf{v}t)\exp\left\{2i\left(\frac{m\mathbf{v}^2}{2}t-m\mathbf{v}\mathbf{x}\right)\right\},$$

$$g_i'(\mathbf{x})=g_i(\mathbf{x}-\mathbf{v}t)\exp\left\{-2i\left(\frac{m\mathbf{v}^2}{2}t-m\mathbf{v}\mathbf{x}\right)\right\}. \tag{47}$$

These expressions lead to the laws of transformations of the quantities $\rho(\mathbf{x})$, $p_i(\mathbf{x})$, $l_i(\mathbf{x})$, and $\underline{l}_i(\mathbf{x})$:

$$\rho'(\mathbf{x})=\rho(\mathbf{x}-\mathbf{v}t),\quad p_i'(\mathbf{x}-\mathbf{v}t)+mv_i,$$

$$l_i'(\mathbf{x})=l_i(\mathbf{x}-\mathbf{v}t),\quad \underline{l}_i'(\mathbf{x})=\underline{l}_i(\mathbf{x}-\mathbf{v}t). \tag{48}$$

Using (47) and (48), we can easily verify that

$$\mathscr{L}'(\mathbf{x})=\mathscr{L}(\mathbf{x}-\mathbf{v}t)-\frac{1}{2}v_i\,\mathrm{curl}_i\underline{l}(\mathbf{x}-\mathbf{v}t). \tag{49}$$

By virtue of (49), the Lagrangian is invariant to Galilean transformations:

$$\int d^3x\mathscr{L}(\mathbf{x})=\int d^3x\mathscr{L}'(\mathbf{x}),$$

and hence Eqs. (43) corresponding to the energy density (45) are also invariant to Galilean transformations. It should be noted that the Mermin–Ho identity also preserves its form under transformations (48).

In conclusion, it is appropriate to make the following remark concerning the dynamics of cyclic variables u_i and ψ appearing in the density of the kinematic component of Lagrangian (12). According to (6), the Hamilton equations of motion for these variables have the form

$$\dot{u}_i=b_{ij}v_j^n,\quad \dot{\psi}+(v_i^n\nabla_i)\psi=-T$$

and can be integrated after finding solutions of Eqs. (43). We can give a simple physical interpretation of the variable $u_i(x,t)$, which is in accord with the meaning of this variable in the density of kinematic component of Lagrangian (4). For this purpose, we define the function $x_i=x_i(\xi,t)$ implicitly by using the equality

$$x_i(\xi,t)=\xi_i+u_i[x(\xi,t),t],\quad \xi_i=\text{const}. \tag{50}$$

Differentiation of both sides of formula (50) with respect to time leads to the relation $\dot{u}_i=b_{ij}x_j$. Consequently, we obtain $\dot{x}_j(\xi,t)=v_j^n$.

Thus, we conclude that the function $x_i(\xi,t)$ which is defined by relation (50) and the quantity u_i are the Euler coordinate and the vector of displacement for the normal component respectively (the quantity ξ_i has the meaning of the Lagrangean coordinate of the same element).

The authors are grateful to M. Yu. Kovalevskii for fruitful discussions of the results.

This research was supported financially by the Ukrainian Foundation of Fundamental Studies, Grant No. 2.4/378.

*E-mail: isayev@kipt.kharkov.ua; spelet@kipt.kharkov.ua

[1)]We disregard the terms containing arbitrary phenomenological constants α, β, γ, which were introduced in Ref. 1 from general symmetry considerations and which cannot be obtained by using purely Hamiltonian formalism.

[1] G. E. Volovik, Usp. Fiz. Nauk **143**, 73 (1984) *Exotic Properties of Superfluid* ^{3}He, World Scientific, Singapore, New Jersey, London, Hong Kong (1992).
[2] D. Vollhardt and P. Wölfle, in *The Superfluid Phases of Helium 3*, (ed. by F. Taylor), Francis, London, New York, Philadelphia (1990).
[3] R. Combescot, Phys. Lett. A **A78**, 85 (1980).
[4] N. D. Mermin and P. Muzikar, Phys. Rev. B **B21**, 980 (1980).
[5] K. Nagai, J. Low Temp. Phys. **38**, 677 (1980).
[6] M. Ishikawa, K. Miyake, and T. Usui, Prog. Theor. Phys. **63**, 1083 (1980).
[7] C. R. Hu and W. M. Saslow, Phys. Rev. Lett. **38**, 605 (1977).
[8] T.-L. Ho, in *Quantum Fluids and Solids* (ed. by S. B. Trickey, E. D. Adams, and J. M. Dufty), Plenum Press, New York, London (1977).
[9] M. Ashida, Prog. Theor. Phys. **65**, 409 (1981).
[10] I. M. Khalatnikov and V. V. Lebedev, Phys. Lett. **A61**, 319 (1977); V. V. Lebedev and I. M. Khalatnikov, Zh. Éksp. Teor. Fiz. **73**, 1537 (1977) [Sov. Phys. JETP **46**, 808 (1977)].
[11] I. E. Dzyaloshinskii and G. I. Volovik, Ann. Phys. **125**, 67 (1980).
[12] A. A. Isayev, M. Yu. Kovalevskii, and S. V. Peletminsky, Fiz. Elem. Chastits. At. Yadra **27**, 431 (1996) [Phys. Part. Nuclei **27**, 203 (1996)].
[13] G. E. Volovik and V. P. Mineev, Zh. Éksp. Teor. Fiz. **81**, 989 (1981) [Sov. Phys. JETP **54**, 524 (1981)].
[14] G. E. Volovik and A. V. Balatskii, J. Low Temp. Phys. **58**, 1 (1985).
[15] A. A. Isayev, M. Yu. Kovalevskii, and S. V. Peletminsky, Teor. Mekh. Fiz. **102**, 283 (1995).
[16] M. Yu. Kovalevskii, S. V. Peletminsky, and A. L. Shishkin, Ukr. Fiz. Zh. **36**, 245 (1991).
[17] A. J. Leggett, Ann. Phys. **85**, 11 (1974).
[18] M. Liu and M. C. Cross, Phys. Rev. Lett. **43**, 296 (1979)

Translated by R. S. Wadhwa

Pinning and dynamics of magnetic flux in YBaCuO single crystals for vortex motion along twin boundaries

A. V. Bondarenko. V. A. Shklovskij, R. V. Vovk, M. A. Obolenskii, and A. A. Prodan

*Kharkov State University, 310077 Kharkov, Ukraine**
(Submitted June 19, 1997)
Fiz. Nizk. Temp. **23**, 1281–1288 (December 1997)

Current-voltage characteristics of YBaCuO single crystals are studied for a Lorentz force aligned along the twin planes. The temperature dependences of the depinning critical currents are determined in magnetic fields that are parallel or tilted with respect to the twin planes for magnetic field vectors oriented almost along axis **c**. A nearly 50% decrease in the critical current in parallel magnetic fields is attributed to the plastic flow of vortices along channels formed by twin boundaries. It is shown that the resistance to the viscous flux flow is described quite correctly by the Bardeen–Stephen model. The peculiarities in the current and temperature dependences of the differential resistivity at temperatures higher than the melting point but lower than the temperature of onset of vortex pinning by twin boundaries are attributed to the coexistence of solid and liquid vortex phases in this temperature region. A large number of peaks observed in the current dependences of the differential resistivity in a parallel field at temperatures below the melting point of the vortex lattice is associated with nonuniform indirect vortex pinning caused by the fluctuations of the separation between twins. © *1997 American Institute of Physics.* [S1063-777X(97)00312-5]

A large number of magnetic[1–5] and resistive[6–9] studies in YBaCuO single crystals have shown that twin boundaries (TB) affect significantly the magnetic flux pinning and dynamics. This influence is associated, on one hand, with the difference in the energies of vortices localized at the TB and those in the bulk of the superconductor and, on the other hand, with an increased pinning of vortices localized at the TB as compared to the vortices lying outside the TB planes as vortices move along twins. In particular, experiments on the decoration of the vortex structure for a magnetic field orientation along the axis **c** have shown that the energy of vortices localized at the TB is about 2% lower than elsewhere in the bulk of the superconductor.[1] This difference in the energy results in a bending of vortex filaments in magnetic fields tilted relative to the TB[10,11] if the disorientation angle θ between the magnetic field vector **H** and the TB plane does not exceed a certain critical value θ^*: for $|\theta| < \theta^*$, a part of the vortex filament is trapped by the TB plane.

The quantity θ^* depends strongly on the orientation of the vector **H** relative to the crystallographic axes. This dependence is determined by the superconductor anisotropy which is estimated for YBaCuO as $\varepsilon \equiv (m/M)^{1/2} = 6$, where m and M are the longitudinal and transverse electron masses relative to the ab planes. Experimental studies have revealed that $\theta^* \simeq 3-7°$ for $\mathbf{H} \perp \mathbf{c}$,[5,6,8] while θ^* may attain values between 15 and 35° for $\mathbf{H} \| \mathbf{c}$.[5–7]

An increase in the pinning of vortices at the TB leads to a specific angular dependence of the critical current J_c: for $|\theta| < \theta^*$, the critical current decreases monotonically with increasing angle θ as the fraction of vortex filaments trapped by TB decreases for $\mathbf{H} \perp \mathbf{c}$.[5,8,12,13] An analogous temperature dependence is also observed for orientation of vector **H** in the vicinity of the axis **c** if the vortex motion is transverse to the TB planes, i.e., if the current vector **J** is parallel to the ab-plane and the TB plane.[9] An entirely different angular dependence of the critical current is observed for orientation of vector **H** in the vicinity of the **c** if vector **J** is oriented at an angle of 45° to the TB plane. For such a geometry of the experiment, the minimum of the critical current observed for $\mathbf{H} \| \mathbf{c}$ is transformed into a peak with increasing electric field, which is used to determine the value of J_c.[7] Experiments on visualization of magnetic flux propagation for $\mathbf{H} \| \mathbf{c}$,[4] in which the induced current vector is also parallel to the ab-plane of the crystal and oriented at an angle of 45° to the TB plane, show that the magnetic field penetrates the crystal along the TB planes. Such a behavior is probably associated with a considerably anisotropy of pinning at the TB: the critical current for transverse motion of vortices (relative to the TB plane) is about 10 times higher than the critical current for longitudinal motion.[14] Such a strong anisotropy of pinning must result in a directed motion of the magnetic flux along the TB planes for $\mathbf{H} \| \mathbf{c}$ and $\angle \mathbf{J}$, TB $= 45°$. Hence the peculiarities of the dependence $J_c(\theta)$ for orientation of vector **H** in the vicinity of the axis **c**, are probably associated with peculiarities of the magnetic flux dynamics for vortex motion along the TB planes.

The present work aims at experimental study of pinning and dynamics of magnetic flux in YBaCuO single crystals for magnetic flux movement along TB planes. We shall present the results of measurements of temperature dependences of the electrical resistance and current–voltage characteristics of bridge 1 in a magnetic field H parallel to TB, as well as in a magnetic field oriented at an angle $\theta = 9°$ rela-

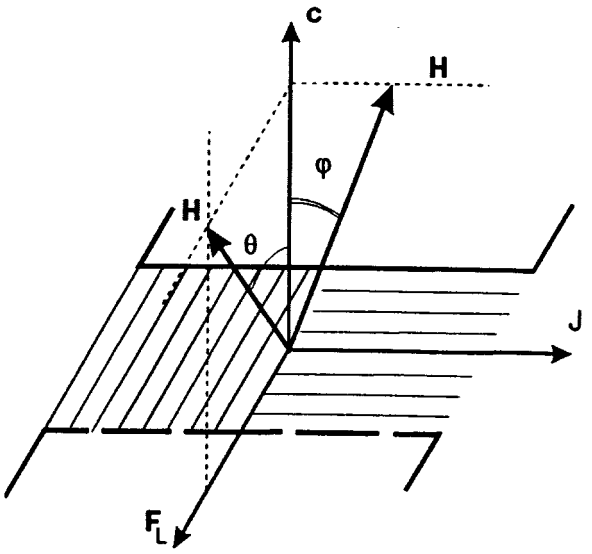

FIG. 1. Schematic diagram of bridges and experimental geometry.

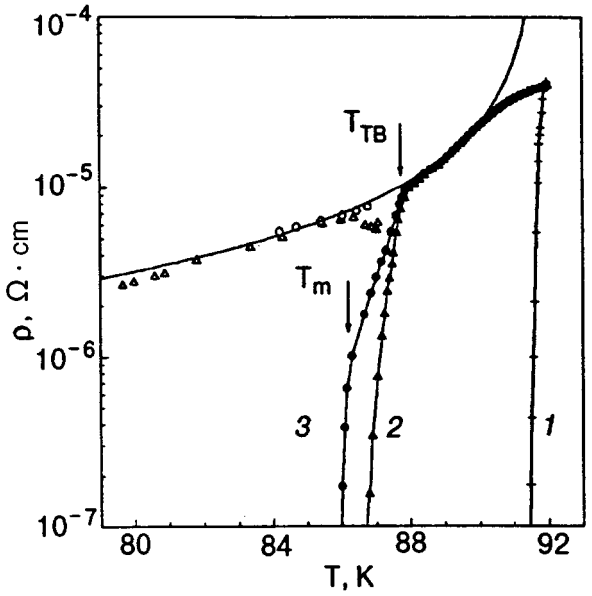

FIG. 2. Temperature dependences of resistivity (light symbols) and resistance to viscous flux flow (dark symbols). Circles correspond to the field orientation $\mathbf{H}\|\mathbf{c}$, while triangles correspond to the field tilted to the TB plane. Crosses show the $\rho(T)$ dependence for $H=0$. Solid curve describes the temperature dependence of the resistance to viscous flux flow in the Bardeen–Stephen model for $H_{c2}/dT=-1.8$ T/K.

tive to the TB plane, if the field vector **H** is oriented in the vicinity of the axis **c**.

Single crystals of YBaCuO were grown by the solution–melt technique in a gold crucible and were saturated in oxygen flow at 420 K for three days. Two bridges of width 0.2 mm were cut from a crystal of size 4×3 mm in the ab-plane and thickness $t=15$ μm as shown in Fig. 1. The transport current passed along the ab-plane. Electrical contacts were made by burning-in of the silver paste. Owing to a large area of the current contacts (about 3 mm^2), the transient electrical resistance was less than $10^{-3}\Omega$, thus enabling measurements in a constant current up to 0.5 A without overheating of the current contacts.

It can be seen from Fig. 1 that the transport current vector is oriented at right angles to twin boundaries in the first bridge and parallel to TB in the second bridge. The goniometer makes it possible to rotate the sample about two mutually perpendicular axes parallel to TB in bridges 1 and 2 and lying in the plane parallel to the ab-plane of the crystal. The error in setting angles was approximately 0.2°. The orientation $\mathbf{H}\|\mathbf{c}$ was determined from the minimum observed on angular dependences of resistance for the orientation of **H** parallel to TB.[6]

The superconducting transition temperature of the sample was 91.8 K for the transition width $\Delta T_c\cong0.3$ K. The average distance d_0 between twins was approximately equal to 2 μm. The measurements were made in direct current in a magnetic field 15 kOe for $\varphi=0$ and for angles θ equal to 0 and 9°.

The temperature dependences of the resistivity $\rho(T)$ measured in zero magnetic field and in the field $H=15$ kOe for $\theta=0$ and 9° are presented in Fig. 2 by curves *1, 2* and *3*, respectively. It can be seen that, for field orientation $\mathbf{H}\|\mathbf{c}$, the resistivity decreases rapidly at $T<T_d^{TB}\cong88$ K. The temperature T_d^{TB} is associated with the beginning of pinning at twin boundaries.[6] It can be seen from Fig. 2 that the melting temperature T_m of vortex lattice in fields 20 kOe is usually 1–2 K lower than T_d^{TB} and is manifested in the form of an additional kink on the $\rho(T)$ curve in magnetic fields tilted relative to TB.[6] Under the given experimental conditions, the value of T_m is approximately equal to 86 K.

According to measurements, the IVC are linear at $T>T_m$, i.e., the vortex liquid is not pinned in this temperature range. The IVC measured at $T<T_m$ for $\varphi=0$ and for angles $\theta=0$ and 9° are shown in Figs. 3a and 3b, respectively. It can be seen that in this temperature range the IVC are essentially nonlinear for low values of transport current density, i.e., the vortex system is in the pinned state. Figure 4 shows the current dependences of differential resistivity $\rho_d(J)=dE/dJ$. It can be seen from the figure that at temperatures smaller than 87 K, the $\rho_d(J)$ dependences attain saturation for large values of J. This means that a transition to the linear dependence $E(J)$ is observed with increasing transport current density, which might indicate the conditions of viscous flux flow for the transport current density J exceeding the critical depinning current J_{cd}. It is assumed that these conditions are characterized by the resistance to viscous flux flow $\rho_{ff}\equiv d\rho/dJ=$const. Temperature dependences of the resistance to viscous flux flow for $\theta=0$ and 9° are shown in Fig. 2.

It can be seen from Fig. 4 that at 87 K$<T<$88 K, the $\rho_d(J)$ dependences do not attain saturation. This is probably due to the fact that in this temperature interval the conditions for viscous flux flow were not created in the current interval under investigation.

The resistance to viscous flux flow in the Bardeen–Stephen model is defined by the relation[15]

$$\rho_{BS}=\rho_N(B/H_{c2}), \tag{1}$$

where ρ_N is the resistance in the normal state, B the magnetic induction, and H_{c2} the upper critical field. It is nor-

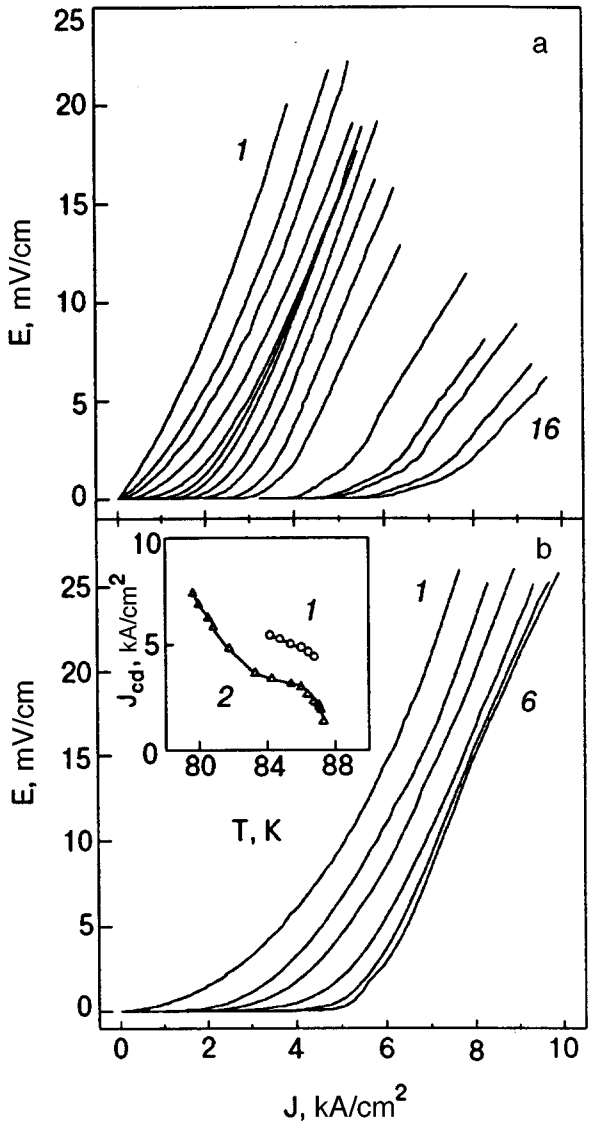

FIG. 3. Current-voltage characteristics in a field parallel (a) and tilted (b) to the TB plane, measured at temperatures T, K: 87.3, 87.15, 87.1, 87.05, 86.9, 86.7, 86.4, 86, 85.4, 84.3, 83.3, 81.8, 80.9, 80.6, 80, and 79.6 (curves *1–16*) (a) and 86.8, 86.4, 86, 85.4, 84.7, and 84.2 (curves *1–6*) (b). The inset shows the temperature dependence of critical depinning current in a field parallel (curve *1*) and tilted (curve *2*) to TB planes in a magnetic fields.

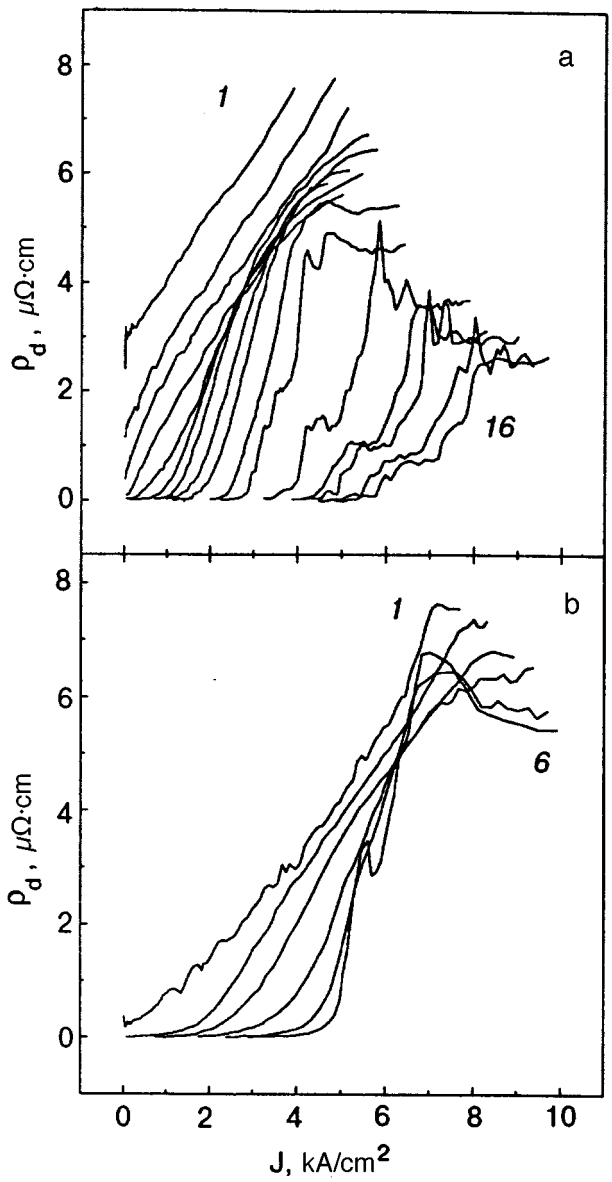

FIG. 4. Current dependences of differential resistivities in a magnetic field parallel (a) and tilted (b) to the TB planes. The numeration on the curves corresponds to that of $E(J)$ dependences shown in Fig. 3.

mally assumed that the temperature dependence of the upper critical field near T_c is determined by the equation $H_{c2}=(dH_{c2}/dT)(T-T_c)$. The best agreement between the temperatures dependences of ρ_{ff} and Eq. (1) is observed for $dH_{c2}/dT=-1.8$ T/K. This value of the derivative is close to the value of $dH_{c2}/dT=-2$ T/K obtained from magnetization measurements for YBaCuO single crystals for the magnetic field orientation $\mathbf{H}\|\mathbf{c}$.[16] This indicates that the linear segments on the $E(J)$ curves for large values of transport current density indeed correspond to the conditions of viscous flux flow. The $\rho_{BS}(T)$ dependence for $dH_{c2}/dT=-1.8$ T/K is shown by solid curve in Fig. 2.

The inset to Fig. 3 shows the temperature dependences of critical depinning current J_{cd} obtained for angles θ equal to 0 and 9°. The value of J_{cd} was determined by extrapolating the linear segments of the $E(J)$ curves corresponding to viscous flux flow to $E=0$. It can be seen that the value of J_{cd} in a tilted field is approximately 1.7 times larger than for $\mathbf{H}\|\mathbf{c}$. This difference in the value of critical current for a relatively small variation of the angle θ can be due to several reasons depending on the ratio of the pinning force at twin boundaries on one hand and the total force of pinning at point defects and indirect pinning on the other hand.

Let us consider this problem in greater detail. It was mentioned above that the effect of TB on pinning and dynamics of Abrikosov vortices in a YBaCuO superconductor is due to a lower energy as well as stronger pinning of vortices localized at TB, which leads to anisotropy of pinning at twins. The value of the ratio $\Delta U/U$ for $\mathbf{H}\|\mathbf{c}$ is estimated as 0.017–0.026.[1,17] Here U is the energy of a vortex filament in the bulk of the superconductor and ΔU the difference in the energy of a vortex in the bulk of the superconductor and a vortex localized in the TB plane. This difference in energy

leads to a step structure of the vortex filament in a magnetic field tilted relative to the TB plane for angles $|\theta| < \theta^*$ as shown in Fig. 5b.[11] The value of the critical angle for an isotropic superconductor is determined by the relations $(1-\cos\theta^*)=(2\Delta U/U)^{1/2}$ (Ref. 11) and $\tan\theta^* = \varepsilon^{-1}=(2\Delta U/U)^{1/2}$ (Ref. 12) for an anisotropic superconductor in the case of a field vector **H** tilted relative to the axis **c**. For YBaCuO superconductors, the anisotropy parameter $\varepsilon \cong 1/6$, and hence the value of the angle θ^* can become as high as 50°. At high temperatures, thermal fluctuations can reduce the value of θ^*, this decrease being determined by the ratio E_p/k_BT, where E_p is the pinning energy.[18] The measurements of angular dependences of electrical resistance[6] and critical current[5,7,12] show that the typical values of the angle θ^* in magnetic fields $H \leqslant 20$ kOe for the orientation of the vector **H** close to the direction of the axis **c** amount to 15–40°. Thus, for $\theta = 9°$, we can expect a step structure for vortex filaments.

Stronger pinning at TB in the case when vortices move along the TB plane can be due to a higher concentration of defects at twins, e.g., oxygen vacancies.[19] In addition, another reason behind stronger pinning at high temperatures can be the suppression of the amplitude of thermal oscillations of vortices localized at TB, which is due to the two-dimensional nature of their thermal oscillations.[10] Obviously, the pinning of a solitary vortex is maximum for the field orientation $\mathbf{H}\|\mathbf{c}$ and decreases with increasing θ due to a decrease in the fraction l_{tr} of the vortex trapped by the TB plane. However, in a strong magnetic field $[a_0 \cong (\Phi_0/B)^{1/2} < d_0]$, the situation can change.[11] If the pinning at twin boundaries and not at point defects plays a decisive role, the difference in the critical currents in fields parallel and tilted to TB planes can be due to the difference in the pinning mechanisms in them.

Thus, we assume that pinning at point defects is negligibly small. In the magnetic field $H = 15$ kOe, the distance a_0 between vortices is approximately equal to 370 Å, i.e., only 1/50 of vortices are localized in the TB plane. If pinning at TB is quite strong, the pinning of vortices located between twin boundaries for $\mathbf{H}\|\mathbf{c}$ will be determined by shear deformation of the vortex lattice. In the theory of elastic medium, the maximum shear stress τ_{max} is attained if the Lorentz force $BJ^c_{sh}/c_0 = 2\tau_{max}/d$. Here $\tau = Dc_{66}$, $d = d_0 - a_0$ is the width of the slip channel in the vortex lattice, $(1/3)\pi \leqslant D \leqslant (1/2)\pi$,[20] and c_0 is the velocity of light. The shear modulus for $\mathbf{H}\|\mathbf{c}$ is defined by the formula $c_{66} = \Phi_0 B(1-b)^2(8\pi\lambda)^{-2}$, where $b = B/B_{c2}$, and λ is the magnetic field penetration depth. Then the critical current controlled by shear deformation of the vortex lattice is given by

$$J^c_{sh} = 2Dc\Phi_0(1-b)^2/[d(8\pi\lambda)^2]. \quad (2)$$

Assuming that $\lambda \cong 3000$ Å, $D \cong 1/10$, $b \ll 1$, and $d_0 \cong 2$ μm, we obtain $J^c_{sh} \cong 5$ kA/cm, which is close to the experimentally observed value of J_{cd}. According to these estimates, the critical current for $\mathbf{H}\|\mathbf{c}$ can be controlled by indirect pinning of the vortex lattice. When the field **H** is tilted to the TB plane, the number of vortices crossing TB planes increases. If t is the thickness of the sample, the width

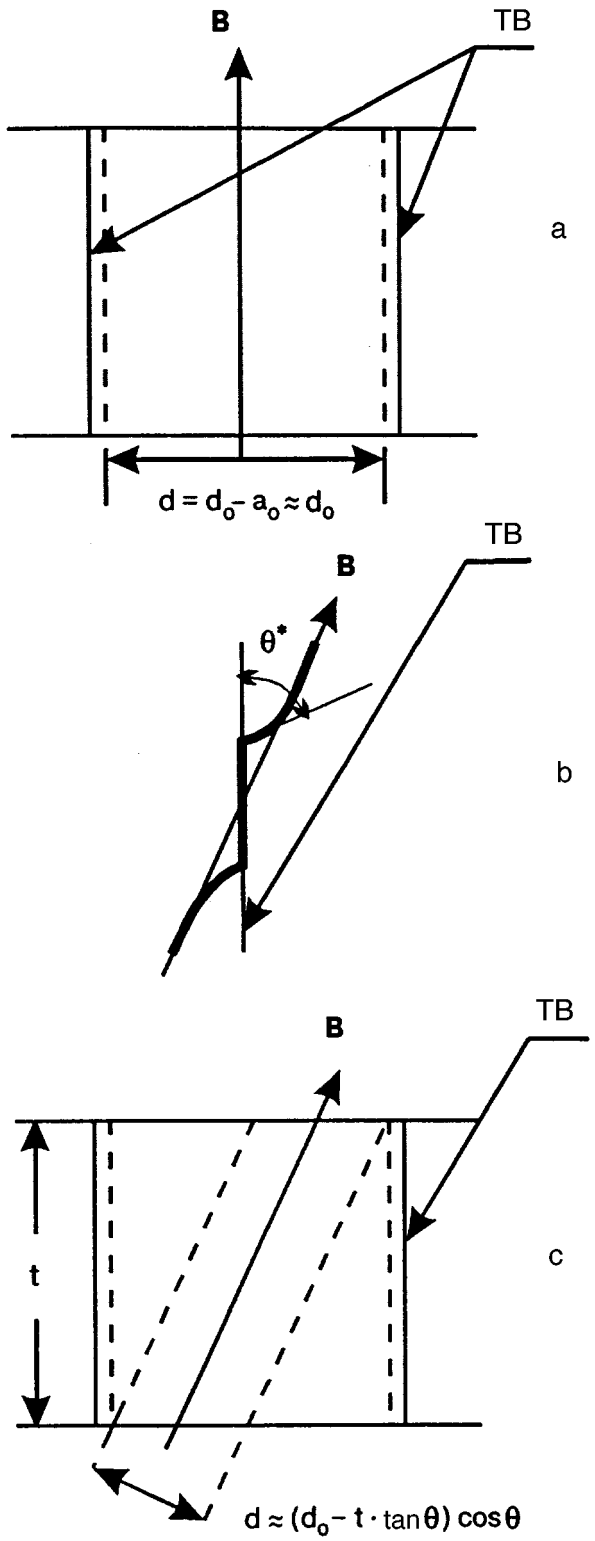

FIG. 5. Schematic diagram of channels for motion of vortices in magnetic fields parallel (a) and tilted (b) to TB planes as well as the structure of a vortex filament in the vicinity of a TB plane in a tilted magnetic field (b).

$d = d_0 a_0 - t\tan\theta$ of the channels in which vortex filaments do not intersect TB planes becomes smaller (see Fig. 5c). In this case, according to formula (2), the critical current J^c_{sh} increases. The increase in the critical current will be observed until indirect pinning becomes stronger than the pin-

ning of vortices trapped by the TB plane. As soon as this condition is observed, the vortex lattice starts moving under the action of the Lorentz force as a single whole, and the critical current decreases with increasing angle θ in view of a decrease in the fraction of vortices trapped by TB planes. Obviously, $\theta_m \leqslant \theta^*$ for $\tan\theta^* \geqslant d_0/t$. Here θ_m is the angle for which the critical current $J_{\rm sh}^c$ attains its maximum value. It should also be noted that the proposed model can be valid for a finite pinning at point defects also. The condition for the applicability of the model is that the force of pinning of vortices crossing the TB plane (which is determined by the pinning at TB as well as at point defects) is larger than the resultant force of pinning of vortices that do not cross the TB plane, which is determined by pinning at point defects and indirect pinning.

The $\rho_{ff}(T)$ dependences obtained by us speak in favor of the proposed model. According to formula (1), the curve $\rho_{BS}(\theta)$ must have a peak at $\theta=0$ since the value of $H_{c2}(\theta)$ in an anisotropic superconductor has the minimum value for $\mathbf{H}\|\mathbf{c}$. However, at $T<86$ K, the resistance to viscous flux flow for $\theta=9°$ is approximately 6% stronger than for $\theta=0$. If vortices localized at TB are pinned for $\mathbf{H}\|\mathbf{c}$, the value of ρ_{ff} in a perfect crystal for $J>J_{\rm sh}^c$ is smaller than ρ_{BS} by $\rho_{BS}(a_0/d_0)\cong 0.02$ which is determined by the fraction a_0/d_0 of vortices localized at TB. However, in the case when TB planes are not oriented strictly along **c**, this difference can be much larger since the fraction of vortices trapped by twin boundaries increases rapidly with the angle θ. For example, in the presence of two blocks in a bridge with the angle of inclination to the axis **c** equal to 1° and for the vector **H** oriented parallel to the axis **c** of one of the blocks, the fraction of vortices intersecting TB in the other block amounts to 20%.

An alternative model explaining the minimum of the critical current for $\mathbf{H}\|\mathbf{c}$ was proposed by Solovjov *et al.*[7] These authors attribute the minimum of $J_c(\theta)$ to an increase in the effective bending modulus c_{44} of the vortex lattice as a result of an increase in magnetic interaction between vortices. The increase in c_{44} leads to an increase in the pinning length $L_c \propto c_{44}^{1/2}$, and hence to a decrease in the efficiency of pinning at point defects. If the pinning at point defects plays a decisive role, this mechanism can lead to a decrease in J_c with the angle θ for $\theta<\theta^*$. However, the change in the value of J_c can attain the value $\Delta J_c \cong J_c(\lambda/d)$ since the magnetic interaction is effective over distances of the order of λ. In the temperature range under investigations, the penetration depth λ is estimated as 3000–4000 Å, and hence for $d=2$ μm we have $\Delta J_c/J_c \cong 0.2$. This value is much smaller than the relative change in critical current ~ 0.7 obtained from experiments.

It is worth noting that the values of ρ_{ff} in parallel and tilted magnetic fields differ considerably, and that the curves $\rho_d(J)$ for $\mathbf{H}\|\mathbf{c}$ intersect in the temperature range $T_m<T<T_d^{TB}$. It was mentioned above that the temperature T_d^{TB} corresponds to the onset of vortex pinning at TB, and the vortices localized at TB are pinned at $T<T_d^{TB}$. The thermal motion of these vortices is partially suppressed owing to two-dimensional nature of thermal fluctuations of these vortices.[10] Since the magnetic interaction between vortices is effective over distances of the order of the magnetic field penetration depth, we can expect that the amplitude of thermal oscillations of vortices separated by a distance λ from TB are also partially suppressed as compared to the amplitude of vortex oscillations in the remaining volume of the crystal. Thus, twin boundaries can serve as centers of nucleation of the crystalline phase; these nuclei grow upon cooling until they occupy the entire volume of the crystal. If the size of a nucleus of the crystalline phase 1 is small in the direction perpendicular to the TB plane, and the pinning of vortices localized at TB is strong, indirect pinning might lead to a transition of the liquid phase to the regime of viscous flux flow under the action of the Lorentz force, the crystalline phase remaining in the pinned state. In this case, the resistance to viscous flux flow of the liquid phase is $\rho_{ff}^l \cong \rho_{BS}(1-l/d_0)$. Putting $l \cong 2\lambda \cong 6000$ Å, we obtain $\rho_{ff}^l \cong 0.7\rho_{BS}$, which is in good agreement with the experimental value of ρ_{ff} at $T \cong 87$ K. In all probability, it is just the relation between the force of pinning in the liquid phase and the force of pinning in the solid phase localized in the vicinity of TB that determines peculiarities in the current dependences of ρ_d in the temperature range $T_m<T<T_d^{TB}$.

Another peculiarity of current dependences of differential resistivity is the presence of numerous peaks on the $\rho_d(J)$ curves at temperatures $T<T_m$. Similar peaks were observed earlier in $NbSe_2$ single crystals in the magnetic field range in which pinning is controlled by plastic deformation of the vortex lattice.[20] Bhattacharya and Higgins[20] attribute the peaks on the curve $\rho_d(J) \propto N_v[dv/dJ]$, where v is the average velocity of the vortex lattice, to the current dependence $N_v(J)$ of the number of moving vortices since the factor in the brackets, which is inversely proportional to the coefficient of friction, varies smoothly with increasing J. It is assumed that the peaks and valleys on the $\rho_d(J)$ curves correspond to peaks and valleys on similar dependences of dN_v/dJ. In other words, pinning is assumed to be nonuniform in the volume of the crystal, and the depinning of the vortex lattice occurs not simultaneously, but with gradual (upon an increase of current) formation of slip channels for the vortex lattice. The formation of such channels is possible if local stresses in the vortex lattice due to frozen disorder exceed the elastic limit of the vortex lattice in the channels.

It was noted above that the critical current of vortices that do not intersect TB planes in twinned YBaCuO single crystals with the magnetic field vector oriented approximately along the axis **c** is controlled by indirect pinning if the pinning force of vortices trapped at twin boundaries is larger than the sum of the forces of pinning at point defects and indirect pinning of vortices located between twins. Since the separations between twins in real crystals are not identical, depinning first takes place in channels with the maximum separation between TB planes because the critical current $J_{\rm sh}^c \propto d^{-1}$. Obviously, the scale of pinning nonuniformity in this case is approximately equal to the separation between twins, and the current dependence of differential resistivity reflects the form of distribution of d_0 in the crystal. The second scale of nonuniformity exceeding the separation between twins can be due to fluctuations of twin boundary density. If the pinning of vortices trapped by twin boundaries

is not stronger than the sum of the pinning at point defects and indirect pinning of vortices located between twins, the current dependence of differential resistivity reflects the type of fluctuations of TB density in the crystal. In magnetic fields tilted to the TB planes for large values of angles $\theta(\tan\theta \geqslant d_0/t)$, when each vortex filament crosses the TB plane, the functions $\rho_d(J)$ can reflect both the form of the distribution of the quantity d_0, and the nature of TB density fluctuations in the crystal depending on the relation between the pinning at TB and at point defects as well as on the distribution of the quantity d_0 and TB density fluctuations in the crystal.

In conclusion, let us briefly formulate the results of this research. Steady-state current-voltage characteristics of a YBaCuO single crystal are considered for the Lorentz force parallel to the twin plane. Measurements are made over a wide range of temperatures and currents in the field $H=1.5$ T directed parallel to the axis **c** and at an angle of 9° to it. It is shown that the critical depinning current in a tilted field is almost twice as strong as that in a parallel field. The proposed physical interpretation of this effect is associated with qualitatively different mechanisms of formation of the critical pinning force in parallel and tilted fields. If $\mathbf{H}\|\mathbf{c}\|$TB, the value of J_{cd} is determined by plastic deformation of vortex bundles relative to vortex rows fixed at twins. However, in a tilted field such a mechanism of movement of segments of the vortex lattice would require the rupture of vortices themselves and not only of bonds between the vortices as in the case when $\mathbf{H}\|\mathbf{c}\|$TB. This would lead to a much larger value of $J_{cd}(\theta=9°)$ than that observed in experiments. Consequently, a simpler version of consolidated depinning of the entire vortex lattice from twins takes place, corresponding to double critical current density. The proposed interpretation is confirmed by a qualitative comparison of the values of resistance ρ_{ff} to viscous flux flow for $J>J_{cd}$. Since some of vortex rows remain fixed at twins for $\mathbf{H}\|\mathbf{c}$ and for the plastic mechanism of J_{cd}, the value of ρ_{ff} under these conditions is systematically smaller than in a tilted field. Plastic mechanism of depinning also leads to a much stronger nonmonotonicity in dE/dJ than in the case of elastic depinning in tilted fields.

*E-mail: mikhail.a.obolenskii@univer.kharkov.ua

[1)]The formula $\tan\theta^* = \varepsilon^{-1}(2\Delta U/U)^{1/2}$ can be easily derived by the method used in Ref. 10 if we take into account the angular dependence of the vortex energy.

[1] L. Ya. Vinnikov, I. V. Grigoreva, L. A. Gurevich, and A. E. Koshelev, Sverkhprovodimost': Fiz., Khim., Tekh. **3**, 1434 (1990).
[2] G. J. Dolan, G. V. Chandrasekhar, T. R. Dinger *et al.*, Phys. Rev. Lett. **62**, 827 (1990).
[3] L. J. Schwartzendruber, A. Roitburg, D. L. Kaiser *et al.*, Phys. Rev. Lett. **64**, 483 (1990).
[4] A. I. Belyaeva, S. V. Vojtsenya, V. P. Yuriyev *et al.*, Solid State Commun. **856**, 427 (1993).
[5] L. M. Fisher, A. V. Kalinov, J. Mirkovic *et al.*, Appl. Suppercond. **2**, 639 (1994).
[6] S. Flesher, W. K. Kwok, U. Welp *et al.*, Phys. Rev. B **47**, 14448 (1993).
[7] V. F. Solovjov, V. M. Pan, and H. C. Freyhard, Phys. Rev. B **50**, 13724 (1994).
[8] M. A. Obolenskii, A. V. Bondarenko, M. G. Revyakina, and V. A. Shklovskij, Sverkhprovodimost': Fiz., Khim., Tekh. **7**, 43 (1994).
[9] M. A. Obolenskii, A. V. Bondarenko, V. A. Shklovskij, *et al.*, Fiz. Nizk. Temp. **21**, 1200 (1995) [Low Temp. Phys. **21**, 917 (1995)].
[10] G. Blatter, J. Rhyner, and V. M. Vinokur, Phys. Rev. B **43**, 7826 (1991).
[11] E. B. Sonin, Phys. Rev. B **48**, 10487 (1993).
[12] M. A. Obolenskii, A. V. Bondarenko, V. A. Shklovskij, and M. G. Revyakina, Low Temp. Phys. **22**, 683 (1996).
[13] L. M. Fisher, A. V. Kalinov, J. Mirkovic *et al.*, Phys. Rev. B , (1997).
[14] M. A. Obolenskii, A. V. Bondarenko, V. I. Beletskii *et al.*, Funktsion. Mater. **2**, 401 (1995).
[15] J. Bardeen and M. J. Stephen, Phys. Rev. A **140**, 1179 (1965).
[16] U. Welp, W. K. Kwok, G. W. Crabtree *et al.*, Phys. Rev. Lett. **61**, 1419 (1989).
[17] L. A. Dorosinskii, V. I. Nikitenko, A. A. Polyanskii, and V. K. Vlasko-Vlasov, Physica C **246**, 283 (1995).
[18] W. K. Kwok, J. A. Fendrich, V. M. Vinokur *et al.*, Phys. Rev. Lett. **76**, 4596 (1996).
[19] R. Schmucker, Philos. Mag. **35**, 431 (1977).
[20] S. Bhattacharya and J. Higgins, Phys. Rev. B **52**, 64 (1995).

Translated by R. S. Wadhwa

On the theory of low-temperature properties of spin systems with magnetic anisotropy

O. B. Zaslavskii, V. V. Ulyanov, and Yu. V. Vasilevskaya

*Kharkov State University, 310077 Kharkov, Ukraine**
(Submitted June 28, 1997)
Fiz. Nizk. Temp. **23**, 1289–1295 (December 1997)

Temperature behavior of easy-axis paramagnets in a transverse magnetic field is considered. It is shown that the low-temperature susceptibility as a function of the field has a peak for all values of spin S. As the temperature increases from zero, this peak is first sharpened (and not blurred), its position changing nonmonotonically. For spins $S<3$, the peak becomes double-humped at a certain temperature, while for $S\geqslant 3$, a flat-top peak is observed. Similar phenomena are also typical of biaxial paramagnets. The energy spectrum of the system coincides with $2S+1$ low-lying energy levels for a particle moving in a potential field of a simple form, which has the shape of a double well for low magnetic fields. This makes it possible to calculate the tunneling velocity by using quantum-mechanical methods. © *1997 American Institute of Physics.* [S1063-777X(97)00412-X]

1. INTRODUCTION

Quantum properties of uniaxial paramagnets were studied by us together with Tsukernik at the beginning of the eighties.[1] Earlier, such systems were analyzed by using semiclassical methods which led to contradictory results. We managed not only to solve the formulated problem, but also work out a number of original approaches for studying more general spin systems, which were developed in our subsequent publications.[2] Another unexpected and important secondary result was the discovery of a new class of potential models with exact solutions of the Schrödinger equation.[3–5]

In a review published in 1992,[2] we summarized the results obtained during ten years of research. Subsequently, new results and a new trend appeared. In the first place, we must mention the extension of the manifold of quasi-exactly solvable models[3] as well as the discovery of similar two-dimensional models and their generalization to multidimensional cases.[6,7]

In this paper, we report on some new results obtained from the study of anisotropic paramagnets. We shall consider here only magnetic susceptibility and spin tunneling. For definiteness, we confine our analysis to spin systems with the Hamiltonian

$$H=\alpha S_z^2-\beta S_y^2-BS_x, \tag{1}$$

describing a so-called biaxial paramagnet with anisotropy constants $\alpha,\beta\geqslant 0$ in a transverse magnetic field proportional to B (S_j are spin projections operators).

2. MAGNETIC SUSCEPTIBILITY OF UNIAXIAL AND BIAXIAL PARAMAGNETS

We begin with a more detailed analysis of the effect of temperature on the susceptibility of a uniaxial paramagnet ($\alpha=0$) for various values of spin S (without loss of generality, we also assume that $\beta=1$). We proceed from the results reported in our initial publication[1] in which specific physical objects and dimensional quantities are considered, and the corresponding dimensionless parameters are introduced; we shall use these characteristics in the present research. In Ref. 1 (see also Ref. 2), the behavior of magnetic susceptibility of a uniaxial paramagnet in the ground state (i.e., at $T=0$) was studied in detail. It was found that the magnetic susceptibility $\chi_0=-2\partial^2 E_0/\partial B^2$ of the ground state as a function of magnetic field has a specific behavior for spin $S\geqslant 2$: the gradual increase in susceptibility with the magnetic field B gives way to a sharp increase with the formation of a well-localized clearly manifested peak having the shape of a ''hump,'' followed by a rapid decrease to small values in the range of ''critical'' magnetic field $B_0=2S+1$ (see Fig. 1, where the susceptibility of the first excited state is also shown for comparison).

In the same publication, graphic explanation of such a phenomenon is given on the basis of a specially developed method of effective potential, which can be described as follows. Since spin is a quantum-mechanical object of essentially discrete nature, equations whose solutions describes the energy spectrum of spin systems have a matrix form. This complicates the analysis of properties of the system by the standard quantum-mechanical methods. It was found, however, that we can introduce a rigorous potential description for a wide class of spin systems, such that the energy spectrum of the spin system coincides with certain energy levels for a particle moving in a potential field of a simple form. Such an exact spin–coordinate correspondence also served as the basis for various approximate methods of description of spin systems, e.g., the perturbation theory and the semiclassical approximation. It is especially important that this leads to new exact solutions of the Schrödinger equation in the corresponding coordinate system.[3–5]

The approach proposed by us lies in the application of the concept of coherent spin states for Hamiltonians constructed from spin operators used in the solution of the problem on their eigenvalues and eigenvectors.[8] In the obtained

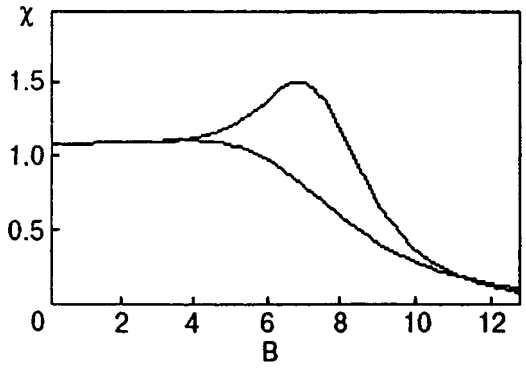

FIG. 1. Typical magnetic-field dependence of susceptibility of a uniaxial paramagnet in the ground state (upper curve) and in the first excited state (lower curve) for $S=6$.

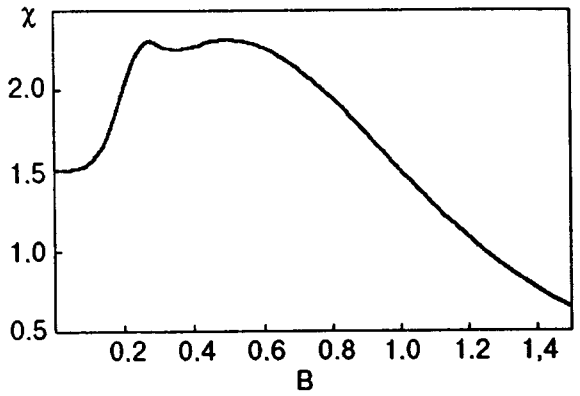

FIG. 3. Two-hump profile of magnetic susceptibility ($S=3/2$, $T=0.0028$).

coordinate representation, such a Hamiltonian becomes a Schrödinger differential operator with a certain effective potential energy. The potentials obtained for simple spin systems either have the shape of nonlocalized wells, or are periodic. In all cases, there exist various symmetric and nonsymmetric multiparametric potential models.

For example, if we are solving the problem on determining stationary states of an easy-axis paramagnet in a transverse magnetic field, i.e., a system with the Hamiltonian $H=-S_y^2-BS_x$, by using the above method, we arrive at the standard one-dimensional Schrödinger equation $d^2\psi/dx^2+[E-U(x)]\psi=0$ for a pseudoparticle with a quadratic energy–momentum relation (spinon), moving in an effective potential field constructed from hyperbolic functions:

$$U(x)=\frac{B^2}{4}\sinh^2 x-B\left(S+\frac{1}{2}\right)\cosh x, \tag{2}$$

where x is a certain dimensionless coordinate. In this case, the eigenvalues of energy E of the spin system coincide with the lower $2S+1$ energy levels of a spinon in the potential field (2).

It was found that the energy spectrum of uniaxial paramagnet has a typical ''fan'' structure corresponding to deformations of effective potential (Fig. 2): from double degeneracy for $B=0$ with pairwise close energy levels for $B\ll B_0$ (tunnel splitting in a double potential well; Fig. 2a) to the energy distribution for $B=B_0$, which is typical of a fourth-degree oscillator $U\sim x^4$ (Fig. 2b), and then to an equidistant structure of the harmonic oscillator spectrum $\sim x^2$ (Fig. 2c). In this case, the most significant rearrangement of the energy spectrum is observed in the ''precritical'' field region $B\lesssim B_0$, in which the ''hump''-type peculiarity of susceptibility is located.

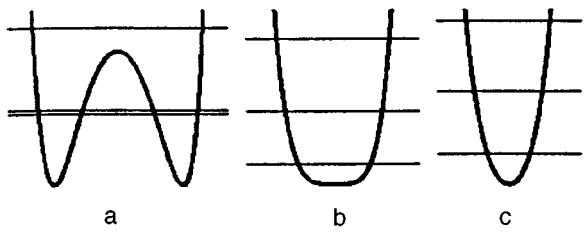

FIG. 2. Typical shapes of the effective potential of a uniaxial paramagnet.

It would be interesting to study the effect of temperature on the behavior of susceptibility. It turns out that, instead of expected blurring of the singularity, an interesting transformation of the ''hump'' takes place, which can be reduced, roughly speaking, to its ''sharpening'' and increase at the beginning followed by gradual blurring and vanishing at a certain critical temperature $T_c\sim S$. In addition, a two-hump profile is formed at the initial stage for not very high values of spin ($S<3$) (Fig. 3), while for large values of spin ($S\geqslant 3$) the top of the hump becomes flat (rudiment doubling). The position of the peak changes nonmonotonically: at first, it is displaced towards higher values of magnetic field B, and then ''starts returning'' down to $B=0$ at T_c.

Some typical stages of these transformations of susceptibility are presented in Fig. 4 along with the standard susceptibility of the ground state, which is described by the dashed curve.

The above-mentioned regularities are determined by the structure of the energy spectrum of a uniaxial paramagnet in

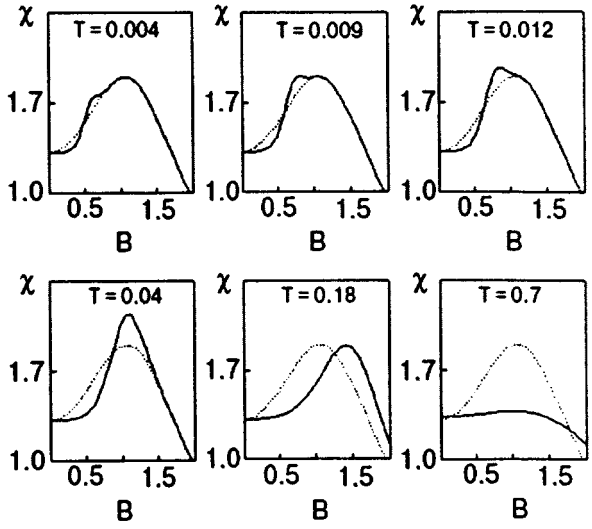

FIG. 4. Some stages of low-temperature transformations of susceptibility ($S=2$).

the region of magnetic fields containing the hump, i.e., a small separation between the ground energy level and the first excited level and a large distance to next excited levels. For example, for $S=3$, the gap $E_1-E_0=0.16$, while $E_2-E_1=3.34$ for $B_{\max}=2.34$.

Thus, the spin system under investigation in the temperature range $0<T<T_c$ behaves as a two-level system. The magnetic susceptibility χ in the two-level approximation can be written by singling out the temperature correction $\Delta\chi$:

$$\chi=\chi_0+\Delta\chi. \tag{3}$$

Considering that energy levels depend on the magnetic field and carrying out simple transformation of the partition function, we obtain the following formula for susceptibility, which contains the main contribution in the form of the susceptibility χ_0 of the ground state and two competing temperature corrections:

$$\chi=\chi_0+\frac{(\Delta')^2}{2T\cosh^2(\Delta/2T)}-\frac{2\Delta''}{1+\exp(\Delta/T)}, \tag{4}$$

where $\Delta\equiv E_1-E_0$, and primes denote derivatives with respect to B.

As $T\to 0, \chi\to\chi_0$ as expected. For any finite T and in the region of small B, where $\Delta\ll T$, we have $\chi=(\chi_1+\chi_0)/2$ (χ_1 is the susceptibility of the first excited state), i.e., the main contribution comes from the second negative correction, while for higher values of B the first positive correction can dominate so that $\chi>\chi_0$. The two-level approximation (4) completely describes the behavior of susceptibility in the most interesting region of low temperatures $0<T<T_c$.

We can now use the power approximation in the magnetic field B for the gap Δ between the ground energy level and the first excited level, which was obtained in Ref. 2:

$$\Delta=cB^{2S}, \quad c=\frac{S^2}{2^{2S-3}(2S)!}, \tag{5}$$

which leads to the following expression for the temperature correction in (3) obtained on the basis of (4):

$$\Delta\chi=T^{(S-1)/S}f_S\left(\frac{cB^{2S}}{T}\right) \tag{6}$$

with the universal function

$$f_S(x)=2S(2S-1)c^{1/S}\frac{x^{(S-1)/S}}{\cosh(x/2)}\left[\frac{Sx}{(2S-1)\cosh(x/2)}-\exp(-x/2)\right]. \tag{7}$$

A comparison of such an approximation for the temperature correction to susceptibility (6) and (7) with the results based on exact formulas for E_0 and E_1 (as well as for χ_0) in the case when $S=3/2$, 2, 5/2, 3, and 7/2 shows that this approximation is fairly accurate in the most interesting temperature region, in which the transformations of the magnetic susceptibility profile described above are observed (for all magnetic fields B).

If we lay the position of $B_{\max}$ and the magnetic susceptibility peak $\chi_{\max}$ on the coordinate axes, the variation of temperature in the range $0\leqslant T\leqslant T_c$ leads to a curve in the form of a spiral loop with an isolated point inside it, which graphically illustrates the above ''anomalies'' in the behavior of the susceptibility peak, i.e., its temperature ''drift'' stage (see Fig. 5). The following characteristic regions and reference points relative to transformations of the magnetic susceptibility profile can be singled out on the temperature scale: $T_0=0$ corresponds to conventional one-hump (standard) profile; the region $T_0\leqslant T\leqslant T_1$ is characterized by small deformations of the left slope of the hump followed by the formation of the second (left) peak; T_1 corresponds to a two-hump profile with the same height of the peaks; in the region $T_1<T<T_2$, the left hump, which is higher than the standard one, increases, becomes sharper, and is shifted to the right; T_2 corresponds to the maximum height of the hump located approximately in the same region as the standard hump; $T_2<T<T_3$ corresponds to further displacement of the peak to the right and its gradual decrease; at T_3 the height of the hump decreases to the standard value with the maximum displacement to the right; in the region $T_3<T<T_4$ the displacement changes direction (to the left), and the peak is blurred; T_4 corresponds to a highly blurred peak in the region of the standard hump; $T_4<T<T_5$ corresponds to a weakly distinguishable peak, which continues its shift to the left; $T_5\equiv T_c$ is the critical temperature at which the weakly manifested peak reaches the point $B=0$ (the susceptibility curve descends smoothly without any singularities), and at $T>T_c$ the value of χ decreases for any B due to activation of the remaining excited energy levels (the two-level approximation becomes inapplicable). Number on the spiral in Fig. 5 indicate the main temperature reference points.

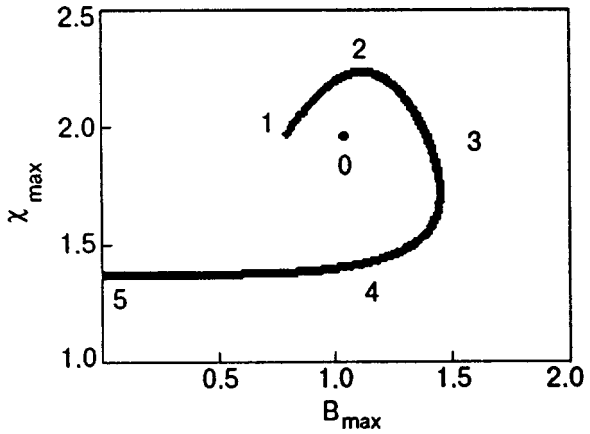

FIG. 5. A typical spiral loop describing the position and magnitude of the maximum susceptibility peak in the low-temperature region $0<T<T_c$ for $S=2$.

As the value of S increases, the spiral curve is shifted towards higher values of B, but all qualitative singularities of transformations are preserved (except the formation of a two-hump profile).

It should be noted that all calculations (apart from the two-level approximation and the power approximation mentioned above) were made on the basis of exact, explicit formulas for the energy levels for $S<4$ and by using exact algebraic equations for the eigenvalues of Hamiltonian (1) for $S\geqslant 4$. Moreover, analytic and numerical methods were

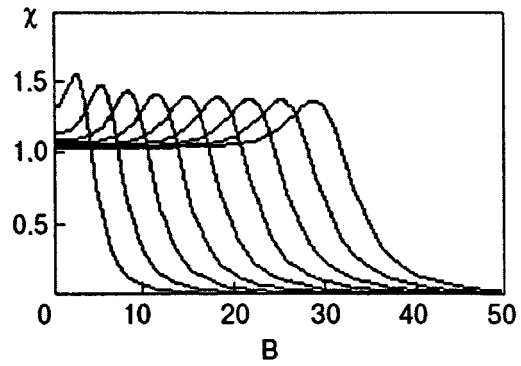

FIG. 6. Magnetic-field dependences of the susceptibility of a biaxial paramagnet for even values of S from 4 to 20.

mutually controlled and verified by plotting graphs.

Another cycle of investigations was devoted to an analysis of the behavior of the magnetic susceptibility of biaxial paramagnets. It was found that all the peculiarities of susceptibility mentioned above are observed for such systems also. For example, Fig. 6 shows a series of typical susceptibility profiles for different values of spin S in the case of equal anisotropy constants $\alpha=\beta$ at $T=0$.

In addition, the general dependence of various effects on the ratio of anisotropy constants was studied separately.

Thus, the peculiarities in the magnetic susceptibility of anisotropic paramagnets observed earlier proved to be stable to the effect of various factors and demonstrated some additional interesting details of the behavior under an increase in temperature T and spin S as well as for different ratios α/β of anisotropy constants.

Finally, in the case of an arbitrarily directed magnetic field, the tensor nature of magnetic susceptibility must be taken into account, i.e., each of its components must be studied in detail. For example, in the uniaxial case we are actually dealing (in view of the symmetry properties) with the three quantities χ_{xx}, χ_{xy}, and χ_{yy}, which should be considered as functions of the magnetic field components B_x and B_y.

3. QUANTUM TUNNELING IN SPIN SYSTEMS

Tunnel effects in various fields of solid state physics have been studied intensely during the last decade (see the review in Ref. 9). Most of such investigations proceeded from the model of a two-level system interacting with the ambient which served as a thermostat. The possibility of replacing a real quantum-mechanical system with a complex energy spectrum by a two-level system by disregarding the contribution from higher energy levels is equivalent to the introduction of effective spin $S=1/2$. In this publication, however, we indicate a field in the physics of tunnel phenomena, in which the spin is not an auxiliary concept, but reflects the real physics of the problem, i.e., tunneling in spin systems (by way of an example, we can mention tunneling in small ferromagnetic particles).[10] The most interesting case is that of large spins $S\gg 1$ rather than the case of small spins.

In spite of the fact that first indications of experimental manifestations of spin tunneling were actually described long ago in the review by Bean and Livingston,[11] the theoretical apparatus for studying this effect was worked out only by the middle of the eighties. This is not accidental. The tunneling of a particle moving in a potential well was explained long ago and is described in textbooks on quantum mechanics. At the same time, spin is an essentially discrete, purely quantum-mechanical variable and cannot be represented in such a visual form. It is remarkable that this has become possible for the spin system as a whole, that is described by a Hamiltonian which is quadratic or quadratic–linear in spin components. Such a spin–coordinate correspondence, which was mentioned in the previous sections of this paper, allows us to translate the problem under consideration into the language of ordinary quantum mechanics and to apply the methods developed earlier, including instanton calculus and semiclassical approximation.

Let us first consider first a uniaxial paramagnet with an easy-axis type anisotropy, which was discussed above for another purpose. Since the energy levels in the spin system coincide (see above) with $2S+1$ low-lying energy levels for a particle moving in a potential field of the form (2), the magnitudes of the tunnel splitting $\Delta=E_1-E_0$ of the ground-state energy also coincide. If we calculate this quantity to the exponential accuracy, the result can be obtained almost immediately. It is well known[12] that this value is determined by the factor $\exp(-W)$, where W is the Euclidean action on a trajectory between two degenerate minima:

$$W=\int_{x_-}^{x_+} dx\sqrt{2m(U-U_-)}.$$

Here m is the effective mass of the particle ($\hbar=1$), and $U_-=U_+$ is the value of the potential at the point of minimum. Thus, if we are not interested in the preexponential factor, we can forget about the equation of the instanton trajectory in explicit form. However, this is essential for calculating the preexponential factor in

$$\Delta=(\omega/\pi)^{1/2}A\ \exp(-W).$$

Here ω is the frequency corresponding to small oscillations near the point of minimum, and the constant A can be determined from the relation

$$\tau=\int_{x_m}^{x} dx\left[\frac{m}{2(U-U_+)}\right]^{1/2},$$

$$x(\tau)\cong x_+-\frac{A}{2\omega\sqrt{m}}\exp(-\omega\tau),\quad \tau\to\infty,$$

where $x_m=0$ corresponds to the midpoint of the potential between two minima, and τ is the Euclidean time. For the uniaxial case under consideration with potential (1) and corresponding dimensionless quantities, the instanton trajectory can be found in explicit form:

$$\tanh\frac{x}{2}=\left(\frac{1-B/B_0}{1+B/B_0}\right)^{1/2}\tanh\frac{\omega\tau}{2},\quad \omega=\sqrt{1-(B/B_0)^2}.$$

Using previous formulas, we obtain

$$\Delta = \frac{8(S+1/2)^{3/2}\omega^{5/2}(1-\omega^2)^S}{\sqrt{\pi}(1+\omega)^{2S+1}} \exp[(2S+1)\omega]. \qquad (8)$$

For $B \ll B_0$, formula (8) for $S \gg 1$ gives the result in the power approximation for the energy gap (6).

The biaxial case can be considered similarly. It is interesting from the general point of view since the energy spectrum of the effective spin potential is a band spectrum.[5] Let us first assume that $B=0$, and S is integral (for half-integral values of spin, degeneracy is not removed). In this case, spin levels correspond to the edges of merged bands, and the splitting of the ground level is equal to the band width. If, however, $B \sim S \gg 1$, the widths of the energy bands containing E_0 and E_1 are much smaller than the separation between the energy levels, so that the splitting can be calculated disregarding the periodic nature of the potential and the band structure (see for details the review in Ref. 2, in which tunneling is considered in special cases when energy levels are near the potential barrier peak).

Moreover, a many-particle system can be approximately reduced in some cases to a one-particle system (as in the case of a Heisenberg magnet with weak anisotropy),[2] and the formulas obtained for paramagnets are applicable for calculating the tunnel splitting.

Finally, for $B \gg B_0$, we can use perturbation theory. It is interesting that degeneracy is removed in the $2S$th order in this case.

CONCLUSION

Thus, the method of effective potential proposed by Tsukernik and developed further by other authors proved to be extremely productive and powerful for studying the low-temperature behavior of susceptibility of anisotropic spin systems as well as for tunnel junctions.

It should be emphasized that, while the classical spin can be parametrized by two variables, in the effective potential method the system is one-dimensional.

At first glance, spin systems with a Hamiltonian of the type (1) appeared as very simple, but further analysis has proved that the problem proposed by Tsukernik at the beginning of the eighties gave rise to a new trend in physics. We believe that this publication is another confirmation of this fact.

The authors are deeply indebted and devote this research to Viktor Moiseevich Tsukernik, remarkable scientist and teacher, considerate and cordial person with whom they made first steps in the development of new methods in the theory of spin systems.

*Email: vladimir.v.ulyanov@univer.kharkov.ua;
oleg.b.zaslavskii@univer.kharkov.ua

[1] O. B. Zaslavskii, V. V. Ulyanov, and V. M. Tsukernik, Fiz. Nizk. Temp. **9**, 511 (1983) [Sov. J. Low Temp. Phys. **9**, 259 (1983)].
[2] V. V. Ulyanov and O. B. Zaslavskii, Phys. Rep. **216**, 179 (1992).
[3] V. V. Ulyanov, O. B. Zaslavskii, and Yu. V. Vasilevskaya, Fiz. Nizk. Temp. **23**, 110 (1997) [Low Temp. Phys. **23**, 82 (1997)].
[4] O. B. Zaslavskii and V. V. Ulyanov, Zh. Éksp. Teor. Fiz. **87**, 1724 (1984) [Sov. Phys. JETP **60**, 991 (1984)].
[5] O. B. Zaslavskii and V. V. Ulyanov, Teor. Mekh. Fiz. **71**, 260 (1987).
[6] A. V. Turbiner, Commun. Math. Phys. **118**, 467 (1988); Contemp. Math. **160**, 263 (1994); A. G. Ushveridze, Fiz. Elem. Chast. Atom. Yadra **20**, 1185 (1989) [Sov. J. Part. Nucl. **20**, 504 (1989)].
[7] O. B. Zaslavskii, Phys. Lett. A **190**, 373 (1994); J. Phys. A **27**, L447 (1994).
[8] A. M. Perelomov, *Generalized Coherent States and Their Applications*, Springer, NY, 1986.
[9] A. J. Leggett, S. Chakravarty, A. T. Dorsey *et al.*, Rev. Mod. Phys. **59**, 1 (1987).
[10] E. M. Chudnovsky and L. Gunther, Phys. Rev. Lett. **60**, 661 (1988); Phys. Rev. B **37**, 9455 (1988); A. Caldeira and K. Furuya, J. Phys. C **21**, 1227 (1988).
[11] C. P. Bean and J. D. Livingston, J. Appl. Phys. **30**, 120S (1959).
[12] S. Coleman, in *The Whys of Subnuclear Physics*, Plenum, New York (1979).

Translated by R. S. Wadhwa

Mechanisms for increasing resolution of high-frequency PC spectroscopy

O. P. Balkashin

*B. Verkin Institute for Low Temperature Physics and Engineering, National Academy of Sciences of the Ukraine, 310164 Kharkov, Ukraine**

(Submitted July 14, 1997)
Fiz. Nizk. Temp. **23**, 1296–1299 (December 1997)

It is shown that the improvement of resolution of high-frequency PC spectroscopy is due to a decrease in the contribution of thermal effects and nonequilibrium phonon reabsorption to the signal being measured. © *1997 American Institute of Physics.* [S1063-777X(97)00512-4]

Point-contact (PC) spectroscopy, i.e., the analysis of inelastic electron energy relaxation by passing current through a bulk sample with a microscopic constriction, has been developed as a relatively simple but effective method of investigation of elementary excitation spectra in pure metals,[1] metallic alloys, and compounds.[2] The efficiency of this method is determined by the relation between the geometrical size of the current concentration region (contact diameter d) and the electron mean free paths l_ε and l_i for energy and momenta relaxation. According to theoretical analysis,[3] in the limiting case of ''dirty'' contacts, when $d \gtrsim \lambda_\varepsilon = (l_i l_\varepsilon)^{1/2}$, the spectroscopy is still possible, but the intensity of spectral lines decreases, tending to zero as $\lambda_\varepsilon / d \to 0$. If reabsorption of nonequilibrium phonons becomes significant in this case, i.e., the diameter d exceeds the mean free path $l_{\mathrm{ph}-e}$ of phonons scattered by electrons, and the contact region experiences Joule heating to temperatures determined by the bias voltage $kT = eV/3.63$, the resolution of the method decreases ($\Delta\varepsilon \propto kT$), and the background signal amplitude increases considerably. In view of computational difficulties, the quantitative analysis of variation of PC spectra upon a transition to the thermal mode was carried out only for the Einstein model of the phonon density of states.[3] The inelastic mean free path for electrons is known to be a function of excess energy determined by the voltage across a point contact [$l_\varepsilon(eV)$]. For this reason, a transition from the spectral mode in the range of low bias voltages to the thermal mode for high bias voltages can be observed for small mean free paths.

Measurements of point-contact spectra at high frequencies $\omega\tau_i \sim 1$, where τ_i are characteristic times of scattering for quasiparticles, make it possible to study the kinetics of relaxation processes in contacts from the frequency dispersion of the signal being measured and to determine the characteristic relaxation time τ_i for quasiparticle excitations of various types.[4–8] Spectral singularities observed in high-frequency spectra of some contacts are absent in the spectra measured by a traditional low-frequency technique.[4,5]

This communication is devoted to an analysis of possible reasons behind the improvement of resolution of PC spectroscopy by using high-frequency modulation. Measurements were made on point contacts between copper and copper-beryllium alloy Cu–Cu(2.7 at. % Be) as well as point contacts Ni–Ni of pure nickel at 4.2 K. We used a modulation technique, involving the recording of the amplitude of second harmonic of modulation current in low-frequency experiments as well as the amplitude of rectified voltage on point contacts exposed to a radiofrequency field of frequency 78 GHz. A detailed description of experimental technique is given in Ref. 4.

The measured low-frequency PC spectra shown in Fig. 1 (curves *1*) are characterized by a low intensity of the peak associated with electron scattering by phonons with transverse polarization (T-peak which normally dominates in spectra), the absence of an L-peak associated with longitudinal phonons, a high background level, and its monotonic increase with the voltage. As a rule, such spectra are observed for ''dirty'' contacts with a small ratio[2] l_i/d.[1)] High-frequency spectra (curves *2* in Fig. 1) exhibit spectral singularities marked by arrows in the figure and absent in rf spectra: L-peaks for copper (29 MeV) and nickel (36 meV) as well as a peak at energies $\sim$40 meV associated with a local vibrational mode for light Be impurity atoms in the copper matrix;[9] besides, the background signal level is much lower.

It was shown in our previous publications[4,5] that a decrease in the background level in the measurements of PC spectra at high frequency exceeding the phonon-electron collision frequency ($\omega > \omega_{\text{ph-e}} = \lambda\omega_D s/v_F$, where λ is the electron-phonon interaction constant, s the velocity of sound, v_F the Fermi velocity, and ω_D the frequency of phonons with the Debye energy) is due to a decrease in the contribution of reabsorption of nonequilibrium phonons to the spectrum being measured.[2)] However, inelastic scattering processes occurring in the point contact (such as spontaneous and induced emission of phonons by conduction electrons with an excess energy eV or reabsorption of phonons) make an additive contribution to the spectrum,[10] and a decrease in the intensity of such a process should not result in the emergence of new spectral singularities. Consequently, the spectral mode of electron movement in the contact region changes during rf measurements.

The heating of a point contact by the transport current can be responsible for deterioration of its spectroscopic potentialities upon an increase in the constant bias voltage. In this case, rf measurements at frequencies[1] $\omega > \omega_T$ (ω_T

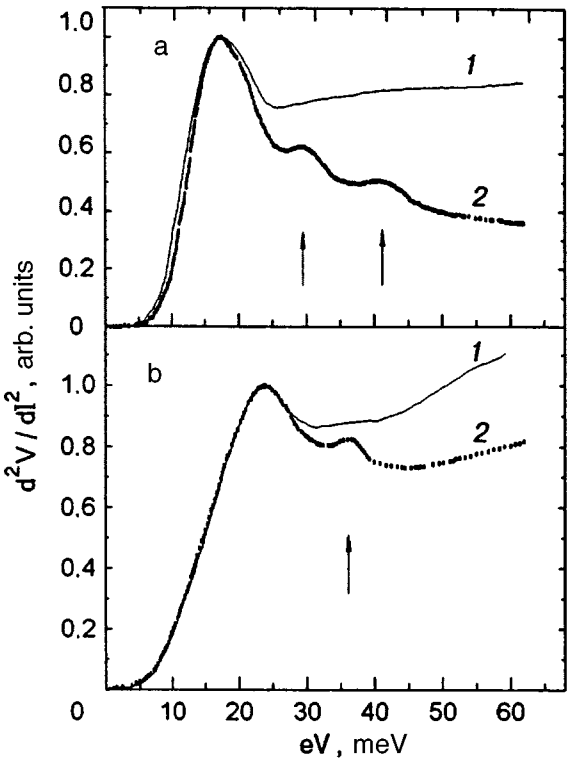

FIG. 1. Point contact spectra for Cu–Cu (2.7 at. % Be) (a) and Ni–Ni (b) measured at a low frequency of 3747 Hz (curve *1*) and at 78 GHz (curve *2*).

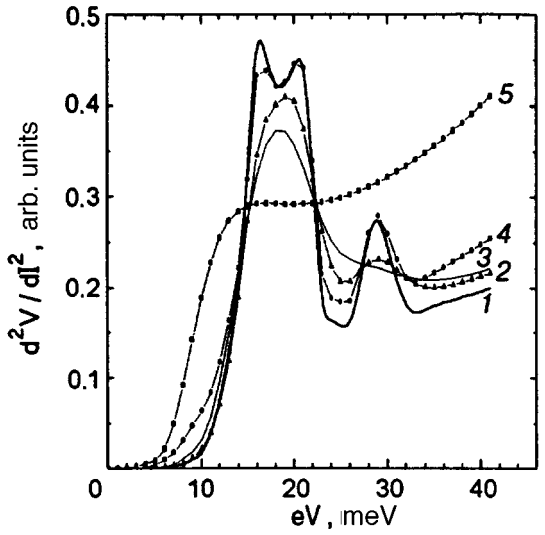

FIG. 2. Evolution of PC spectra of a Cu–Cu contact for various values of overheating $\Delta T = eV/k\gamma$ for $\gamma = \infty$ (curve *1*), 40 (curve *2*), 20 (curve *3*), and 4 (curve *5*); curve *4* corresponds to overheating of the phonon subsystem only ($\gamma = 4$).

$\propto sl_i/d^2 \sim 1$ GHz is the temperature relaxation frequency for the contact) must reduce the influence of thermal effects considerably, thus improving spectral resolution. In order to verify this assumption, we calculated the current-voltage characteristics (IVC) and their second derivatives (PC spectra) under the condition of contact overheating by displacement current. Calculations were made for a copper contact with the resistance $R_0 = 5\Omega$ at the helium bath temperature $T_0 = 1.5$ K by using tabulated values of the point-contact electron-phonon interaction function $g_{pc}(\varepsilon)$.[1] The following expression was used for IVC[11,12]:

$$I(V) = \frac{V}{R_0} - C\int_0^\infty \left[\frac{\varepsilon - eV}{e^{\beta(\varepsilon - eV)} - 1} - \frac{\varepsilon + eV}{e^{\beta(\varepsilon + eV)} - 1} + 2eVN(\varepsilon) \right] g_{pc}(\varepsilon)\, d\varepsilon, \quad (1)$$

where $C = 8d/3e\hbar v_F R_0$; $\beta = 1/kT$; R_0 is the contact resistance at zero bias voltage, and T the temperature. The nonequilibrium phonon distribution function $N(\varepsilon)$ for complete reabsorption of phonons is taken in the form

$$N(\varepsilon) = \frac{1}{4\varepsilon}\left[\frac{2\varepsilon}{e^{\beta e} - 1} + \frac{\varepsilon - eV}{e^{\beta(\varepsilon - eV)} - 1} + \frac{\varepsilon + eV}{e^{\beta(\varepsilon + eV)} - 1} \right]. \quad (2)$$

The point contact temperature was defined in the form $T = T_0 + \Delta T$, where $\Delta T = eV/k\gamma$. Figure 2 shows the initial PC spectrum without overheating (curve *1*) and various modifications of the spectrum for several values of the coefficient γ: from $\gamma = 4$, which is typical of the thermal mode, to $\gamma = 40$. Curve *4* in this figure shows the point contact spectrum in the case when only the subsystem of nonequilibrium phonons excited by electrons is heated for $\gamma = 4$, i.e., we assume that an equilibrium distribution sets in the phonon system with the temperature determined by the constant bias voltage. In this case, we take into account the fact that the total number of phonons coincides with their number in the absence of equilibrium heating of the entire contact:

$$\int_0^\infty N(\varepsilon, T) g_{pc}(\varepsilon)\, d\varepsilon = \int_0^\infty N(\varepsilon, T_0) g_{pc}(\varepsilon)\, d\varepsilon.$$

Comparing the experimental and theoretical spectra, we can see that curves *1* in Fig. 1 and curve *3* in Fig. 2 are similar. The theoretical spectrum, as well as the experimental spectrum, contains no L-peak and displays a high background level. As the overheating becomes smaller, the quality of theoretical spectra is improved. A similar improvement of the spectra is also observed upon an increase in the voltage modulation frequency to 78 GHz (curves *2* in Fig. 1). Naturally, the calculations made for a static IVC cannot be directly compared with the results of measurements in the dynamic rf mode, but the similarity in the observed effects is obvious. Moreover, for ''dirty'' contacts studied experimentally, the effect of heating must be manifested even more strongly than in the calculations made for the ballistic mode.

Thus, the improvement of resolution of PC spectroscopy in high-frequency measurements ($\omega > \omega_T, \omega_{\text{ph-e}}$) can be attributed to the weaker effects of nonequilibrium phonon reabsorption and point contact heating. Such measurements do not affect spontaneous emission of phonons by nonequilibrium electrons in view of the inequality $\omega \ll \omega_{\text{e-ph}} \sim 10^4$ GHz. It should be noted that in experiments with low-frequency interruption of rf radiation $\omega_M \tau_i \ll 1$ (quasistatic mode), the signal being measured contains a contribution of the bolometric effect due to the presence of nonequilibrium phonons induced by rf current in the contact. The amplitude of the bolometric signal increases with the bias voltage across the

contact, leading to the emergence of residual background in rf spectra. For this reason, dynamic measurements of two mixed rf signals or second harmonic amplitude at a high frequency are preferable.[4]

The author is grateful to O. I. Shklyarevskii and A. G. Shkorbatov for fruitful discussions of the results of this research.

*E-mail: balkashin@ilt.kharkov.ua

[1)]The value of the ratio l_i/d estimated from the intensity of the PC spectrum[8] for a given contact is ~ 0.01.

[2)]The characteristic electron-phonon scattering frequency is 5 GHz for copper[4] and ~ 6 GHz for nickel according to estimates.

[1] I. K. Yanson and A. V. Khotkevich, *Atlas of Point Contact Spectra of Electron-Phonon Interaction in Metals* [in Russian], Naukova Dumka, Kiev (1986).
[2] I. K. Yanson and O. I. Shklyarevskii, Fiz. Nizk. Temp. **12**, 899 (1986) [Sov. J. Low Temp. Phys. **12**, 509 (1986)].
[3] I. O. Kulik and M. V. Moskalets, Fiz. Nizk. Temp. **15**, 405 (1989) [Sov. J. Low Temp. Phys. **15**, 229 (1989)].
[4] O. P. Balkashin, I. K. Yanson, and Yu. A. Pilipenko, Fiz. Nizk. Temp. **13**, 389 (1987) [Sov. J. Low Temp. Phys. **13**, 222 (1987)].
[5] O. P. Balkashin, I. K. Yanson, and Yu. A. Pilipenko, Fiz. Nizk. Temp. **17**, 221 (1991) [Sov. J. Low Temp. Phys. **17**, 114 (1991)].
[6] O. P. Balkashin and I. I. Kulik, Fiz. Nizk. Temp. **21**, 45 (1995) [Low Temp. Phys. **21**, p. 32 (1995)].
[7] O. P. Balkashin, Physica B **B218**, 54 (1996).
[8] O. P. Balkashin and Yu. A. Pilipenko, Fiz. Tverd. Tela (Leningrad) **33**, 2584 (1991) [Sov. Phys. Solid State **33**, 1460 (1991)].
[9] Yu. G. Naidyuk, N. A. Chernoplekov, Yu. A. Shitikov *et al.*, Zh. Éksp. Teor. Fiz. **83**, 1177 (1982) [Sov. Phys. JETP **56**, 671 (1982)].
[10] O. P. Balkashin, I. K. Yanson, V. S. Solov'ev, and A. Yu. Krasnogorov, Zh. Tekh. Fiz. **52**, 811 (1982) [Sov. Phys. Tech. Phys. **27**, 522 (1982)].
[11] I. O. Kulik, Fiz. Nizk. Temp. **11**, 937 (1985) [Sov. J. Low Temp. Phys. **11**, 516 (1985)].
[12] O. P. Balkashin and I. I. Kulik, Fiz. Nizk. Temp. **18**, 1357 (1992) [Sov. J. Low Temp. Phys. **18**, 946 (1992)].

Translated by R. S. Wadhwa

A new variational method in the problem of the spectrum of elementary excitations in an edge-dislocation crystal

I. M. Dubrovskii

Institute of Metal Physics, National Academy of Sciences of the Ukraine, 252142 Kiev, Ukraine
(Submitted May 23, 1997; revised July 28, 1997)
Fiz. Nizk. Temp. **23**, 1300–1304 (December 1997)

A new method based on a combination of the direct variational method and perturbation theory is proposed to calculate approximately the eigenvalues and eigenfunctions of ground state and the states close to it. The new method is applicable to the Schrödinger equation with a potential proportional to the dilatation produced by an edge dislocation. The ground-state energy obtained in this case is lower than the theoretical values obtained in other works. The energy value is obtained for the lowest state for which the eigenfunction is odd in the azimuthal angle. It is assumed that the spectrum may be described only statistically near the condensation point. © *1997 American Institute of Physics.* [S1063-777X(97)00612-9]

1. While applying the variational method for calculating the spectrum of the Schrödinger equation, the ground-state function is chosen in such a form that it depends on several variational parameters, and the average Hamiltonian for this function is minimized with respect to the parameters. The functions corresponding to the excited states must also satisfy the orthogonality conditions. Hence attempts are made sometimes to select straightaway a system of orthogonal functions of which one (without any nodal surfaces) will be the ground state function. If this system of functions is not complete, it may lead only to a certain sequence of eigenvalues instead of the entire spectrum in a certain interval. The results depend on the appropriate choice of the form of the trial function, and there is no technique for estimating the correctness. Trial functions are not an approximation of true eigenfunctions and cannot be used, say, for approximate calculation of the probability of transitions between stationary states.

The approach proposed in this work is free from the above-mentioned drawbacks of the variational technique since it is a combination of the variational technique and the perturbation theory. The initial Hamiltonian $\hat{H}$ can be represented in the form

$$\hat{H} \equiv \hat{H}_0(\{\alpha_i\}) + \hat{H}_1(\{\alpha_i\}), \tag{1}$$

where $\{\alpha_i\}$ is a certain set of parameters and $\hat{H}_0$ the Hamiltonian whose spectrum and eigenfunctions can be determined, say, by separation of variables. If $\hat{H}$ commutes with a certain operator $\hat{A}$, it is desirable to choose $\hat{H}_0$ in such a way that it also commutes with $\hat{A}$. The values of the parameters $\{\alpha_i\}$ are determined in the course of the variational procedure. For the rest, the splitting in (1) is arbitrary, and there are no general criteria for its choice although, as will be shown below, this choice determines the closeness of the obtained results to the exact values of the principal and low-excitation eigenvalues of $\hat{H}$. The system of eigenfunctions $\hat{H}_0$ is used as trial functions in the standard variational procedure. The average value of $\hat{H}$ in the ground state $\hat{H}_0$ is minimized with respect to the parameters $\{\alpha_i\}$, and an approximate value is obtained for the minimum eigenvalue of $\hat{H}$ and the set of values of $\{\alpha_i\}_{\min}$. It can be assumed that the mean values of $\hat{H}$ in the functions of the excited states $\hat{H}_0$ for the values of $\{\alpha_i\}_{\min}$ are approximate values for the corresponding eigenvalues of $\hat{H}$. This approximation can be evaluated by turning to the Rayleigh–Schrödinger perturbation theory. In this theory, the obtained eigenvalues are the first approximation in the perturbation $\hat{H}_1$ for the values of $\{\alpha_i\}_{\min}$. The quality of the approximation can be estimated by calculating the values of the expansion parameters $\langle n|\hat{H}_1|m\rangle/(E_n - E_m)$ in the perturbation theory. In this case, it is obvious that the convergence of series in the perturbation theory may be different for different eigenvalues, since $\hat{H}_1$ is generally not proportional to the small parameter. For example, if the spectrum of $\hat{H}_0$ consists of discrete and continuous parts whose boundary is the point of condensation of discrete values, the perturbation theory is not applicable for values close to this point. If the decomposition (1) can be chosen in such a way that the expansion parameters are smaller than unity at least for the ground state, the perturbation theory can be used not only to estimate the accuracy of the obtained value, but also to improve it. Indeed, the second-approximation correction for the ground state energy is always negative. Hence the second approximation will always give a smaller, i.e., more precise, value. Generally speaking, the value of $\{\alpha_i\}_{\min}$ should be determined from the condition of minimum of the expression for the ground state energy in the second approximation of perturbation theory. This would correspond to the use of functions in the first approximation in $\hat{H}_1$ as trial functions in the variational procedure. It can be shown that an improvement (i.e., decrease) in the ground-state energy in comparison with the values obtained by using the above procedure is of the fourth order of the expansion parameter in perturbation theory. There is simply no need to resort to minimization of the ground-state energy if we somehow determine the parameters $\{\alpha_i\}$ of the decomposition (1) in such a way that the parameters of the perturbation theory are smaller than unity. The parameters $\{\alpha_i\}_{\min}$ are simply the best choice of the separation param-

eters for which the series in the perturbation theory converge in the best way (for a given choice of the decomposition (1)). If $\hat{H}$ commutes with a certain operator $\hat{A}$, the spectrum of $\hat{H}$ can be divided into subsystems of levels, each of which corresponds to one eigenvalue of $\hat{A}$. Each subsystem has its own state with the minimum eigenvalue of $\hat{H}$, which can be determined in the same manner by requiring additionally that the functions are the eigenfunctions of $\hat{A}$ for a certain eigenvalue. In this case, the values of $\{\alpha_i\}^A_{\min}$ may be different for different subsystems, but it is necessary that $\hat{A}$ commute with $\hat{H}_0$ also. In each subsystem, the excited states can be determined with the help of the perturbation theory for values of $\{\alpha_i\}^A_{\min}$ obtained for the ground state, while the corresponding parameters in the perturbation theory are quite small.

2. To illustrate the potentialities of this method, we consider the equation

$$-\frac{\partial^2\psi}{\partial\rho^2}-\frac{1}{\rho}\frac{\partial\psi}{\partial\rho}-\frac{1}{\rho^2}\frac{\partial^2\psi}{\partial\varphi^2}-\frac{\cos\varphi}{\rho}\psi=\varepsilon\psi. \tag{2}$$

Many problems in the physics of crystals which contain edge dislocations (see Refs. 1–3) can be reduced to this equation in dimensionless polar coordinates, that does not contain any parameters. The density of negative values of ε near zero was estimated semiclassically by Lifshits and Pushkarov.[1] Nabutovskii and Shapiro[2] used the conventional variational technique to obtain the ground-state energy, while Slyusarev and Chishko[3] obtained a better (lower) value for this energy. The Hamiltonian in Eq. (2) commutes with the operator reversing the sign of φ, hence the levels are split into two subsystems corresponding to functions that are even and odd in φ. Levels corresponding to even functions only are considered in Ref. 3.

In problems that are usually solved by using perturbation theory, the Hamiltonian naturally splits into the zeroth Hamiltonian for which the eigenvalue problem is easily solved, and a perturbation that is proportional to a small parameter. The expansion parameters in the perturbation theory are proportional to this small parameters and therefore are also small. Such a natural splitting does not occur for Eq. (2), and hence the perturbation theory was not applied to them. We choose

$$\hat{H}_0=-\frac{\partial^2}{\partial\rho^2}-\frac{1}{\rho}\frac{\partial}{\partial\rho}-\frac{1}{\rho^2}\frac{\partial^2}{\partial\varphi^2}-\frac{q\cos\varphi}{2\rho^2}+\frac{\alpha_1}{4\rho^2}-\frac{\alpha_2}{\rho}. \tag{3}$$

Here, the vibrational parameters are denoted by q, α_1, and α_2. Note that $\hat{H}_0$ contains a potential proportional to ρ^{-2}, and hence has eigenfunctions satisfying the conventional continuity and integrability conditions only if $2q>\alpha_1$, i.e., if the sign of this potential varies with φ. It will be shown below that the Hamiltonian $\hat{H}_0$ has a spectrum consisting of a discrete part and a continuous part, as well as $\hat{H}$. Moreover, it also has a similar angular dependence of the potential. In the eigenvalue problem for $\hat{H}_0$, the variables are separated, and the complete system of eigenfunctions can be expressed in terms of known transcendental functions. It is hard to formulate any additional concepts determining the choice of $\hat{H}_0$ in the form (3). This is probably not the only possible choice, and may not even be the best one. The final confirmation about the propriety of such a choice of decomposition of $\hat{H}$ comes from the computation of the expansion parameters in the perturbation theory. The variables in the equation $\hat{H}_0\psi=\varepsilon^{(0)}\psi$ can be separated, and the equation for the function $\Phi(\varphi)$ assumes the form

$$\frac{d^2\Phi}{dz^2}+(a-2q\cos 2z)\Phi=0. \tag{4}$$

Here, we have made the substitution $\varphi=2z+\pi$ to transform the above expression into Matthieu's canonical equation (see Ref. 4). The condition of periodicity in φ with a period 2π is satisfied by Matthieu's functions $ce_{2m}(z,q)$ and $se_{2m}(z,q)$ with the even index. They form a complete system of functions on the segment $-\pi/2\leqslant z\leqslant\pi/2$. For each q, the separation constant a assumes an infinite set of discrete values depending on the index and parity of the functions. The function $ce_0(z,q)$ does not have zeros; hence this is the function corresponding to the ground state. The solution of the radial equation is known (see Ref. 5). The ground-state function has the form

$$\psi_{00}=A_{00}\pi^{-1/2}ce_0(z,q)\exp(-\beta\rho)\rho^\gamma, \tag{5}$$

where β and γ are certain functions of q, α_1 and α_2, and A_{00} is the normalization constant. The mean value of the total Hamiltonian from Eq. (2) in the function ψ_{00}, which must be minimized, assumes the following form after integration with respect to z:

$$\varepsilon_{00}=A_{00}^2\int_0^\infty\exp(-\beta\rho)\rho^{\gamma+1}\left[\left(-\frac{d^2}{d\rho^2}-\frac{1}{\rho}\frac{d}{d\rho}+\frac{C_0^2}{4\rho^2}-\frac{C_0^2-a_0}{2q\rho}\right)\exp(-\beta\rho)\rho^\gamma\right]d\rho. \tag{6}$$

Here, $a_0(q)<0$ is the eigenvalue of Eq. (4) for $\Phi=ce_0(z,q)$, and

$$C_0^2=-\frac{2}{\pi}\int_{-\pi/2}^{\pi/2}ce_0(z,q)\frac{d^2}{dz^2}ce_0(z,q)dz=\frac{2}{\pi}\int_{-\pi/2}^{\pi/2}\left[\frac{d}{dz}ce_0(z,q)\right]^2dz. \tag{7}$$

The last term in the integrand operator is calculated by multiplying Eq. (4) for $\Phi=ce_0(z,q)$ by $ce_0(z,q)$, and integrating with respect to z. Instead of minimizing in α_1 and α_2, we can make use of the fact that the minimum of ε_{00} is attained by the eigenfunction of the integrand operator for any $q>0$. In this case, we obtain

$$\beta(q)=\frac{C_0^2-a_0}{2q(C_0+1)},\quad \gamma(q)=\frac{C_0}{2},\quad \varepsilon_{00}(q)=-\beta^2. \tag{8}$$

It remains for us to minimize $\varepsilon_{00}(q)$ in q by numerical tabulation according to Ref. 6. In order to compute C_0^2 in this case, we use the expansion of $ce_0(z,q)$ into a Fourier series, whose coefficients are given in Ref. 6. We obtain

$$q_{\min}=4\pm 0.05,\ \ \varepsilon_{00}^{(0)}=-0.1053,\ \ C_0/2=0.6466. \tag{9}$$

The eigenfunctions and eigenvalues of the Hamiltonian $\hat{H}_0$ are classified according to three quantum numbers, viz., radial quantum number $n=0,1,2,\ldots$, the quantum number $\sigma=0,1$ determining the parity of a function relative to the reversal of sign of z [the eigenvalue of the sign-reversal operator $(-1)^{\sigma}$], and m the index of the Mathieu function, which assumes all even values starting from zero for $\sigma=0$ and from 2 for $\sigma=1$. They have the following form:

$$|n\sigma m\rangle=\frac{A_{n\sigma m}}{\sqrt{\pi}}\exp(\rho\sqrt{-\varepsilon_{n\sigma m}^{(0)}})\rho^{\mu}F(-n,2\mu+1,2\rho\sqrt{-\varepsilon_{n\sigma m}^{(0)}})[\delta_{\sigma 0}ce_m+\delta_{\sigma 1}se_m],$$

$$\mu(\sigma,m)=\frac{1}{2}(\delta_{\sigma 0}a_m+\delta_{\sigma 1}b_m+\alpha_1)^{1/2},$$

$$\varepsilon_{n\sigma m}^{(0)}=-\frac{\alpha_2^2}{(2\mu+2n+1)^2},$$

$$A_{n\sigma m}=\frac{(2\sqrt{-\varepsilon_{n\sigma m}^{(0)}})^{\mu+1}}{\Gamma(2\mu+1)}\left(\frac{\Gamma(2\mu+n+1)}{n!(2\mu+n+1)}\right)^{1/2}. \tag{10}$$

Here, $F(-n,2\mu+1,2\rho\sqrt{-\varepsilon_{n\sigma m}^{(0)}})$ is the degenerate hypergeometric function, $A_{n\sigma m}$ the normalized constant of the radial function (see Ref. 7 for computing this function as well as other functions encountered in the computation of matrix elements), and δ_{ik} the Kronecker delta. According to Ref. 4, the eigenvalues of Mathieu functions are denoted by a_m for even functions and by b_m for odd functions. For the value of q obtained above, all these eigenvalues are positive except a_0. Comparing (10) with (5) and considering (8), we obtain

$$\alpha_1=C_0^2-a_0=5.9529;\ \ \alpha_2=\frac{\alpha_1}{2q}=0.7441. \tag{11}$$

The correction to the ground-state energy in the first approximation of perturbation theory is equal to zero. Averaging of the total Hamiltonian $\hat{H}$ in the functions (10) gives values of the excited-state energy in the first approximation of perturbation theory that are different from $\varepsilon_{n\sigma m}^{(0)}$. These values have meaning only for the excited states for which perturbation theory is applicable.

Let us calculate the highest term in the second approximation of perturbation theory for the ground-state energy:

$$\hat{H}_1=-\frac{q_{\min}\cos 2z}{2\rho^2}-\frac{C_0^2-a_0}{4\rho^2}+\frac{C_0^2-a_0}{2q_{\min}\rho}+\frac{\cos 2z}{\rho}. \tag{12}$$

The matrix elements of $\hat{H}_1$ on functions for the ground state and others with $m=0$ are equal to zero. The closest state with a nonzero matrix element is $|002\rangle$. In this case,

$$\langle 000|\hat{H}_1|002\rangle=0.0336,\ \frac{\langle 000|\hat{H}_1|002\rangle}{\varepsilon_{000}-\varepsilon_{002}}=-0.4264,$$

$$\varepsilon_{000}^{(2)}=-0.1196. \tag{13}$$

Thus, the obtained value of the ground-state energy is lower than the best value (-0.1111) obtained by Slyusarev and Chishko.[3] The relative decrease is more than 8%. Another result having a physical meaning is the lowest exponent of ρ as $\rho\to 0$. The value of this exponent obtained in Ref. 3 is equal to 0.75, while in the method considered here, $\mu_{00}=0.6466$.

Similarly, we can calculate the energy and exponent for the lowest odd state:

$$q_{\min}=25,\quad \alpha_1=34.9688,\quad \alpha_2=0.6994,$$

$$\mu_{012}=1.8476,$$

$$\left|\frac{\langle 210|\hat{H}_1|014\rangle}{\varepsilon_{012}-\varepsilon_{014}}\right|=0.458,\quad \varepsilon_{012}^{(2)}=-0.0252. \tag{14}$$

3. The above example shows that the new method allows us to obtain better and more comprehensive results than the conventional variational procedure. The results for eigenvalues can be improved further by calculating other terms also in second order perturbation theory. However, for levels for which perturbation theory is applicable, the eigenfunctions in the first approximation in perturbation theory can be regarded as approximate expressions for true eigenfunctions. This means that they can be used to calculate the matrix elements for other operators with the same accuracy as the eigenvalues.

The restriction on the applicability of perturbation theory for the ground state and low-excited states in the case when the spectrum has a condensation point is probably of fundamental importance. If the variables in the eigenvalue problem for the Hamiltonian $\hat{H}$ are separable, this problem can be considered by using the WKB approach in the vicinity of the condensation point.[8] This technique can be used to justify a transition to the classical integrable problem. The point of condensation of eigenvalues corresponds to a separatrix dividing the regions of finite and infinite motion of the corresponding classical particle. If the variables can be separated only in the Hamiltonian $\hat{H}_0$, the correction $\hat{H}_1$ corresponds to the loss of all integrals of motion except the energy. The WKB approach becomes inapplicable, and there are no methods known which would permit the calculation of the eigenvalues $\varepsilon(n)$ for large n, where n is the level number counted from the ground state in ascending order. In classical mechanics, the loss of integrals of motion leads to random motion of a particle, especially near the separatrix.[9] It can be assumed that this corresponds to the absence of an algorithm for calculating $\varepsilon(n)$ for large n in the eigenvalue problem. In this case, the spectrum can be described by using statistical concepts only, like the density of states. For the equation considered in Sec. 2, such a description was used in Ref. 1.

[1] I. M. Lifshits and Kh. I. Pushkarov, Pis'ma Zh. Éksp. Teor. Fiz. **11**, 456 (1970) [JETP Lett. **11**, 310 (1970)].
[2] V. M. Nabutovskii and B. Ya. Shapiro, Pis'ma Zh. Éksp. Teor. Fiz. **26**, 624 (1977) [JETP Lett. **26**, 473 (1997)].
[3] V. A. Slyusarev and K. A. Chishko, Fiz. Met. Metalloved. **58**, 877 (1984).

[4] *Handbook of Mathematical Functions* (edited by M. Abramowitz and I. Steegun), Dover, New York, 1965.
[5] V. L. Bonch-Bruevich, Fiz. Tverd. Tela (Leningrad) **3**, 47 (1961).
[6] *Tables for Computing Matthieu Functions* [in Russian], Comp. Center, USSR Acad. Sci., Moscow (1967).
[7] L. D. Landau and E. M. Lifshitz, *Quantum Mechanics* [in Russian], Fizmatgiz, Moscow (1967).
[8] N. Fröman and P. Fröman, *JWKB Approximation*, Amsterdam (1965).
[9] G. M. Zaslavskii, *Chaos in Dynamical Systems*, Harwood, Chur, 1985.

Translated by R. S. Wadhwa

Hyperfine-interaction-driven Aharonov–Bohm effect in mesoscopic rings

I. D. Vagner,[1] A. S. Rozhavsky,[2] and P. Wyder[1]

[1]*Grenoble High Magnetic Field Laboratory Max-Planck-Institut für Festkörperforschung and Centre Nationale de la Recherche Scientifique, BP 166, 38042 Grenoble Cedex 09, France**
[2]*B. I. Verkin Institute for Low Temperature Physics and Engineering, National Academy of Sciences of Ukraine, 47, Lenin Ave., 310164, Kharkov, Ukraine***

(Submitted April 21, 1997; revised July 23, 1997)
Fiz. Nizk. Temp. **23**, 1305–1308 (December 1997)

It is shown qualitatively that lifting of the electron spin degeneracy by a hyperfine field, which is generated by a nonequilibrium nuclear spin distribution, and breaking of the left-right symmetry by the spin-orbit interaction in a closed ring produces under certain conditions a persistent current, which demonstrates the Aharonov–Bohm-like oscillations with time in GaAs/AlGaAs-based mesoscopic rings even in the absence of an external magnetic field. The typical time interval of these (meso-nucleospinic) oscillations is of the order of several seconds, which is typical of the nuclear spin relaxation times in heterojunctions. © *1997 American Institute of Physics.* [S1063-777X(97)00712-3]

The persistent currents (PC) in multiconnected mesoscopic conductors reflect the broken clockwise-anticlockwise symmetry, which is usually caused by the external vector potential. Experimentally, PCs are observed when an adiabatically slow, time-dependent, external magnetic field is applied along the ring axis.[1–3] The magnetic field variation results in the oscillatory behavior, with the magnetic flux quantum $\Phi_0 = hc/e$ (or its harmonics), of the diamagnetic moment (the PC), which is a manifestation of the Aharonov–Bohm effect.[4]

We propose that the persistent current exist in a GaAs/AlGaAs quantum ring with a nonequilibrium nuclear spin population, even in the absence of an external magnetic field. We predict the ABE-like oscillations of PC with time during the time interval of the order of nuclear spin relaxation time T_1, which is known to be long in semiconductors at low temperatures. The physics behind these oscillations can be understood along the following lines. The hyperfine field, which is caused by the nonequilibrium nuclear spin population,[5] breaks the spin symmetry of conduction electrons which, combined with a strong spin-orbit coupling, results under certain conditions in the breaking of the rotational symmetry of diamagnetic currents in a ring. Under the topologically nontrivial spin distribution, the hyperfine field produces the Berry phase analogous to one which emerges in textured mesoscopic rings.[7–11]

We note that this is the first of a series of ''meso-nucleospinic'' effects, which take place in different systems with broken symmetry due to the combined action of the hyperfine field and spin-orbit coupling.

Let us first examine the nature of the hyperfine electron-nuclear spin interaction and of the electron spin-orbit interaction in typical heterojunctions.

The hyperfine interactions in GaAs heterojunctions and similar quantum Hall systems attracted recently sharply growing theoretical[12] and experimental[13–15] attention. The main physical interest in this subject is based on the fact that the discrete nature of the electron spectrum in these systems results in the exponential ($\exp(\Delta/T)$, where Δ is the mean electron energy spacing, and T is the temperature dependence of the nuclear spin relaxation times T_1 on the system parameters). We assume here that similar law should apply for the nanostructures with well-defined size quantization of the electron spectrum. Note that in this case T_1 is very sensitive to the potential fluctuations caused by the inhomogeneous distribution of impurities in a heterojunction. Indeed, as it was discussed in Ref. 16, the impurity potential modulates the spacing, thus providing faster nuclear relaxation.

Intensive experimental studies of this phenomenon have provided a more detailed knowledge of the hyperfine interaction between the nuclear and electron spins in heterojunctions and quantum wells. It was observed that the nuclear spin relaxation time in GaAs/AlGaAs is rather long (up to 10^3 sec)[13] and the hyperfine field acting on electron spins in this material is extremely high, up to 10^4 g.[14,15] Based on this knowledge we suggest that once the nonequilibrium population of nuclear spins is created, the hyperfine field may strongly influence the electron transport and persistent currents in nanostructures in sufficiently long time.

In this brief note we show qualitatively that the combined action of the hyperfine nuclear field and the electron spin-orbit interaction breaks the time reversal symmetry in a mesoscopic ring (i.e., a sufficiently small ring so that quantum-mechanical phase coherence is preserved), formed in a GaAs/AlGaAs 2DEG, which results in an oscillating persistent current at millikelvin temperatures. The detailed theory will be published elsewhere.

The contact hyperfine interaction between the electron and nuclear spins is described by the following term in the Hamiltonian:[6]

$$\hat{H}^{en}_{chf} = \frac{8\pi}{3}\,\mu_B \gamma_h \hbar^2 \sum_i I_i S\,\delta(r_e - R_i) \qquad (1)$$

where μ_B and γ_h are the conduction electron and the nuclear magnetons; I, S, R_i, and r_e are the nuclear and the electron spins and position vectors, respectively; and $\delta(r_e - R_i)$ reflects the fact that the s-electrons have a nonvanishing probability on the nuclei. Since the conduction quasiparticle wavelength in GaAs is much larger than the internuclei distance, it follows from Eq. (1), that once the nuclear spins are polarized, i.e., if $\langle \Sigma_i I_i \rangle \neq 0$ (Refs. 13–15), the electron spins will experience an effective hyperfine field, which lifts the electron spin degeneracy even in the absence of an external magnetic field. In GaAs/AlGaAs one may achieve the spin splitting due to hyperfine field of the order of the Fermi energy: $\mu_B H_{chf} \cong \varepsilon_F$ (Refs. 14 and 15), which is of the order of 1 K.

Let us assume, therefore, that only one electron spin orientation is populated during the time interval of the order of the nuclear spin relaxation time T_1. It is quite obvious that under the topologically nontrivial spin texture (see below) switching on electron spin-orbit interaction in the system of spin-polarized electrons will produce a persistent current.

The standard expression for the spin-orbital interaction

$$\hat{H}_{\rm so} = \frac{\hbar}{4m^2c^2} [\nabla V \times \mathbf{p}] \tag{2}$$

can be rewritten in the form: $\hat{H}_{\rm so} = \mathbf{p}\hat{\mathbf{A}}_{\rm eff}$, where the effective vector potential operator reflects the combined action of the hyperfine field and of the spin-orbit interaction:

$$\hat{\mathbf{A}}_{\rm eff}(t) = \frac{\hbar}{4mc^2} [\sigma(t) \times \nabla V] = \hat{\mathbf{A}}^0_{\rm eff} \exp\left(- \frac{t}{T_1} \right). \tag{3}$$

In what follows we restrict the discussion to the case of GaAs/AlGaAs heterostructure-based mesoscopic rings. Spin-orbit interaction in semiconductors can be caused by impurities, boundaries, etc. In GaAs there is a well-known mechanism, attributable to the crystal anisotropy,[17] which can be presented as

$$\hat{H}_{\rm so} = \frac{\alpha}{\hbar} \sum_i [\sigma_i \times \mathbf{p}] v. \tag{4}$$

Here $\alpha = 0.6 \times 10^{-9}$ eV·cm for holes with $m^* = 0.5 m_0$ (m_0 is the free electron mass); σ and $\mathbf{p}$ are the charge carrier spin and momentum; and v is the normal to the surface.

We obtain for the effective vector potential operator [Eq. (3)] the estimate

$$\hat{A}^{\rm GaAs}_{\rm eff} \cong \frac{\alpha m^*}{\hbar}. \tag{5}$$

Under real conditions we have $\mu_B H_{ehf} \gg \alpha / L$, where L is the loop perimeter, and the electron spin projection is a well-defined quantum number. The vector potential [Eq. (5)] generates a persistent current, which is the sum over the partial current carried by the individual energy levels with different projections of the electron spin.

The result of summation is an oscillatory dependence of PC on the effective flux across the loop:

$$2\pi\varphi = \frac{1}{\hbar} \oint dl \langle A^{\rm GaAs}_{\rm eff} \rangle = \frac{L \langle\langle \alpha \rangle\rangle}{\hbar^2} \langle \sigma(t) \rangle, \tag{6}$$

where the brackets stand for quantum averaging, and the double brackets denote

$$\langle\langle \alpha \rangle\rangle = \frac{1}{L} \oint \alpha(t) dl. \tag{7}$$

For a micron ring formed in a GaAs/AlGaAs 2DEG, $2\pi\varphi \sim 30 \langle \sigma(t) \rangle$. The value of $\langle \sigma(t) \rangle$ depends on the particular features of the relaxation dynamics.

To estimate the amplitude of a PC generated by a time-dependent flux [Eq. (6)], we must establish the hierarchy of time scales in a micron ring at the level of millikelvins.

The time scales are the nuclear magnetization relaxation time T_1, the ballistic time $\hbar/\Delta \propto L/V_F$, the phase-breaking time $\tau_\varphi \cong \tau_{\rm in}$, where $\tau_{\rm in}$ is the time of inelastic electron scattering, and τ_e is one of the elastic processes.

The time τ_e in quasi-one-dimensional GaAs/AlGaAs rings is governed mainly by smooth tails of the impurity potential located in the ''spacer''.[20,21] In an actual experiment[3] the elastic mean free path is of the order of 10 μm.

The inelastic time $\tau_{\rm in}$ in quasi-one-dimensional quantum rings is defined by a combined action of the electron-phonon scattering and the elastic scattering.[20] Under the condition $\mu_B H_{ehf} \sim \varepsilon_F \gg \Delta \gg T$ the electron-spin-lattice[22] scattering in a ring is suppressed. It is estimated[20] to be $\tau_\varphi \cong 10^{-7} - 10^{-8}$ sec.

In our case the time T_1 far exceeds all the microscopic electron times, $T_1 \gg (\hbar/\Delta, \tau_\varphi, \tau_e)$, which evidently means that energy relaxation restores the equilibrium distribution of the electron levels, and we have a thermodynamic situation.[20] When $L \sim l_e \ll L_\varphi$, the persistent current can be calculated as[4]

$$j_{PC} = -c \frac{\partial F}{\partial \Phi_{\rm ext}} \Big|_{\Phi_{\rm ext}=0}, \tag{8}$$

where F is the free energy, and $\Phi_{\rm ext}$ is the probe external flux. The thermodynamic value of $\langle \sigma(t) \rangle$ in Eq. (6) is $\mu_B H_{ehf}(t)/\varepsilon_F \cong 1$.

In light of the above discussion, we estimate the persistent current in a fully spin-polarized gas when $\Delta \gg T$ to be

$$j_{PC} \cong \frac{eV_F}{L} \sum_{k=1}^{\infty} \frac{\sin(2\pi k \varphi_0 \exp(-t/T_1))}{k}, \tag{9}$$

where $\varphi_0 \cong L \langle\langle \alpha \rangle\rangle \hbar^{-2} m^*$.

The oscillations of persistent current arise due to the exponential time dependence of the phase $\varphi_0 \exp(-t/T_1)$ in Eq. (9), with the time constant T_1, which in GaAs can be of the order of several seconds at a temperature of several millikelvins.[5] We note the marked difference between the time dependence of standard AB oscillations, which are usually observed under the condition of linear time variation of the applied magnetic field, and the hyperfine driven oscillations, which die out due to the exponential time dependence of the nuclear polarization.

Let us now consider experimental feasibility of the proposed effect. A nuclear spin configuration should be created when the circulation of the effective vector potential is a nonzero topological invariant [Eq. (6)]. In the geometry

where the vector v in Eq. (4) is normal to the heterojunction, either the nuclei, which are pumped along some direction in the plane of the ring, or the spin-orbit coupling should be inhomogeneous along the perimeter, say, due to the inhomogeneous distribution of impurities. Since in a GaAs/AlGaAs heterojunction the characteristic length of the impurity potential is of the order of several hundreds Å, i.e., comparable to the ring width, the mesoscopic sensitivity to a single impurity position may produce a nonvanishing phase [Eq. (6)]. The influence of the long range impurities on the nuclear spin-relaxation time in heterojunctions was studied in Ref. 16. Note that the spin-orbit-produced PC considered above is not averaged in a single ring, in marked contrast with the situation considered in Refs. 8 and 9.

Other mechanisms connected with external potentials like boundaries, heavy-atom impurities along the ring perimeter, and other imperfections, which may enhance the spin-orbit interaction in these systems, will be considered in detail elsewhere.

In summary we propose here the first in a family of hyperfine-field-driven mesoscopic (mesospinic) orbital effects: the Aharonov–Bohm-like oscillations of a persistent current in a GaAs/AlGaAs mesoscopic ring in the absence of external magnetic field. We note that the large (of the order of 1 T) hyperfine field acts on the electron spins only, which results in the nonequilibrium electron spin population. The later, at millikelvin temperatures, under the conditions of the topologically nontrivial texture, $\langle\langle \alpha \rangle\rangle \neq 0$, via the spin-orbit coupling, results in weak persistent currents, which decrease with time due to the nuclear depolarization, during the time interval of the order of the nuclear spin-relaxation time T_1 which can be sufficiently long at low temperatures.

We acknowledge illuminative discussions with Yu. Bychkov, A. Dyugaev, I. Krive, L. Levy, G. Platero, and A. Zyuzin.

I. V. and P. W. acknowledge the support by GIF-German Israeli Foundation for Scientific Research and Development, Grant No. 1-0222-136.07/91.

*E-mail: vagner@labs.polycurs.-gre.fr
**E-mail: rozhavsky@ilt.kharkov.ua

[1] L. P. Levy, G. Dolan, J. Dunsmuir, and H. Bouchiat, Phys. Rev. Lett. **64**, 2074 (1990).
[2] V. Chandrasekhar *et al.*, Phys. Rev. Lett. **67**, 3578 (1991).
[3] D. Mailly, C. Chapelier, and A. Benoit, Phys. Rev. Lett. **70**, 2020 (1991); Physica B **197**, 514 (1994).
[4] See for a review: I. V. Krive and A. S. Rozhavsky, Int. J. Mod. Phys. B **6**, 1255 (1992); A. A. Zvyagin and I. V. Krive, Fiz. Nizk. Temp. **21**, 688 (1995) [Low Temp. Phys. **21**, 533 (1995)].
[5] M. I. Dyakonov and V. I. Perel, in *Modern Problems in Condensed Matter Sciences*, F. Meier and B. P. Zakharchenya (Eds.), North-Holland, Vol. 8 (1984), p. 11.
[6] C. P. Slichter, *Principles of Magnetic Resonance*, Springer-Verlag (1991), Second ed.
[7] D. Loss, P. Goldbart, and A. V. Balatsky, Phys. Rev. Lett. **65**, 1655 (1990).
[8] E. N. Bogachek, I. V. Krive, I. O. Kulik, and A. S. Rozhavsky, Mod. Phys. Lett. B **5**, 1607 (1991).
[9] A. G. Aronov and Y. B. Lyanda-Geller, Phys. Rev. Lett. **70**, 343 (1993).
[10] A. V. Balatsky and B. L. Altshuler, Phys. Rev. Lett. **70**, 1678 (1993).
[11] T.-Z. Qian and Z.-B. Su, Phys. Rev. Lett. **72**, 2311 (1994).
[12] I. D. Vagner and T. Maniv, Phys. Rev. Lett. **61**, 1400 (1988); see for a recent review I. D. Vagner, Yu. A. Bychkov, A. M. Dyugaev, and T. Maniv, Phys. Scr. **66**, 158 (1996).
[13] A. Berg, M. Dobers, R. R. Gerhardts, and K. von Klitzing, Phys. Rev. Lett. **64**, 2563 (1990).
[14] K. Wald, L. P. Kouwenhoven, P. L. McEuen, N. C. Van der Vaart, and C. T. Foxon, Phys. Rev. Lett. **73**, 1011 (1994).
[15] S. E. Barret *et al.*, Phys. Rev. Lett. **75**, 4290 (1995); see for a review R. Tycko *et al.*, Science **268**, 1460 (1995).
[16] S. V. Iordanskii, S. V. Meshkov, and I. D. Vagner, Phys. Rev. B **44**, 6554 (1991).
[17] Yu. A. Bychkov and E. I. Rashba, JETP Lett. **39**, 78 (1984).
[18] Y. Meir, Y. Gefen, and O. Entin-Wohlman, Phys. Rev. Lett. **63**, 798 (1989).
[19] O. Entin-Wohman, Y. Gefen, Y. Meir, and Y. Oreg, Phys. Rev. B **45**, 11890 (1992).
[20] E. N. Bogachek, Yu. M. Galperin, M. Jonson, R. I. Shekhter, and T. Swahn, J. Phys.: Condens. Matter **8**, 2603 (1996).
[21] A. S. Rozhavsky, J. Phys.: Condens. Matter **9**, 1521 (1997).
[22] R. J. Elliott, Phys. Rev. **96**, 266 (1954).

This article was published in English in the original Russian journal. It was edited by S. J. Amoretty.

Classical mesoscopic effect in the resistance of point contacts

Yu. A. Kolesnichenko[1] and A. N. Omelyanchouk[1]

[1]*B. I. Verkin Institute for Low Temperature Physics and Engineering of National Academy of Science of Ukraine, 47 Lenin Ave., 310164 Kharkov, Ukraine**

N. van der Post[2] and A. I. Yanson[1,2]

[2]*Kamerlingh Onnes Laboratorium, Leiden University, P.O. Box 9506, 2300 RA Leiden, The Netherlands***

(Submitted May 22, 1997)
Fiz. Nizk. Temp. **23**, 1309–1314 (December 1997)

The mesoscopic effect of the dependence of the point-contact conductance on the spatial distribution of the impurities is theoretically studied. It is shown that the resistance dependence on the diameter d is not only determined by the electron mean free path l_i, but also by the average distance between the impurities. In the case of two types of impurities with different concentrations the mesoscopic effect is predicted for a dirty point contact ($d \gg l_i$) due to the scattering at specific (e.g., magnetic) impurities with a low concentration. Such contacts were numerically modeled for random distributions of the two types of impurities. © *1997 American Institute of Physics.* [S1063-777X(97)00812-8]

The break-junction technique[1] makes it possible to study electron transport through microconstrictions few nanometers in diameter. The conducting properties of such small contacts are affected by quantum effects such as the $2e^2/h$ conductance quantization observed while changing the diameter of the contact,[2,3] conductance fluctuations due to electron wave interference,[4,5] etc. In ultrasmall contacts, besides the quantum effects,[6,7] the presence of impurities in the contact region produces noticeable classic effects. Such ''classical mesoscopic effects'' cause conductance fluctuations due to the displacement of individual scatterers, and also its stochastic-like dependence on the magnetic field.[8] It was shown in Ref. 9 that individual point defects, which are located at a distance from the constriction comparable to its diameter d, cause a deviation of the size-dependence of a ballistic contact's resistance $R(d)$ from Sharvin's formula.[10,11] If the average distance between the impurities appears greater than or equal to d, we obtain a classical mesoscopic effect—the dependence of additional contact resistance due to the defects on their spatial distribution. We will demonstrate below that an analogous dependence can be also observed in contacts with a short electron mean free path for two types of scatterers of different concentrations. Such a situation can take place, for instance, in experimental observations of size effects in metallic point contacts with magnetic impurities,[12] where a rare spin-flip electron scattering is accompanied by many scatterings at regular impurities which inevitably appear at the point contacts.

We restrict the analysis of classical mesoscopic effects to the semiclassical approximation, assuming that the size is considerably larger than the de Broglie wavelength of electrons.

Assuming that the point contact is an orifice of diameter d in the insulating partition Σ, and separating the two metallic half-spaces, we obtain a situation which is illustrated in Fig. 1. It is assumed that the metal has two types of defects of different effective scattering cross section. The characteristic distance r_0 between the defects of first type (their concentration is $n_i = r_0^{-3}$) is assumed to be smaller than the contact diameter, which allows us to average all equations over the coordinates of these impurities. We call such defects ''the background defects''. The concentration of second-type defects n_i^*, whose interaction with electrons determines the mesoscopic effects, is such that their separation, $r_0^* = n_i^{*-1/3}$, is comparable to d. Such defects are referred to as ''specific impurities.''

The current through the contact can be expressed in terms of the Green–Keldysh function $g_{\mathbf{p}}^K(\mathbf{r},\varepsilon)$ integrated with respect to the energy variable $\xi = \varepsilon_{\mathbf{p}} - \varepsilon_F$ (ε_F is the Fermi energy)[13]:

$$I = \frac{\pi}{2} eN(0) \int_S d^2\rho \int \frac{d\varepsilon}{2\pi} \langle v_z g_{\mathbf{p}}^K(\rho,\varepsilon) \rangle. \tag{1}$$

In this formula the integration with respect to $d^2\rho$ is carried out over the area S of the contact, and v_z is the component of the electron velocity $\mathbf{v} = \partial\varepsilon/\partial\mathbf{p}$ parallel to the contact axis. The angle brackets denote averaging over the directions of the momentum $\mathbf{p}$ at the Fermi surface $\varepsilon_{\mathbf{p}} = \varepsilon_F$, where the density of states is $N(0)$.

In the Keldysh method[13] the retarded $g_{\mathbf{p}}^R$ and advanced $g_{\mathbf{p}}^A$ Green's functions appear along with $g_{\mathbf{p}}^K$. The matrix

$$\hat{g}_{\mathbf{p}} = \begin{bmatrix} g_{\mathbf{p}}^A & g_{\mathbf{p}}^K \\ 0 & g_{\mathbf{p}}^R \end{bmatrix}, \tag{2}$$

which satisfies the normalization condition $\hat{g}_{\mathbf{p}}^2 = 1$ for a nonsuperconducting metal, is the solution of the equation[14]

$$i\mathbf{v}\nabla\hat{g}_{\mathbf{p}} + [\hat{g}_{\mathbf{p}}\Sigma] = [\hat{t}, \nabla\hat{g}_{\mathbf{p}}^{(0)}]. \tag{3}$$

In this equation $\hat{g}_{\mathbf{p}}^{(0)}$ is the matrix of the Green's function for a pure point contact with only the background impurities, the scattering of electrons on which is described by the coordinate-independent matrix of self-energy functions $\hat{\Sigma} = (i/2\tau_i)\langle g_{\mathbf{p}} \rangle$, where τ_i is the characteristic time of the elastic relaxation. The electron interaction with the specific defects is associated with the right side of Eq. (3) which

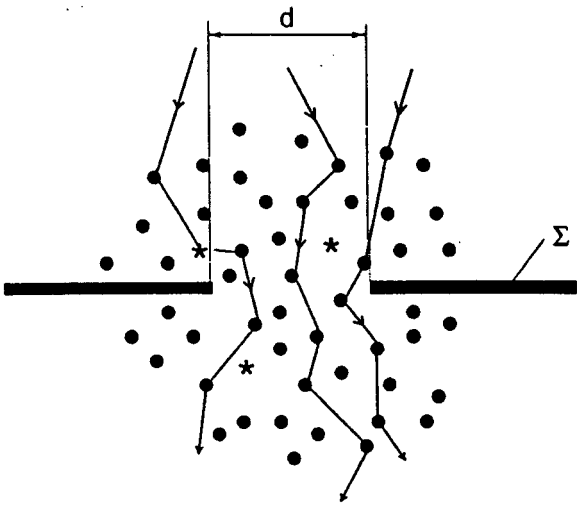

FIG. 1. A model of the point contact as a circular orifice in an insulating partition Σ. The dots represent the background and the stars symbolize the specific defects. The broken lines represent the electron trajectory through the contact.

contains the scattering matrix $\hat{t}$. This matrix can be determined from the Lippman–Schwinger equation

$$\hat{t}=\hat{V}-i\pi N(0)\hat{V}\langle\hat{g}_{\mathbf{p}}^{(0)}\rangle\hat{t}, \tag{4}$$

where $\hat{V}=\hat{V}(\mathbf{r})$ is the scattering potential. Note that the structures of matrices $\hat{\Sigma}$ and $\hat{t}$ are similar to that of (2).

According to Eq. (3) and the normalization condition, the functions $g_{\mathbf{p}}^{R,A}$ in a normal metal are equal to their equilibrium values $g_{\mathbf{p}}^{R}=-g_{\mathbf{p}}^{A}=1$. Taking into account relation (4), the equation for $g_{\mathbf{p}}^{K}$ can be written in the form

$$\mathbf{v}\nabla\hat{g}_{\mathbf{p}}^{K}-I_i(\hat{g}_{\mathbf{p}}^{K})=I_i^*(\hat{g}_{\mathbf{p}}^{(0)K}), \tag{5}$$

where

$$I_i(\hat{g}_{\mathbf{p}})=\frac{1}{\tau_i}\,[\langle g_{\mathbf{p}}\rangle-g_{\mathbf{p}}];\quad I_i^*(\hat{g}_{\mathbf{p}})=2\ \mathrm{Im}\ t^A[\langle g_{\mathbf{p}}\rangle-g_{\mathbf{p}}].$$

The boundary condition

$$g_{\mathbf{p}}^{K}(\mathbf{r},\varepsilon)=G_0\left(\varepsilon-\frac{1}{2}\,eU\ \mathrm{sign}\ z\right)\quad \text{for } |z|\to\infty \tag{6}$$

ensures the restoration of equilibrium in the electron system at the contact banks. In Eq. (6) $G_0(\varepsilon)=2\tanh(\varepsilon/2T)$ is the equilibrium Green's function (T is the temperature), U is the voltage applied to the point contact.

Following the authors of Ref. 15, the function $g_{\mathbf{p}}^{(0)K}(\mathbf{r},\varepsilon)$ can be conveniently expressed as

$$g_{\mathbf{p}}^{(0)K}(\mathbf{r},\varepsilon)=\alpha_{\mathbf{p}}(\mathbf{r})G_0\left(\varepsilon+\frac{eU}{2}\right)+(1-\alpha_{\mathbf{p}}(\mathbf{r}))G_0\left(\varepsilon-\frac{eU}{2}\right), \tag{7}$$

where the voltage-independent function $\alpha_{\mathbf{p}}(\mathbf{r})$ is the probability that an electron arrives at the point $\mathbf{r}$ from $-\infty$ with the momentum $\mathbf{p}$ after being scattered only by the background impurities. The function $\alpha_{\mathbf{p}}(\mathbf{r})$ satisfies a homogeneous equation similar to the one for $g_{\mathbf{p}}^{(0)K}$

$$\mathbf{v}\nabla\alpha_{\mathbf{p}}(\mathbf{r})-I_i(\alpha_{\mathbf{p}}(\mathbf{r}))=0 \tag{8}$$

and also the condition for $|\mathbf{r}|\to\infty$

$$\alpha_{\mathbf{p}}(\mathbf{r}\to\infty)=\theta(z), \tag{9}$$

which is derived from (6).

We write the particular solution $\delta g_{\mathbf{p}}^{K}(\mathbf{r},\varepsilon)$ of a nonhomogeneous equation (5) using the corresponding Green's function $g_{\mathbf{pp}'}(\mathbf{r},\mathbf{r}')=g_{-\mathbf{p}',-\mathbf{p}}(\mathbf{r}',\mathbf{r})$:

$$\delta g_{\mathbf{p}}^{K}(\mathbf{r})=\int d\mathbf{p}'d\mathbf{r}'g_{\mathbf{pp}'}(\mathbf{r},\mathbf{r}')I_i^*(g_{\mathbf{p}}^{(0)K}). \tag{10}$$

The function $g_{\mathbf{pp}'}$ should be determined from the relations

$$\mathbf{v}\,\frac{\partial}{\partial\mathbf{r}}\,g_{\mathbf{pp}'}(\mathbf{r},\mathbf{r}')-I_i(g_{\mathbf{pp}'})=\delta(\mathbf{p}-\mathbf{p}')\,\delta(\mathbf{r}-\mathbf{r}'), \tag{11}$$

$$g_{\mathbf{pp}'}(\mathbf{r},\mathbf{r}'\to\infty)=0. \tag{12}$$

Substituting the value of $\delta g_{\mathbf{p}}^{K}$ in Eq. (1), we obtain the expression for the change in the electric current ΔI due to specific defects

$$\Delta I=-\frac{\pi e}{2}\,N(0)\int dS\int\frac{d\varepsilon}{2\pi}\,\langle v_z\delta g_{\mathbf{p}}^{K}(\rho)\rangle$$

$$=-\frac{\pi e}{2}\,N(0)\int\frac{d\varepsilon}{2\pi}\int d\mathbf{p}\int d\mathbf{r}G_{\mathbf{p}}(\mathbf{r})I_i^*(g_{\mathbf{p}}^{(0)K}(\mathbf{r})), \tag{13}$$

where

$$G_{\mathbf{p}}(\mathbf{r})=\int_S d^2\rho\int d\mathbf{p}'v_z'g_{\mathbf{p}'\mathbf{p}}(\rho,\mathbf{r}). \tag{14}$$

Multiplying Eq. (11) by v_z and integrating it by ρ over the contact area and momentum $\mathbf{p}$, we obtain the following equation for the function $G_{\mathbf{p}}(\mathbf{r})$:

$$\mathbf{v}\,\frac{\partial}{\partial\mathbf{r}}\,G_{\mathbf{p}}(\mathbf{r})+I_i(G_{\mathbf{p}}(\mathbf{r}))=-\delta(z). \tag{15}$$

The probability $\alpha_{\mathbf{p}}(\mathbf{r})$ satisfies Eq. (8), which combined with Eq. (15) yields the relation[15]

$$G_{\mathbf{p}}(\mathbf{r})=\alpha_{-\mathbf{p}}(\mathbf{r})-\theta(z). \tag{16}$$

Substituting (7) and (16) into the expression for the point-contact current correction (13), we find

$$\Delta I=-\pi eN(0)\int\frac{d\varepsilon}{2\pi}\left\{G_0\left(\varepsilon+\frac{eU}{2}\right)-G_0\left(\varepsilon-\frac{eU}{2}\right)\right\}\int d\mathbf{r}\int d\mathbf{p}\alpha_{-\mathbf{p}}(\mathbf{r})I_i^*(\alpha_{\mathbf{p}}(\mathbf{r})). \tag{17}$$

Relation (17) has a wide range of applications. It is valid for any mean free path as to the electron scattering on background impurities l_i in case their separation distance r_0 is much smaller than the contact diameter d, and also for arbitrary relation between the value d and the distance between the specific defects r_0^*, which provide the mean free path for electron scattering on these defects, $l_i^*\gg d,l_i$.

The following calculations depend on the properties of both types of scatterers and their concentrations. The integrodifferential equation for the probability $\alpha_{\mathbf{p}}$ (8) can be

solved analytically for extreme cases in which the mean free path l_i is much greater or much smaller than the diameter d. For the ballistic regime of electron motion through the contact we obtain

$$\alpha_{\mathbf{p}}(\mathbf{r})=\begin{cases}\theta(-z)+\text{sign } z, & -\mathbf{v}\in\Omega(\mathbf{r})\\ \theta(-z), & -\mathbf{v}\notin\Omega(\mathbf{r}),\quad l_i\gg d\end{cases} \tag{18}$$

$\Omega(\mathbf{r})$ is a solid angle at which the aperture is seen from the point $\mathbf{r}$; $\theta(z)$ is the (Heaviside) unit step function.

For the diffusive regime of the electron motion through the contact $\alpha_{\mathbf{p}}$ can be expanded in a series in a small relaxation time τ_i (Ref. 15)

$$\alpha_{\mathbf{p}}(\mathbf{r})=\langle\alpha_{\mathbf{p}}(\mathbf{r})\rangle-\tau_i\mathbf{v}\nabla\langle\alpha_{\mathbf{p}}(\mathbf{r})\rangle+\ldots\quad l_i\ll d, \tag{19}$$

where

$$\langle\alpha_{\mathbf{p}}(\mathbf{r})\rangle=\theta(z)-\text{sign } z\,\frac{1}{\pi}\arctan\frac{1}{Q}; \tag{20}$$

$$Q^2=\frac{2r^2}{d^2}-\frac{1}{2}+\left[\left(\frac{2r^2}{d^2}-\frac{1}{2}\right)^2+\frac{4z^2}{d^2}\right]^{1/2}. \tag{21}$$

The solution of Eq. (4) for the scattering matrix is complicated and can be found only in some special cases. For example, if the interaction with a single impurity located at $\mathbf{r}_i$ is described by the spin-independent operator $\hat{V}(\mathbf{r})=V\hat{I}\delta(\mathbf{r}-\mathbf{r}_i)$ ($\hat{I}$ is a singular matrix, $V=\text{const}$), then for an arbitrary interaction potential V the $\hat{t}$ matrix will have the form

$$\hat{t}=\frac{\hat{V}\hat{I}-i\pi V^2\langle\hat{g}^{(0)}_{\mathbf{p}}\rangle N(0)}{1+[\pi N(0)V]^2}\,\delta(\mathbf{r}-\mathbf{r}_i). \tag{22}$$

In the case of a scattering center with nonzero spin $\mathbf{s}$ the electron interaction energy with such a scatterer contains the component $\hat{V}=J\hat{\sigma}\hat{\mathbf{s}}\delta(\mathbf{r}-\mathbf{r}_i)$ ($\hat{\sigma}$ is an electron spin operator, and J is an exchange interaction constant). At temperatures T above the Kondo temperature $T_K\sim\varepsilon_F\exp(-1/N(0)J)$ we can construct the Born series for the scattering matrix. Standard calculations[16] in the second Born approximation give

$$t^K=\frac{i}{2}\,\Gamma(\mathbf{r},\varepsilon)\langle g^{(0)K}_{\mathbf{p}}\rangle;\quad t^{R,A}=\int\frac{d\varepsilon}{2\pi}\frac{\Gamma(\mathbf{r},\varepsilon)}{\varepsilon-\varepsilon'\pm i0},$$

where

$$\Gamma(\mathbf{r},\varepsilon)=\pi N(0)J^2s(s+1)\left[1-\frac{JN(0)}{2}\int d\varepsilon'\,\frac{\langle g^{(0)K}_{\mathbf{p}}\rangle}{\varepsilon-\varepsilon'}\right]\delta(\mathbf{r}-\mathbf{r}_i). \tag{23}$$

If we have $N\gg1$ specific defects which yield an electron mean free path $l_i^*\gg\max(d,l_i)$, the calculation of the current through the contact can be performed by ignoring the correlation between the individual scattering events and writing the operator $\hat{t}$ of the system in the form of the sum of $\hat{t}$-operators of scattering by isolated defects. In this approximation, in the case of isotropic scattering by zero-spin impurities the resistance R of a point contact has the form

$$R^{-1}=R_c^{-1}\left\{1-\frac{\sigma^*}{S}\sum_{\mathbf{r}_i}M(\mathbf{r}_i)\right\}; \tag{24}$$

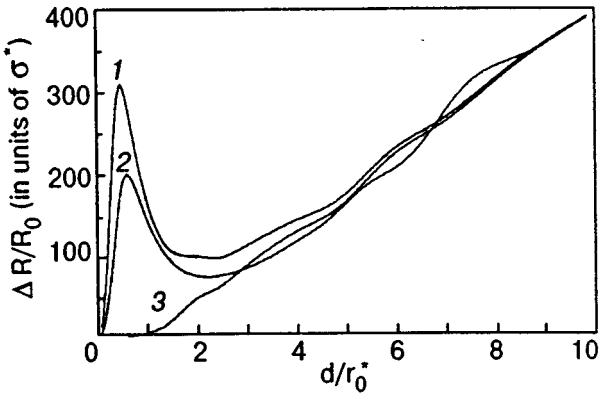

FIG. 2. The dependence of the relative correction $\Delta R/R_0$ for the ballistic resistance of the point contact R_0 versus the ratio between its diameter and the characteristic distance r_0^* between the defects for three random distributions in the contact region. Curves *1* and *2* represent the cases in which one of the impurities is located in the contact region, and curve *3* is the case in which there is no such impurity present.

$$R_c^{-1}=e^2N(0)\int_S d^2\rho\langle v_z\alpha_{\mathbf{p}}(\rho)\rangle; \tag{25}$$

R_c is the contact resistance without the specific impurities,[13]

$$\sigma^*=\frac{\text{Im } t^A}{v_F}=\frac{\pi V^2N(0)}{v_F[1+(\pi N(0)V)^2]}$$

is the effective cross section of scattering by the specific impurities.

$$M(\mathbf{r}_i)=4\frac{R_c}{R_0}\langle\alpha_{-\mathbf{p}}(\mathbf{r}_i)[\langle\alpha_{\mathbf{p}'}(\mathbf{r}_i)\rangle-\alpha_{\mathbf{p}}(\mathbf{r}_i)]\rangle; \tag{26}$$

$R_0^{-1}=1/2e^2v_FN(0)S$, and R_0 is the resistance of a ballistic contact (Sharvin formula).[10,11]

The sum of the $M(\mathbf{r}_i)$ functions depends on the specific configuration of the impurities and describes the classical mesoscopic effects in the conductivity of point contacts. For the ballistic case in which the function $\alpha_{\mathbf{p}}$ is determined by Eq. (18), we have[9]

$$M(\mathbf{r}_i)=\left[\frac{\Omega(\mathbf{r}_i)}{2\pi}\right]^2. \tag{27}$$

Figure 2 shows the results of a numerical calculation for Eqs. (24) and (27). In the mesoscopic region ($d\sim r_0^*$) the behavior of the resistance is essentially determined by the presence of impurities at distances $r_i\sim d$ from the aperture. If there are some impurities, then we will have N-shaped dependences $(\Delta R/R_0)(d)$ (curves *1* and *2* in Fig. 2), otherwise, we have a monotonic $(\Delta R/R_0)(d)$ dependence (curve *3* in Fig. 2). It should be noted that while d/r_0^* is increased from some point, the value of $\Delta R/R_0$ stays below its asymptotic value:

$$\frac{\Delta R}{R_0}=\frac{16}{3\pi}n_i^*\sigma^*d. \tag{28}$$

Figure 3 illustrates a situation that might be observed in experiments[12] when the defects are concentrated in a thin layer near the contact. In such a case the contaminated region

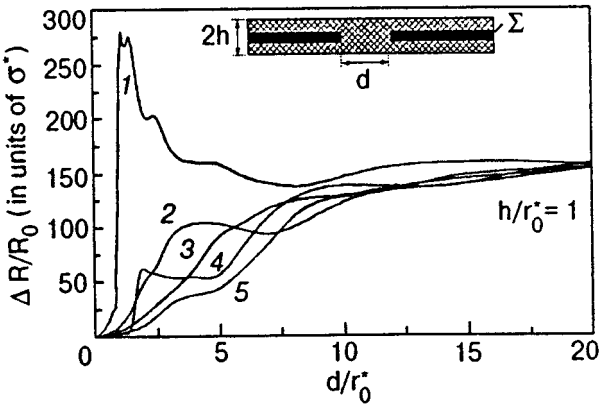

FIG. 3. Relative correction $\Delta R/R_0$ for the resistance of a ballistic contact for the various spatial distributions of impurities when the defects are located in a thin layer in the insulating plane (curves *2–5*). Curve *1* represents a rare case in which one of the impurities initially appears in the near contact region.

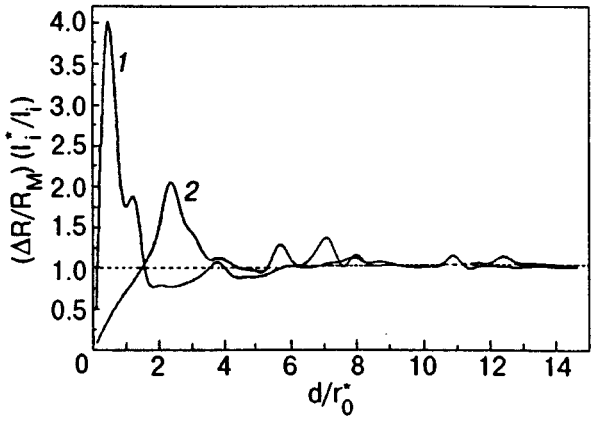

FIG. 4. Dependence of the relative correction $\Delta R/R_M$ for the resistance of a contact with small mean free path on the ratio between its diameter d and the characteristic distance between the specific defects r_0^*. Curves *1* and *2* correspond to two different distributions of these defects.

plays the role of a barrier with effective transparency D. It is known[17] that the relative change $\Delta R/R_0$ in the resistance of a ballistic contact due to the translucent barrier is $1-D$ and does not depend on the diameter d. The assumption made is supported by the results of a numerical calculation (Fig. 3), which shows a fairly weak $(\Delta R/R_0)(d)$ dependence for contact sizes, of the order of the thickness of a layer in which the scatterers are concentrated.

For contacts with a small mean free path, using Eqs. (19) and (26), we obtain

$$R_c^{-1}=R_M^{-1}=\frac{2}{3}\,e^2 v_F N(0) l_i d; \tag{29}$$

R_M is the resistance of the diffusion contact (Maxwell's equation);

$$M(\mathbf{r}_i)=\frac{l_i}{\pi d}\,\frac{1}{(Q^2+1)(Q^2+4z_i^2/(Q^2d^2))}, \tag{30}$$

where $Q^2(\mathbf{r}_i)$ is defined by Eq. (21). If the characteristic distance between the specific scatterers r_0^* is much larger than the contact size $r_0^* \gg d$, the impurities located at distances $r_i \gg d$ from the orifice yield $M(\mathbf{r}_i)\simeq (l_i/d)(S^2/r_i^4)$. Separating the contribution of distant defects, we obtain for a relative correction to the resistance

$$\frac{\Delta R}{R_M}\simeq\frac{\sigma^*}{S}\sum_{r_i\lesssim d} M(\mathbf{r}_i)+\frac{l_i}{l_i^*}\,\frac{S}{r^* d}, \tag{31}$$

where $l_i^{*-1}=\sigma^* n^*$, $l_i=v_F\tau_i$, and $r^*\approx r_0^*$. The first term in Eq. (31) is the contribution of specific defects in the contact region to the contact resistance. The partial contribution of every scatterer to the ΔR value is of the order of $\sigma^* d/S l_i$ and increases as the diameter is reduced. In a real situation for $r_0^* \gg d$ there might be no defects at distances $r_i \lesssim d$ from the contact, and the relation $\Delta R/R_0$ is proportional to d.

Now if $d \gg r_0^*$, the location of defects has no effect on the resistance of a point contact. Such inequality allows us to switch in (24) from a sum over the impurity coordinates r_i to an integral over the whole space. This yields for the circular contact

$$R^{-1}=R_M^{-1}(1-l_i/l_i^*). \tag{32}$$

Note that Eq. (32) can be directly obtained from expression (29) for the resistance of a short mean free path contact in which, according to Matthiessen's rule, l_i^{-1} should be replaced by $l_i^{-1}+l_i^{*-1}$, bearing in mind that $l_i \ll l_i^*$.

The $(\Delta R/R_M)(d)$ dependence, which is determined by analytical equations (31) and (32), is illustrated in Fig. 4, showing the results of the numerical calculation using Eqs. (24) and (30) for various random distributions of the specific scatterers. The mesoscopic regime in the conductance of point contacts is observed up to the values of d/r_0^* of about 5–10.

For the electron scattering by specific impurities with nonzero spin, substituting expression (23) for t^A into (17) at temperatures above the Kondo temperature, we can formally write the differential resistance of a point contact in the form (24), denoting by σ^* the following function of the voltage and temperature:

$$\sigma^*=\frac{\pi N(0) J^2 s(s+1)}{2v_F}\left[1-\frac{JN(0)}{4}\,\frac{dF(eU)}{deU}\right], \tag{33}$$

where

$$F(eU)=\int_0^\infty d\varepsilon\ \varepsilon G_0(\varepsilon)\int_0^\infty \frac{d\varepsilon'}{\varepsilon^2-\varepsilon'^2}\,[G_0(\varepsilon'-eU) - G_0(\varepsilon'+eU)].$$

The second term in square brackets of expression (33), which is a function of voltage and temperature, describes the Kondo anomaly on the current-voltage characteristic of the point contact. Note that the value σ^*, evaluated in the second Born approximation, does not depend on the scattering by background defects, and Eq. (33) is valid for any relation between the contact diameter d and the mean free path l_i.

Therefore, the increase in concentration of the specific impurities n_i^*, which leads to the alteration of the ratio between the characteristic separation of the impurities r_0^*

$=(n_i^*)^{-1/3}$ and the contact diameter, changes the size-dependence of the resistance of a point contact, $R(d)=R_M+\Delta R$:

$$\frac{\Delta R}{R_M}\sim\begin{cases} l_i/l_i^*, & r_0^*\ll d \quad l_i^*\ll d\ll l_i, \\ \dfrac{dl_i}{r_0^* l_i^*}+\dfrac{N_0\sigma^*}{dl_i^*} & r_0^*\gg d, \end{cases}$$

where N_0 is the number of defects in contact region. The influence of specific defects on the resistance for low concentrations ($r_0^*\gg d$) is determined by their spatial distribution, which leads to diverse (random) dependences $\Delta R(d)$. They can be split into two groups: 1) $(\Delta R/R_M)(d)$ increases with decreasing d if at least one of the specific impurities is located at a distance $r\ll d$ from the contact aperture; 2) the ratio $(\Delta R/R_M)$ decreases with decreasing d if all impurities are located far enough from the contact. As mentioned above, the total contribution from all defects at different distances from the contact can lead to the appearance of a minimum on the curve $(\Delta R/R_M)(d)$. For high concentrations ($r_0^*\ll d$) the relative change in resistance is independent of the contact size, $\Delta R/R_M=\text{const}(d)$. Thus the functional dependence of the point contact resistance versus its diameter can serve as a criterion for determining the concentration of the specific impurities, and also their distribution in the contact region. Note that due to the ''screening'' effect of background impurities the classical mesoscopic effect in the diffusive contact is weakened $d/l_i>1$ times compared to the ballistic case described in Ref. 7. If the specific impurities are magnetic impurities, they lead to a nonlinear dependence of the correction for the contact resistance versus the applied voltage. Such dependence can be extracted in standard experiments in point-contact spectroscopy. In this case the distribution of impurities in the contact region affects the intensity and displacement (on the voltage scale) of the Kondo anomaly in the point contact spectrum.

*E-mail: kolesnichenko@ilt.kharkov.ua
**E-mail: post@rulgm1.leidenuniv.nl

[1] C. J. Muller, J. M. van Ruitenbeek, and L. J. de Jongh, Physica C **191**, 485 (1992).
[2] E. N. Bogachek, A. N. Zagoskin, and I. O. Kulik, Sov. J. Low Temp. Phys. **18**, 796 (1990).
[3] J. M. Krans, J. M. van Ruitenbeek, V. V. Fisun, I. K. Yanson, and L. J. de Jongh, Nature (London) **375**, 767 (1995).
[4] P. A. M. Holweg, J. A. Kokkedee, J. Caro, A. H. Vebruggen, S. Radelaar, A. G. M. Jansen, and P. Wyder, Phys. Rev. Lett. **67**, 2549 (1991).
[5] V. I. Kozub, J. Caro, and P. A. M. Holweg, Phys. Rev. B **50**, 15126 (1994).
[6] E. G. Haanappel and D. van der Marel, Phys. Rev. B **39**, 5484 (1989).
[7] A. M. Zagoskin, S. N. Rashkeev, R. I. Shekhter, and G. Wendin, J. Phys.: Condens. Matter **7**, 6253 (1995).
[8] Yu. M. Gal'perin and V. I. Kozub, Sov. J. Low Temp. Phys. **18**, 336 (1992).
[9] Yu. A. Kolesnichenko, A. N. Omelyanchouk, and I. G. Tuluzov, Low Temp. Phys. **21**, 655 (1995).
[10] Yu. V. Sharvin, Sov. Phys. JETP **21**, 655 (1965).
[11] I. O. Kulik, A. N. Omelyanchouk, and R. I. Shekhter, Sov. J. Low Temp. Phys. **3**, 740 (1977).
[12] I. K. Yanson, V. V. Fisun, R. Hesper, A. V. Khotkevich, J. M. Krans, J. A. Mydosh, and J. M. Ruitenbeek, Phys. Rev. Lett. **74**, 302 (1995).
[13] L. V. Keldysh, Sov. Phys. JETP **20**, 1018 (1964).
[14] G. Eilenberger, Z. Phys. **214**, 195 (1968).
[15] I. O. Kulik, R. I. Shekhter, and A. G. Shkorbatov, Sov. Phys. JETP **54**, 1130 (1981).
[16] Yu. M. Ivanchenko and G. A. Trush, Sov. Phys. JETP **67**, 352 (1974).
[17] R. I. Shekhter and I. O. Kulik, Sov. J. Low Temp. Phys. **9**, 46 (1983).

This article was published in English in the original Russian journal. It was edited by S. J. Amoretty.

Raman investigations of orientational ordering in $NiSiF_6 \cdot 6H_2O$, $NiSiF_6 \cdot 6D_2O$, and $ZnSiF_6 \cdot 6H_2O$ crystals

V. V. Eremenko, A. V. Peschanskii, and V. I. Fomin

*B. Verkin Institute for Low Temperature Physics and Engineering, National Academy of Sciences of the Ukraine, 310164 Kharkov, Ukraine**

(Submitted May 27, 1997; revised July 2, 1997)
Fiz. Nizk. Temp. **23**, 1315–1324 (December 1997)

The results of investigations of polarized Raman spectra in $ZnSiF_6 \cdot 6H_2O$ and $NiSiF_6 \cdot 6D_2O$ single crystals in the temperature range 2–300 K are presented. It is found that the crystals are orientationally ordered at low temperatures. The orientational disordering is described by a model in which the rotational motion of the SiF_6^{2-} complex is determined by a two-well asymmetric potential function. The parameters of the model are determined from the temperature behavior of the Raman spectral lines. The calculated values of concentration for two orientational positions of the SiF_6^{2-} complex at room temperature are in good agreement with the x-ray data. © *1997 American Institute of Physics.* [S1063-777X(97)00912-2]

According to the results of x-ray diffraction analysis at $T=300$ K,[1] orientational disorder of octahedral ions SiF_6^{2-} each of which can occupy one of two energetically inequivalent positions which are not connected through a symmetry element is a structural peculiarity of hexahydrates of nickel and zinc fluorosilicates ($NiSiF_6 \cdot 6H_2O$ and $ZnSiF_6 \cdot 6H_2O$) under investigation. In these orientations, octahedrons are distributed randomly over the crystal, their population densities for Ni- and Zn-based compounds at $T=300$ K being in the ratio 0.33/0.67.[1] The temperature evolution of orientational disorder of the crystals has not yet been studied.

Anomalous temperature behavior of lattice parameters discovered in low-temperature x-ray studies[2,3] was attributed by the authors of these publications to a second-order phase transition (PT). The crystals of $NiSiF_6 \cdot 6H_2O$ at $T \simeq 220$ K [2] and $ZnSiF_6 \cdot 6H_2O$ at $T \simeq 200$ K [3] exhibit a change of rhombohedral modifications differing in the temperature expansion coefficients of the lattice. An analysis of the permittivity[4] of the crystals revealed that $NiSiF_6 \cdot 6H_2O$ and $ZnSiF_6 \cdot 6H_2O$ crystals in the temperature range 150–250 K experience dielectric losses indicating the existence of temperature-activated motion of electric dipole moments. The observed behavior of dielectric response indicates a significant change in the nature of vibrational mobility of ions in this temperature range.

The space symmetry group of the crystal lattice of the crystal under investigation is $R\bar{3}(C_{3i}^2)$, and the unit cell contains one structural unit ($z=1$).[1] An analysis of fundamental oscillations[5] shows that the ordered structure can have 78 vibrational modes:

$$\Gamma_{\text{vib}} = 12A_g + 12E_g + 14A_u + 14E_u .$$

In the Raman scattering (RS), the A_g and E_g modes with nonzero components of the Raman scattering tensor are active: XX, YY, ZZ for A_g and XX, YY, XY, XZ, and YZ for E_g.

The Raman spectra were studied earlier for $NiSiF_6 \cdot 6H_2O$[5–10] and $ZnSiF_6 \cdot 6H_2O$[8,9,11] crystals. Jenkins and Lewis[6,7] paid main attention to the temperature dependence of intrinsic vibrations of H_2O. The observed Raman spectral lines were classified for $NiSiF_6 \cdot 6H_2O$ and $NiSiF_6 \cdot 6D_2O$ crystals at 300, 110, and 10 K in Ref. 5, for $ZnSiF_6 \cdot 6H_2O$ at 20 K in Ref. 11, and for $MeSiF_6 \cdot 6H_2O$ (Me=Zn, Ni, Co, Fe, and Mn) at $T=300$ K in our earlier publication.[9] Jenkins and Lewis[8] compared the Raman spectra for zinc and nickel fluorosilicates with the corresponding spectra for fluorotitanates.

In our earlier publication,[10] we thoroughly analyzed the temperature behavior of Raman spectra in a $NiSiF_6 \cdot 6H_2O$ crystal. It was found that at $T>130$ K, the spectrum acquires an additional low-frequency line in the lattice vibration region, whose intensity increases anomalously with temperature. The emerging additional line is not a result of a PT; its behavior reflects orientational ordering upon cooling in the proposed model of an asymmetric two-well potential describing vibrations of SiF_6^{2-} ions.

In order to verify the proposed mechanism of orientational disordering, we analyze here the Raman spectra over wide temperature interval for $NiSiF_6 \cdot 6D_2O$ and $ZnSiF_6 \cdot 6H_2O$ crystals having the same structure and similar types of disorder. We shall also consider estimates of the parameters of the orientational ordering model proposed in Ref. 10.

DISCUSSION OF EXPERIMENTAL RESULTS

Experiments were made on single crystals of high optical quality. The coordinate system was determined by crystal faceting in the form of a combination of a hexagonal prism and a rhombohedron. The X-axis was parallel to the hexagonal growth plane and perpendicular to the axis C_3, $Z \| C_3$, and $Y \perp X, Z$. The Raman spectra were excited by the 4880 Å line emitted by an Ar laser with a power of 200–300 mW. The light scattered by a sample at an angle of 90° was analyzed by a double monochromator JOBLIN YVON U-1000 and recorded by a cooled photomultiplier in the photon count mode.

Structural peculiarities and measuring technique are described in detail in Ref. 10.

Low-Temperature Raman Spectra

We investigated Raman spectra of $NiSiF_6 \cdot 6D_2O$ and $ZnSiF_6 \cdot 6H_2O$ crystals at $T=2$ K in the frequency range $0-3600$ cm^{-1}. Figures 1a–c show the Raman spectra with different components of the Raman tensor for a $ZnSiF_6 \cdot 6H_2O$ crystal. The same figure shows for comparison the spectra for $NiSiF_6 \cdot 6H_2O$ and $NiSiF_6 \cdot 6D_2O$ (Figs. 1d and 1e, respectively). The above frequency range can be divided into two.[5,8–11] The first (from 0 to 140 cm^{-1}) corresponds to the lattice vibrations region containing $2A_g+2E_g$ rotational oscillations of octahedral complexes. The range $190-800$ cm^{-1} contains lines of intrinsic vibrations of $Me(H_2O)_6^{2+}$ and SiF_6^{2-} complexes as well as broad (even for $T=2$ K) lines corresponding to librational vibrations of $H_2O(D_2O)$.

Table I contains values of frequency corresponding to Raman lines, attributed to the first-order spectrum, in comparison with the available data. It can be seen that the number and polarization of lines observed in the Raman spectrum at low temperatures are in good agreement with the calculations based on the group theory for an ordered crystal lattice described by the space group $C_{3_i}^2(z=1)$.

Experimentally obtained frequencies of vibrations in the $ZnSiF_6 \cdot 6H_2O$ crystal are in good agreement with the available data (see Table I), but the interpretation of the spectrum differs from that described in Ref. 11, in which the vibration at a frequency of 401 cm^{-1} was attributed to intrinsic vibrations of the $Zn(H_2O)_6^{2+}$ complex, while the vibration at 381 cm^{-1} was classified as an intrinsic vibration of the SiF_6^{2-} complex. The classification carried out here is based on a comparison of the Raman spectra of the crystals under inves-

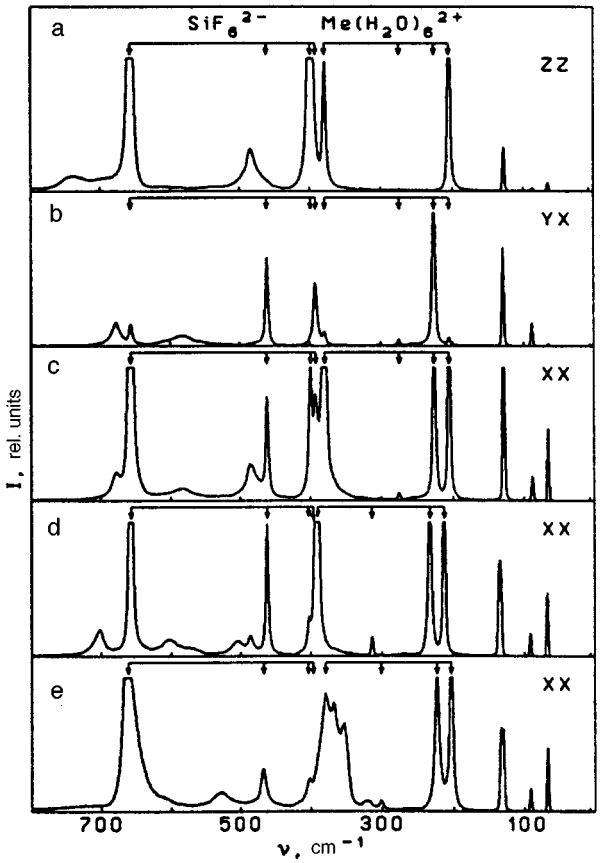

FIG. 1. Raman spectra of $ZnSiF_6 \cdot 6H_2O$ (a–c), $NiSiF_6 \cdot 6H_2O$ (d), and $NiSiF_6 \cdot 6D_2O$ (e) crystals in experimental geometries $Z(XX)Y$, $Z(YX)Y$, and $X(ZZ)Y$ at $T=2$ K. The spectral resolution is 3 cm^{-1}.

TABLE I. Frequency (in cm^{-1}) and symmetry of fundamental vibrations in $ZnSiF_6 \cdot 6H_2O$, $NiSiF_6 \cdot 6H_2O$, and $NiSiF_6 \cdot 6D_2O$ crystals which are active in Raman scattering.

Symmetry and identification of vibrations		$ZnSiF_6 \cdot 6H_2O$			$NiSiF_6 \cdot 6H_2O$	$NiSiF_6 \cdot 6D_2O$	
		Our results $T=2$ K	[Ref. 11] $T=20$ K	[Ref. 8] $T=15$ K	[Ref. 10] $T=2$ K	Our results $T=2$ K	[Ref. 5] $T=10$ K
		–	–	–	–	–	38
Lattice vibrations	A_g	66	65	66	68	68	68
	E_g	89	90	89	92.5	92	94
	A_g	129	129	–	134.5	131	130
	E_g	130	132	130	137	134.5	–
Intrinsic vibrations of $Me(H_2O)_6^{2+}$	A_g	206	206	207	214	204	203
	E_g	227	227	228	234	224	225
	E_g	276	276	278	314.5	302	300
	A_g	380	401	380	391.5	380	380
Intrinsic vibrations of SiF_6^{2-}	E_g	392.5	393	395	394.5	403.5	–
	A_g	400	381	401	403	398	405
	E_g	462	462	462	463	468.5	462
	A_g	658	657	658	659	665.5	661
Rotational vibrations of $H_2O(D_2O)$	A_g	485.5	486	490	485.5	353.5	–
	A_g	–	–	–	505.5	369	–
	E_g	~555	–	–	573	449.5	–
	E_g	583	~590	587	604	484	–
	E_g	679	680	676	704	527.5	–
	A_g	740	~740	–	767	578	–

tigation, which shows that the frequencies of intrinsic vibrations of the $Me(H_2O)_6^{2+}$ complex in Ni- and Zn-containing crystals differ significantly, while the frequencies of the complex SiF_6^{2-} have close values. In addition, in comparison with the data presented in Ref. 11 containing the most complete information on the vibrational spectrum, two lines (at 1616 and 1640 cm^{-1}) of deformational vibrations of H_2O are observed as well as a line at a frequency ~ 555 cm^{-1} corresponding to the rotational E_g-vibration of H_2O (see Table I). The missing line corresponding to the A_g rotational vibration of an H_2O molecule (see Table 1) apparently lies in the region 480–500 cm^{-1}, but it is difficult to single out this line due to the complex form of the line at 485.5 cm^{-1} (see Figs. 1a and c).

It should be noted that the Raman spectra of the $ZnSiF_6 \cdot 6H_2O$ as well as $NiSiF_6 \cdot 6H_2O$ crystals[10] exhibit four narrow lines in the lattice vibration regions, indicating a high extent of orientational ordering at low temperatures.

Raman spectra for a $NiSiF_6 \cdot 6(D_{1-x}H_x)_2O$ crystal (which will be henceforth denoted by $NiSiF_6 \cdot 6D_2O$) have a more complex structure. In view of incomplete substitution of deuterium for hydrogen, the spectra contain rotational vibrations of D_2O, HOD, and H_2O (see Fig. 1e), deformational vibrations of D_2O at 1196 $cm^{-1}(A_g)$ and 1207 $cm^{-1}(E_g)$, of HOD at 1435 $cm^{-1}(A_g)$ and 1446 $cm^{-1}(E_g)$, and of H_2O at 1635 $cm^{-1}(E_g)$ as well as valence vibrations of D–O (in the range 2500–2650 cm^{-1}) and H–O (in the range 3450–3550 cm^{-1}). An estimate of the extent of deuterization of the crystal was obtained from the ratio of intensities of the spectral lines corresponding to deformational vibrations of D_2O, HOD, and H_2O and amounts to 75–80% of deuterium ($x = 0.2–0.25$). Incomplete substitution of D for H is manifested in depolarization of lines corresponding to valence vibrations of H–O and D–O. In contrast to strictly polarized lines in the $NiSiF_6 \cdot 6H_2O$ crystal, the lines of rotational vibrations of D_2O, HOD, and H_2O are predominantly polarized.

Processing of Raman spectra as a superposition of Lorentzians on a microcomputer made it possible to determine the frequencies of all rotational lines of D_2O (see Table I) and most of lower-intensity lines of HOD and H_2O. All the lines attributed in Ref. 10 to vibrations of H_2O in a $NiSiF_6 \cdot 6H_2O$ crystal are as a result of deuterization to the low-frequency region are displaced to the low frequency region as a result of deuterization, which confirms the correctness of their interpretation.

Substitution of deuterium leads to a considerable decrease in frequencies of all intrinsic vibrations of the $Ni(D_2O)_6^{2+}$ complex (see Table I). The effect of deuterization on the frequencies of intrinsic vibrations of the SiF_6^{2-} complex is worth noting. For example, the lines at frequencies 463 and 659 cm^{-1} for the $NiSiF_6 \cdot 6H_2O$ crystal are displaced by 6–7 cm^{-1} to the high-frequency region as a result of deuterization (see Table I). A similar increase in the frequencies of corresponding intrinsic vibrations of the TiF_6^{2-} complex was observed in $MnTiF_6 \cdot 6D_2O$ and $ZnTiF_6 \cdot 6D_2O$ crystals.[12] The asymmetric shape of the line at frequency 665.5 cm^{-1} in a $NiSiF_6 \cdot 6D_2O$ (Fig. 1e) is apparently associated with different surroundings of the SiF_6^{2-} complex in the case of incomplete deuterization (from completely D_2O environment to completely H_2O environment with different probabilities).

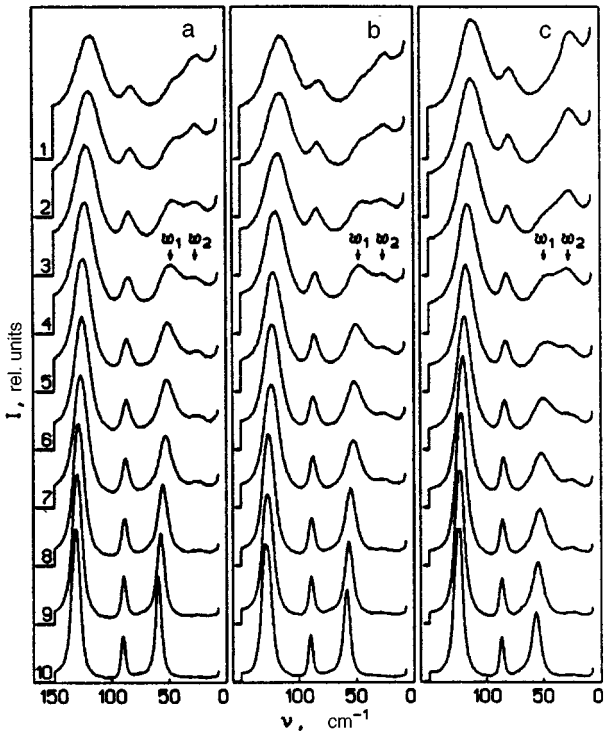

FIG. 2. Temperature behavior of Raman spectra with the Raman tensor component XX in the range of lattice vibrations in $NiSiF_6 \cdot 6H_2O$ (a), $NiSiF_6 \cdot 6D_2O$ (b), and $ZnSiF_6 \cdot 6D_2O$ (c)crystals at various temperatures T, K: 300 (curve *1*), 280 (curve *2*), 260 (curve *3*), 240 (curve *4*), and 215 (curve *5*) (a,b), 220 (curve *5*) (c), 200 (curve *6*), 185 (curve *7*) (a,b), 180 (curve *7*) (c), 155 (curve *8*) (a,b), 160 (curve *8*) (c), 135 (curve *9*) (a,b), 140 (curve *9*) (c), 115 (curve *10*) (a,b), and 120 (curve *10*) (c). The spectral resolution is 3 cm^{-1}.

Disordering in H and D is not manifested in the spectrum of lattice vibrations. Four polarized and narrow lines (whose half-width is determined by the apparatus function) are observed in the frequency range 0–150 cm^{-1} (see Fig. 1e) as in a $NiSiF_6 \cdot 6H_2O$ crystal. Deuterization leads to a displacement of two of lattice vibrations to the low-frequency region (see Table I).

Small damping of lattice vibrations in the crystals under investigation at low temperatures indicates a high degree of their orientational ordering. A comparison of the spectra for these crystals has made it possible to classify vibrations unambiguously.

Temperature Behavior of Raman Spectrum

As in the case of $NiSiF_6 \cdot 6H_2O$ crystal, the heating of $ZnSiF_6 \cdot 6H_2O$ and $NiSiF_6 \cdot 6D_2O$ crystals leads to qualitative and quantitative changes in the Raman spectrum, which are manifested most strongly in the low-frequency spectral region (Fig. 2). As the temperature increases, the spectra with XX, YY, and ZZ components of the Raman tensor for all the three compounds exhibit an increase in the intensity of scattering in the low-frequency region adjoining the excitation line and the emergence of a new line ω_2 denoted by ν_R in Ref. 10. In spectra with nondiagonal Raman tensor compo-

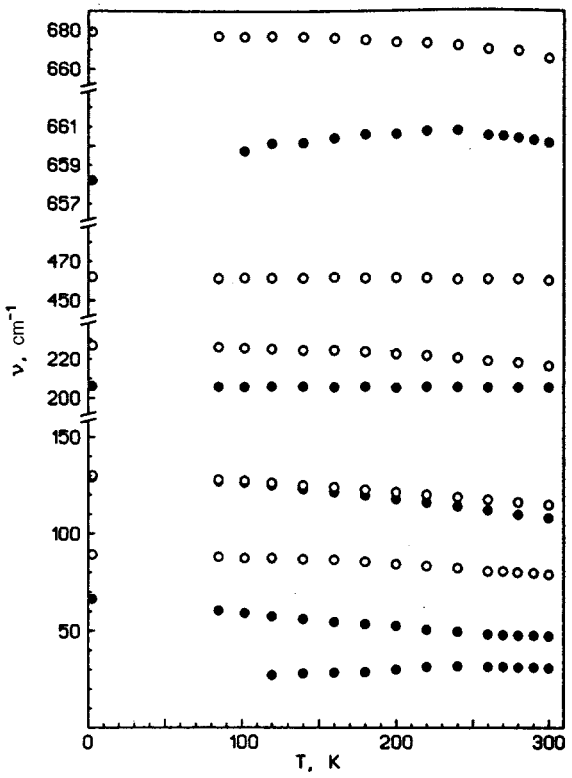

FIG. 3. Temperature dependence of vibrational frequencies in the $ZnSiF_6 \cdot 6H_2O$ crystal: A_g vibrations (●) and E_g vibrations (○). The error in frequency measurements does not exceed the size of the symbols.

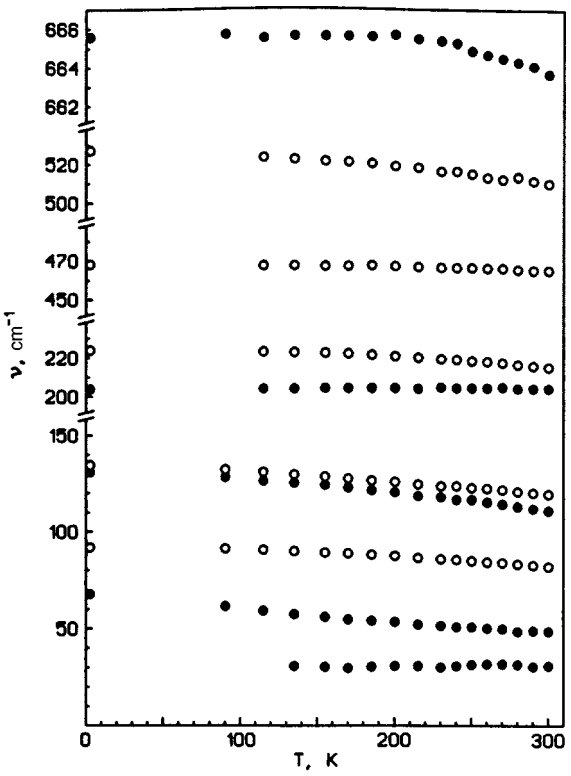

FIG. 4. Temperature dependence of vibrational frequencies in the $NiSiF_6 \cdot 6H_2O$ crystal: A_g vibrations (●) and E_g vibrations (○). The error in frequency measurements does not exceed the size of the symbols.

nents, no line ω_2 and no low-frequency wing are observed, but the background scattering increases upon heating. It can be seen from Fig. 2c that an additional low-frequency line emerges in Raman spectra of the $ZnSiF_6 \cdot 6H_2O$ crystal with diagonal Raman tensor components at a lower temperature ($\sim$120 K).

Temperature evolution of the Raman spectra for $NiSiF_6 \cdot 6H_2O$ and $ZnSiF_6 \cdot 6H_2O$ crystals is qualitatively the same (Figs. 2a and c). The processing of spectra on a microcomputer is described in detail in Ref. 10. Figure 3 shows the temperature behavior of lattice vibration frequencies as well as A_g(658 cm^{-1}) and E_g(462 cm^{-1}) modes of intrinsic vibrations of the SiF_6^{2-} complex, A_g(206 cm^{-1}) and E_g(227 cm^{-1}) modes of the $Zn(H_2O)_6^{2+}$ complex, and the temperature behavior of the rotational mode of H_2O (679 cm^{-1}). All the peculiarities in the temperature behavior of vibrational frequencies observed earlier[10] for the $NiSiF_6 \cdot 6H_2O$ crystal also take place for the $ZnSiF_6 \cdot 6H_2O$ crystal.

Experiments with the $NiSiF_6 \cdot 6D_2O$ crystal revealed that the substitution of deuterium for hydrogen virtually did not affect the Raman spectra of lattice vibrations (see Figs. 2a and b). The temperature corresponding to the emergence of an additional line ω_2 and its evolution are the same as for the $NiSiF_6 \cdot 6H_2O$ crystal. The temperature behavior of frequencies of lattice vibrations, intrinsic vibrations of the $Ni(D_2O)_6^{2+}$ complex, and rotational vibration of D_2O (Fig. 4) is the same as that observed in a nondeuterized crystal.[10] It can be seen from Fig. 4 that the line at frequency 665.5 cm^{-1} (completely symmetric vibration of the Si-F_6^{2-} complex) also exhibits an anomalous temperature behavior, which, however, differs from that of a nondeuterized crystal in which the vibrational mode frequency (659 cm^{-1}) increases upon heating to $T \simeq 220$ K.[10] As a result of heating, the shape of this line in a deuterized crystal becomes symmetric.

It was noted earlier[10] that additional lines in the Raman spectrum of crystals can appear as a result of PT. It can be seen from Fig. 2 that additional peculiarities are observed experimentally in the low-temperature spectra at much lower temperatures than those corresponding to the second-order PT for $NiSiF_6 \cdot 6H_2O$ and $ZnSiF_6 \cdot 6H_2O$ crystals (220 and 200 K, respectively).[2,3] Moreover, the intensity of the line ω_2 increases monotonically with temperature without exhibiting any peculiarities in this temperature range. These facts confirm that the emergence of an additional line is associated with the evolution of orientational disorder and is not the result of a PT.

Model of Orientational Disorder

According to x-ray data,[1] octahedral SiF_6^{2-} ions in fluorosilicates under investigation at room temperature can occupy (with different probabilities) two orientational positions that are not associated with a symmetry element and that can be transformed into each other by rotation around the axis C_3 through an angle $\sim 30°$. As a result, the potential function of rotational vibrations of SiF_6^{2-} ions must have two minima having different depths and separated by a potential barrier

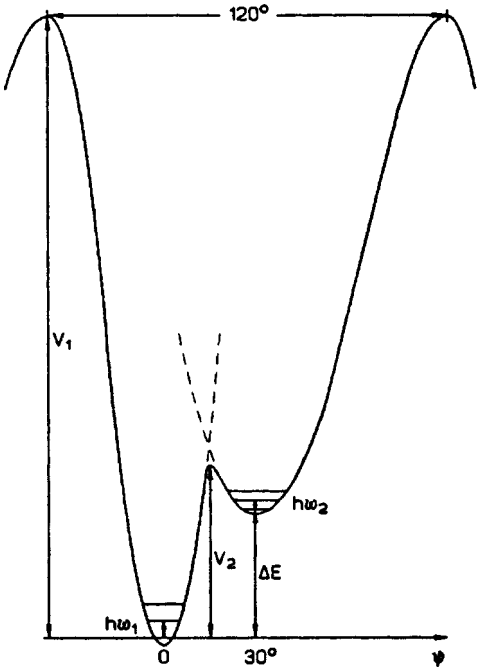

FIG. 5. Schematic representation of a segment of the potential function of rotational vibrations of the SiF_6^{2-} complex around the crystallographic axis C_3.

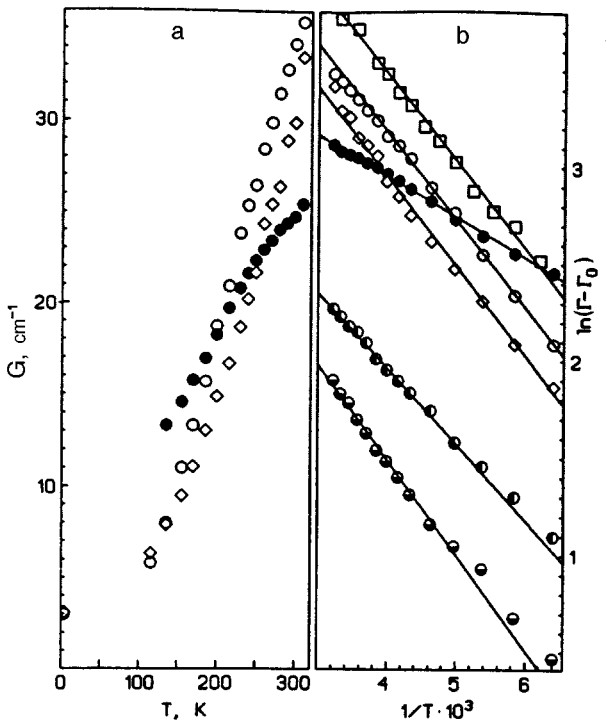

FIG. 6. Temperature dependence of line half-width of lattice vibrations (a) and dependence of the logarithm of half-width on reciprocal temperature (b) for certain vibrations in the $NiSiF_6 \cdot 6H_2O$ crystal: ω_2 (●), ω_1 (○), the line at frequency 134.5 cm^{-1} (A_g of lattice vibrations) (◇), A_g of intrinsic vibrations of the SiF_6^{2-} complex (659 cm^{-1}) (◒), A_g of intrinsic vibrations of the $Ni(H_2O)_6^{2+}$ complex (214 cm^{-1}) (◐) (symbols on the curve are lowered by unity along the Y-axis), and E_g of rotational vibration of H_2O (□).

V_2 (Fig. 5). The lines in Raman spectra attributed to rotational vibrations in these wells are obviously polarized identically, but may have different frequencies.[10]

At low temperatures, only the energy levels of the deeper potential well are populated, the crystals are ordered, and the Raman spectra contain a line of frequency ω_1 (68 cm^{-1} for a $NiSiF_6 \cdot 6H_2O$ crystal; see Table I). In the course of heating, the energy levels in the potential well separated from the deeper well by ΔE become populated as a result of thermal activation (see Fig. 5). The spectra acquire an additional line of frequency ω_2, whose intensity depends on the population density of the metastable state. The relaxation peak[10] in this model is due to thermally activated jumps of SiF_6^{2-} ions through the barrier V_2 and is observed in the Raman spectra with the same components of the Raman tensor as for vibrations in the potential wells (see Fig. 2).

The frequencies ω_1 and ω_2 can be different due to a change in the moments of inertia of octahedral complexes SiF_6^{2-} as well as due to a change in force constants. It was found[1] that the lengths of hydrogen bonds O–H...F and the angles formed by H–O–H bonds differ significantly for two orientational positions of octahedrons. At the same time, octahedrons in these positions differ insignificantly in shape and parameters.[1] A detailed analysis of the shape of the line at frequency 659 cm^{-1} for the $NiSiF_6 \cdot 6H_2O$ crystal[10] and 658 cm^{-1} for the $ZnSiF_6 \cdot 6H_2O$ crystal, which is identified with the A_g ''compression–expansion'' mode of the octahedron SiF_6^{2-}, revealed that it can be described satisfactorily by a Lorentzian at any temperature. The lack of symmetry for this line indicates that the splitting that can emerge upon heating due to the difference in the shape of octahedrons is small, which is in accord with the results obtained in Ref. 1. The anomalous temperature dependence of the frequency of this mode (see Fig. 3) in the crystals under investigation can be due to a change in the force constant of the Si-F bond and apparently reflects the change in the temperature behavior of the crystal lattice parameters observed in Refs. 2 and 3 at $T \simeq 220$ K for a $NiSiF_6 \cdot 6H_2O$ crystal and at $T \approx 200$ K for $ZnSiF_6 \cdot 6H_2O$.

The estimated value of the potential barrier V_1 for 120° reorientations of the SiF_6^{2-} ion in $NiSiF_6 \cdot 6H_2O$ and $ZnSiF_6 \cdot 6H_2O$ crystals is 5.5 kcal/mole (~ 2770 K).[4] The barrier height V_2 can be estimated from the temperature dependence of the line widths of the vibrational spectrum since reorientational motion is one of the reasons behind their broadening. It is well known that broadening is described by the formula

$$\Gamma(T) = \Gamma_0 + aT + be^{-V/kT},$$

where Γ_0 is the line half-width at a low temperature. Figure 6a shows the half-widths Γ of the lines of A_g lattice vibrations as functions of temperature, while Fig. 6b shows the dependence of $\ln(\Gamma - \Gamma_0)$ on reciprocal temperature for these vibrations as well as for intrinsic vibrations of the complexes $Ni(H_2O)_6^{2+}$ and SiF_6^{2-} and rotational vibrations of H_2O. It can be seen that the linear contribution is much smaller than the exponential one, and the broadening at $150\ \text{K} < T < 300$ K can be satisfactorily described by an exponential (see Fig. 6). The barrier height obtained from the temperature dependence of half-width of the line ω_2 differs significantly from the values obtained from the broadening

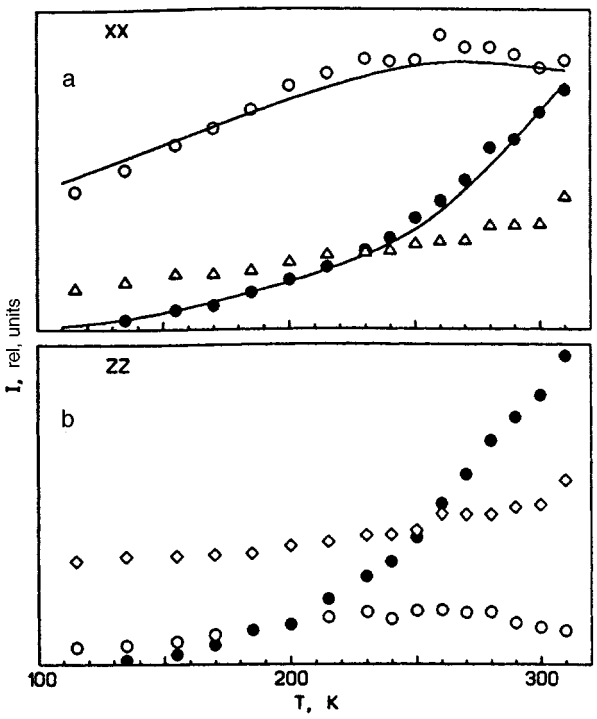

FIG. 7. Experimental and theoretical temperature dependences of line intensities in the $NiSiF_6 \cdot 6H_2O$ crystal: XX Raman spectra (a), ZZ Raman spectra (b); ω_2 (●), ω_1 (○), the lines at frequency 92.5 cm^{-1} (△) and at frequency 134.5 cm^{-1} (◇) (Table I). Solid curves are calculated by formulas (3) and (4).

of other lines. This confirms the hypothesis that the additional line ω_2 is associated with rotational vibrations of the octahedron SiF_6^{2-} in the metastable state (see Fig. 5). A similar behavior of line broadening is observed for $NiSiF_6 \cdot 6D_2O$ and $ZnSiF_6 \cdot 6H_2O$ crystals. The potential barrier height obtained from the broadening of the ω_2 line is (210 ± 20), (170 ± 20), and (190 ± 20)K for $NiSiF_6 \cdot 6H_2O$, $ZnSiF_6 \cdot 6H_2O$, and $NiSiF_6 \cdot 6D_2O$ crystals, respectively. The estimate of the barrier height obtained from the broadening of other lines lies in the intervals 400–480, 410–500, and 400–480 K for these crystals.

Figure 7 shows the temperature dependence of the integral intensities of lattice vibration lines in the $NiSiF_6 \cdot 6H_2O$ crystal for Raman spectra with Raman tensor components XX and ZZ. Anomalous behavior is observed for the intensity of not only the line ω_2, but also of the ω_1 line. The temperature behavior of the intensity of the E_g mode (92.5 cm^{-1}; see Table I) and the A_g mode (134.5 cm^{-1}, see Table I) with the normal temperature dependence is also shown for comparison. It can be seen from Fig. 7 that the ω_1 and ω_2 lines have qualitatively similar temperature dependences of intensities for both polarizations. The normalization of intensities of the lattice vibrational spectra was carried out for all temperatures and experimental geometries XX and ZZ to the intensity of the A_g intrinsic vibrational mode of the SiF_6^{2-} complex with frequency 659 cm^{-1}, which is characterized by a normal temperature dependence of intensity. In addition, the normalization of ZZ-spectra was verified from the behavior of the intensity of the line at 214 cm^{-1} (A_g is the intrinsic vibrational mode for the complex $Ni(H_2O)_6^{2+}$).

The value of the parameter ΔE can be determined from the ratio of the intensities of the ω_1 and ω_2 lines. The expressions for the concentrations N_1 and N_2 for two different orientational positions of the octahedral ion SiF_6^{2-} and for intensities I_1 and I_2 of the ω_1 and ω_2 lines in the proposed model were obtained in the harmonic approximation[13]:

$$N_1 = c\ \exp\left(-\frac{h\omega_1}{2kT}\right)\left[1-\exp\left(-\frac{h\omega_1}{kT}\right)\right]^{-1}, \tag{1}$$

$$N_2 = c\ \exp\left(-\frac{\Delta E}{kT}\right)\exp\left(-\frac{h\omega_2}{2kT}\right)\left[1-\exp\left(-\frac{h\omega_2}{kT}\right)\right]^{-1}. \tag{2}$$

$$I_1 = K_1 c\ \exp\left(-\frac{h\omega_1}{2kT}\right)\left[1-\exp\left(-\frac{h\omega_1}{kt}\right)\right]^{-2}, \tag{3}$$

$$I_2 = K_2 c\ \exp\left(-\frac{\Delta E}{kT}\right)\exp\left(-\frac{h\omega_2}{2kT}\right) \times\left[1-\exp\left(-\frac{h\omega_2}{kT}\right)\right]^{-2}. \tag{4}$$

where c is the factor responsible for redistribution of concentrations with orientations N_1 and N_2 upon heating, which was obtained from the condition $N = N_1 + N_2 = 1$:

$$c = \left\{\exp\left(-\frac{h\omega_1}{2kT}\right)\left[1-\exp\left(-\frac{h\omega_1}{kT}\right)\right]^{-1} + \exp\left(-\frac{\Delta E}{kT}\right)\exp\left(-\frac{h\omega_2}{2kT}\right) \times\left[1-\exp\left(-\frac{h\omega_2}{kT}\right)\right]^{-1}\right\}^{-1};$$

and K_1 and K_2 are coefficients independent of the vibrational quantum number. The expression for ΔE in this case has the form

$$\frac{\Delta E}{kT} = \ln\frac{I_1}{I_2} - \ln\frac{K_1}{K_2} - \ln\frac{\exp(-h\omega_1/2kT)}{\exp(-h\omega_2/2kT)} - 2\ln\frac{1-\exp(-h\omega_2/kT)}{1-\exp(-h\omega_1/kT)}. \tag{5}$$

Figure 8a shows the right-hand side of expression (5) (without the contribution from the value of $\ln(K_1/K_2)$) as a function of reciprocal temperature. We assume that $\ln(K_1/K_2)$ is independent of temperature and gives only a constant shift of the curve in this case. The intensities I_1 and I_2 were taken from the spectra with the XX Raman tensor component since the integral intensities of these lines in the indicated experimental geometry can be determined with a smaller error than for spectra with the ZZ component. Assuming that ΔE is constant for low concentrations N_2 and using formula (5), we can determine ΔE from the slope of the straight line in Fig. 8a. The deviation of experimental points from the straight line upon heating can indicate that the value of ΔE changes.

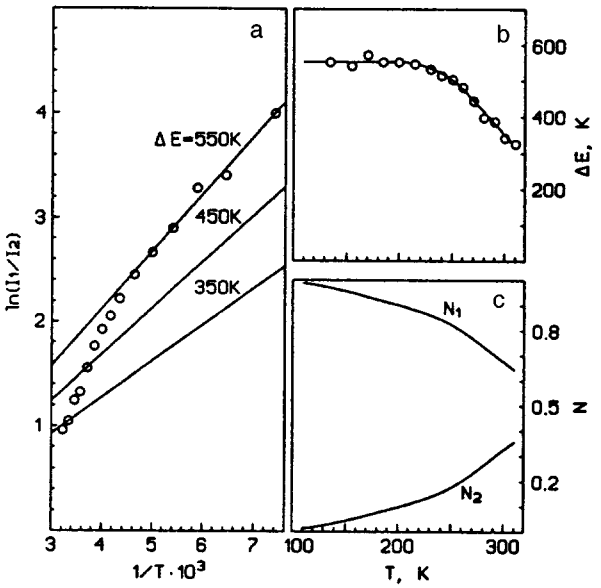

FIG. 8. Temperature dependence of the model parameters for a $NiSiF_6 \cdot 6H_2O$ crystal: logarithms of the intensity ratio as functions of reciprocal temperature (a), difference in energy ΔE between the minima of potentials (b), and concentrations N_1 and N_2 (c).

In the temperature range 135–215 K in which the intensity ratio is described by a straight line on a semilogarithmic scale (see Fig. 8a), i.e., for a constant ΔE, we can calculate $\ln(K_1/K_2)$ by using formula (5). Substituting the value of $\ln(K_1/K_2)$ into (5), we determine ΔE for the entire temperature interval. The results of such calculations for a $NiSiF_6 \cdot 6H_2O$ crystal are illustrated in Fig. 8b. The solid curve corresponds to the averaged value of ΔE for experimental values shown by circles. Using the averaged value of ΔE (see Fig. 8b), we calculate by formulas (1) and (2) the concentrations N_1 and N_2 whose temperature dependence is shown in Fig. 8c.

Similar calculations were made for the XX Raman spectra for $ZnSiF_6 \cdot 6H_2O$ and $NiSiF_6 \cdot 6D_2O$ crystals for which the parameter ΔE exhibits the same temperature dependence as for the $NiSiF_6 \cdot 6H_2O$ crystal, but the parameter ΔE for the Zn-based compound becomes variable above $T \approx 200$ K, while its value below this temperature amounts to 520 K.

The values of N_2 and N_1 obtained at room temperature are 0.33/0.67, 0.37/0.63, and 0.35/0.65 for $NiSiF_6 \cdot 6H_2O$, $ZnSiF_6 \cdot 6H_2O$, and $NiSiF_6 \cdot 6D_2O$ crystals, respectively and are in good agreement with the values obtained from x-ray data.[1]

The temperature dependence of ΔE was obtained from the intensity ratio. In the temperature interval where the value of ΔE is constant, we calculate the intensities by using formulas (3) and (4) (to within the coefficients K_1 and K_2). Comparing these values with experimental intensities at these six temperatures (135–215 K), we determine the average value of the scaling factors K_1 and K_2. Using formulas (3) and (4), we determine the line intensities in the entire temperature range from the averaged value of ΔE (see Fig. 8b), K_1, and K_2. The results of calculations for the XX Raman spectra of the $NiSiF_6 \cdot 6H_2O$ crystal are shown in Fig. 7a by solid curves.

It should be noted that the values of intensities and concentrations were calculated in the harmonic approximation i.e., all the formulas were obtained for a harmonic oscillator (with an infinite number of energy levels). In addition, we assume that the vibrations ω_1 and ω_2 do not interact. It can be seen from Fig. 5 that in the real case we must take into account a finite number of transitions in both wells of the potential function as well as transitions occurring above the barrier V_2. The latter have a lower frequency and cannot be determined from experiments unambiguously in view of the presence of a high-intensity relaxation peak and the line ω_2 in the spectra. This can lead to lower calculated values of ω_2 since the profile of this line contains a line with a lower frequency corresponding to transitions above V_2. Naturally, such an approximation introduces an error in the determination of ΔE and the $\Delta E(T)$ dependence at high temperatures.

The temperature range in which the quantity ΔE becomes variable ($T \approx 220$ K for $NiSiF_6 \cdot 6H_2O$ and $NiSiF_6 \cdot 6D_2O$ crystals and $T \approx 200$ K for $ZnSiF_6 \cdot 6H_2O$) coincides with temperatures at which the thermal expansion coefficient for the crystal lattice changes.[2,3] Such a behavior of the parameters can be due to the formation of a large number of octahedrons in the metastable orientation position as well as due to thermal activation of transitions above the barrier V_2 (see Fig. 5).

CONCLUSIONS

An analysis of Raman spectra in crystals with isomorphic substitution has made it possible to identify all the observed lines. It was found that $NiSiF_6 \cdot 6H_2O$ and $ZnSiF_6 \cdot 6H_2O$ crystals are ordered at low temperatures.

The obtained results do not confirm the existence of a second-order phase transition in the $NiSiF_6 \cdot 6H_2O$ crystal at $T \approx 220$ K and in the $ZnSiF_6 \cdot 6H_2O$ crystal at $T \approx 200$ K.

The evolution of orientation disorder in the crystals under investigation is associated with thermal population of the metastable orientational state of SiF_6^{2-} ions. The concentration of ions in the metastable state increase upon heating and may cause a decrease in the energy difference ΔE between the ground state and the metastable state, which in turn can lead to a change in the elastic properties of crystals. The anomalies in the temperature expansion of the lattice of the $NiSiF_6 \cdot 6H_2O$ crystal at $T \simeq 220$ K[2] and in the $ZnSiF_6 \cdot 6H_2O$ crystal at $T \simeq 200$ K,[3] whose temperatures coincide with those at which the parameter ΔE becomes variable, are probably associated just with this process.

The temperature dependences of concentrations N_1 and N_2 were calculated on the basis of the obtained experimental data on the temperature behavior of frequencies and intensities of the lines for two orientational positions of the SiF_6^{2-} complex in the crystals under investigation. In the above approximations, the values of N_1 and N_2 obtained from Raman spectra at room temperature are in good agreement with the x-ray data.[1]

The authors are grateful to B. Ya. Sukharevskii and V. P. D'yakonov for single crystals presented for our experiments and for their interest in this research.

*E-mail: peschansky@ilt.kharkov.ua

[1] S. Ray, A. Zalkin, and D. H. Templeton, Acta Crystallogr., Sect. B: Struct. Crystallogr. Cryst. Chem. **29**, 2741 (1973).
[2] S. K. Asadov, E. A. Zavadskii, V. I. Kamenev *et al.*, Ukr. Fiz. Zh. **36**, 293 (1991).
[3] S. K. Asadov, È. A. Zavadskii, V. I. Kamenev *et al.*, Fiz. Tekh. Vys. Davl. **2**, 104 (1992).
[4] R. Rommetveit and I. Svare, Phys. Scr. **17**, 27 (1978).
[5] J. Lewis and T. E. Jenkins, J. Raman Spectrosc. **8**, 111 (1979).
[6] T. E. Jenkins and J. Lewis, J. Raman Spectrosc. **11**, 1 (1981).
[7] T. E. Jenkins and J. Lewis, Phys. Scr. **18**, 351 (1978).
[8] T. E. Jenkins and J. Lewis, Spectrochim. Acta A **37A**, 47 (1981).
[9] V. P. Gnezdilov, V. V. Eremenko, A. V. Peschanskii, and V. I. Fomin, Fiz. Tverd. Tela (Leningrad) **32**, 841 (1990) [Sov. Phys. Solid State **32**, 496 (1990)].
[10] V. V. Eremenko, V. S. Kurnosov, A. V. Peschanskii, and V. I. Fomin, Fiz. Nizk. Temp. **20**, 330 (1994) [Low Temp. Phys. **20**, 263 (1994)].
[11] H. Poulet and J.-P. Mathieu, Compt. Rend. **286**, 331 (1978).
[12] P. Choudhury, B. Ghosh, M. B. Patel, and H. D. Bist, J. Raman Spectrosc. **16**, 149 (1985).
[13] M. M. Sushchinskiĭ, *Raman Spectra of Molecules and Crystals*, Israel Program for Sci. Trans., Jerusalem, 1973.

Translated by R. S. Wadhwa

A new dynamic mechanism of topological charge creation in a commensurate one-dimensional charge density wave near the contact with a normal metal

A. S. Rozhavsky, Yu. V. Pershin, and A. S. Kovalev

*B. Verkin Institute for Low Temperature Physics and Engineering, National Academy of Sciences of the Ukraine, 310164 Kharkov, Ukraine**

(Submitted July 11, 1997; revised August 3, 1997)
Fiz. Nizk. Temp. **23**, 1325–1330 (December 1997)

The dynamics of conversion of conduction electrons into topological solitons of a charge density wave (CDW) commensurability in an external electric field is investigated. A novel mechanism of initiation of a nonlinear CDW current in the vicinity of the interface between a CDW and a normal metal is revealed and explained. The nonlinear current is produced by the conduction solitons created by the moving profile of the order parameter, formed during the conversion of electrons into collective phase excitations of a CDW. The field dependence of the current is of threshold nature and has no analogs in the bulk mechanisms of CDW nonlinearity. © *1997 American Institute of Physics.* [S1063-777X(97)01012-8]

INTRODUCTION

It is well known that several quasi-one-dimensional metals are transformed into the Peierls–Fröhlich phase as a result of cooling, which is accompanied by the emergence of a lattice superstructure along the unidimensionality direction with a period π/k_F. The static lattice deformation modulus creates a gap 2Δ in the one-electron spectrum, while the phase of the order parameter $\Delta\exp(i\varphi)$ is electrically active and causes a collective response of a Peierls insulator (PI) to an external field. The deformations of the lattice are called charge density waves (CDW).

Study of quasi-one-dimensional conductors with CDW is interesting primarily because they exhibit nonlinear electrical conductivity in very weak electric fields (see, for example, the reviews in Refs. 1 and 2). The nonlinear conductivity is of the threshold type and has always been attributed to processes occurring in the bulk of the conductor. There are two theoretical approaches to this phenomenon, viz., the classical approach and the quantum approach.[1,2] In both approaches, the charge transport in a CDW is presented as a collective mode, i.e., the Peierls–Fröhlich order parameter phase, when the charge fluctuations $\delta\rho$ and the CDW current j are described by Fröhlich relations for a single chain (see, for example, Ref. 1):

$$\delta\rho=\frac{e}{\pi}\frac{\partial\varphi}{\partial x},\quad j=-\frac{e}{\pi}\frac{\partial\varphi}{\partial t}, \tag{1}$$

where x is the direction of unidimensionality.

The CDW on a single chain is always described by the sine-Gordon (SG) equation. The SG solitons play the role of charge carriers.

In the classical model, the nonlinearity of electrical conductivity has the form[1]

$$j\sim\sqrt{E^2-E_T^2},\quad E>E_T. \tag{2}$$

The threshold field E_T is connected with the bulk term in the SG equation.

The quantum model connects the nonlinearity with the tunnel creation of soliton–antisoliton $(s\,\overline{s})$ pairs by an electric field, and the current is defined as[2]

$$j\sim(E-E_T)\exp\left(-\frac{E_0}{E-E_T}\right),\quad E>E_T. \tag{3}$$

The threshold field E_T is determined by the Coulomb interaction between a soliton and an antisoliton.

However, the modern state of the experiment does not permit us to give preference to any of the models, hence both approaches are equivalent at present, and probably complement each other.

It has become clear recently that an important role in the conductivity of CDW is played by contact phenomena at the interface between a CDW and a normal metal, where the conduction electron current is transformed into the collective CDW current. Qualitatively, the need for the existence of a conversion channel is dictated by the instability of a free electron or hole in a quasi-one-dimensional Peierls lattice to self-trapping with the formation of a collective charge.[3,4] This channel causes a finite conduction through the metal-CDW interface at temperatures $T\ll\Delta$, when the conventional one-electron current is exponentially suppressed $[\sim\exp(-\Delta/T)]$ (see, for example, Ref. 5).

It is not obvious beforehand whether an additional nonlinearity emerges in the conversion channel. This problem is studied in the present work where it is shown that a nonlinear conductivity emerges in a simplified one-dimensional model. This conductivity has a structure different from Eqs. (1) and (2):

$$j\sim\frac{\sqrt{E-E_T}E}{A+\sqrt{E-E_T}}, \tag{4}$$

where E_T is defined by the bulk term in the sine-Gordon equation like in the classical model.

Investigations of the dynamics of the conversion process were started in Refs. 6 and 7. An instanton mechanism was proposed in Ref. 6 for the transition of free charges from the chemical potential level at the metal-CDW interface to the PI condensate (valence band) with the formation of a collective charge (CDW phase profile) localized at distances of the order of $\xi_0=\hbar V_F/\Delta$ from the interface. Transition to the condensate is always made by two electrons, which is reminis-

cent of Andreev scattering from the point of view of the outer boundary relative to the PI. Unlike the case of superconductors in which Δ is the only parameter determining the space and time dynamics of the order parameter, three well-defined time scales exist in a PI[2,3,6,7]:

(1) the time of formation of the quasiparticle spectrum $\tau_S \sim \hbar/\Delta$;
(2) the time of deformation of the order parameter modulus $\tau_\Delta \sim \overline{\omega}^{-1}$, where $\overline{\omega}$ is of the order of Debye frequency $\overline{\omega} \ll \Delta$;
(3) the phase evolution time of the order parameter $\tau_\varphi \gg \tau_\Delta \gg \tau_s$.

These parameters make it possible to formulate and consistently solve the problem of transformation of electron charge through the interface. A quasiparticle level is formed on gap fluctuation (instanton) over a time τ_s. The fluctuation itself takes place over a time τ_Δ, the bound level is absorbed by the valence band, and the initial condition $\delta\varphi = \varphi(x=\infty) - \varphi(x=0) = 2\pi$ is formed for the problem on the evolution of the phase from the boundary $x=0$ towards $x>0$. This condition corresponds to a charge $2e$ [see Eq. (1)]. A steadily moving CDW profile is obtained from the initial condition in time τ_φ.[7]

Earlier, we studied[7] the evolution of the initial condition in a cluster of the nearest chains carrying a noncommensurate CDW. The role of the bulk term in the sine-Gordon equation was played by interaction of the type $\sin(\varphi_i - \varphi_{i+1})$ between chains. In the equation for a commensurate CDW, each chain acquires an additional term $\sin(M\varphi_i)$, where M is an integer.[1,2] Accordingly, a topological soliton has an asymptotic form $\delta\varphi = \varphi(x=\infty) - \varphi(x=-\infty) = 2\pi/M$. Such a soliton is a stable carrier of the fractional charge $2e/M$ in a CDW.[2] It is certainly interesting to study the evolution of the initial condition $\delta\varphi = 2\pi$ in M solitons and to study their dynamics in an electric field. Such a problem is formulated and solved in the present work for a single chain.

In Ref. 7, we reduced the Cauchy problem for a CDW to an exactly integrable problem and solved it by the inverse scattering problem method. In an external electric field, the exact integrability is violated on the right-hand side of the sine-Gordon equation, and the equation is solved numerically. It was found that $s\bar{s}$ pairs are created in an electric field with an intensity inversely proportional to time $\overline{\tau}$ (14), which determines the current (4).

We believe that the nonlinear conductivity (4) can be explained as follows: the initial CDW profile at the interface has an energy of the order Δ which is considerably higher than static energy of a topological soliton carrying a charge $2e/M$. Away from the interface, nonlinear deformations are created in the moving front region from the high-energy initial profile in a time τ_0. During a time of the order of $\sqrt{2d/(E-E_T)}$ (d is the soliton width), these deformations are transformed into topological solitons with an asymptotic form $\delta\varphi = 2\pi/M$, or antisolitons with $\delta\varphi = -2\pi/M$ (depending on the direction of the electric field) moving behind the front along or against the field. Accordingly, the total time for the creation of a stable topological charge $\pm 2e/M$ is $\overline{\tau} = \tau_0 + \sqrt{2d/(E-E_T)}$. The creation frequency $\overline{\tau}^{-1}$ determines the number of charges created, i.e., the nonlinear conductivity (4).

A similar dynamic effect of multiple creation of domain walls for a moving domain boundary was studied in Ref. 8.

MODEL AND NUMERICAL ANALYSIS

Suppose that a CDW occupies a semi-axis $x \geqslant 0$. The Lagrangian of the CDW in a field is defined as (see, for example, Ref. 2)

$$L = \frac{1}{\pi\hbar V_F}\left\{\frac{\Delta^2}{\overline{\omega^2}}\left(\frac{\partial\varphi}{\partial t}\right)^2 - \frac{\hbar^2 V_F^2}{4}\left(\frac{\partial\varphi}{\partial x}\right)^2 + \frac{\Delta^2}{\overline{\omega^2}}\frac{2}{M^2}\,\omega_0^2\cos M\varphi + \frac{e}{\pi}\hbar V_F E(\varphi-\varphi_0)\right\}, \tag{5}$$

where ω_0 is the commensurability frequency. Here, φ_0 is the phase for $x \to \pm\infty$. Such a form of notation for the last term in Eq. (5) takes into account the fact that the electric field acts on CDW only in the region where $|\partial\varphi/\partial x| \neq 0$.

In a nonzero field E, the quantity φ_0 is renormalized as seen from the equation of motion, which can be represented in dimensionless units

$$\tau = \omega_0 t\sqrt{2/M}, \quad y = x\left(\frac{\hbar V_F\overline{\omega}}{2\Delta\omega_0}\sqrt{M/2}\right), \tag{6}$$

for the variable $\chi = \varphi - \varphi_0$.

The equation of motion has the form

$$\frac{\partial^2\chi}{\partial\tau^2} - \frac{\partial^2\chi}{\partial y^2} + \sin M(\chi+\varphi_0) = \varepsilon, \tag{7}$$

where

$$\varepsilon = \frac{e}{2\pi}\hbar V_F\frac{M\overline{\omega^2}}{\Delta^2\omega_0^2}E \tag{8}$$

and $\varphi_0 = \arcsin\varepsilon$.

Equation (7) is supplemented by the initial and boundary conditions corresponding to the above hierarchy of time in the conversion problem:

$$\left.\frac{\partial\chi}{\partial\tau}\right|_{r=0} = 0, \tag{9a}$$

$$\chi(\tau=0) = -2\pi\theta(\overline{\xi_0}-y) - \varphi_0'(\varepsilon), \tag{9b}$$

$$\chi(y=0) = -2\pi - \varphi_0(\varepsilon), \tag{9c}$$

where $\overline{\xi_0}$ is the coherence length $\xi_0 = \hbar V_F/\Delta$ in dimensionless variables (6), $\overline{\xi_0} \ll 1$, and $\theta(y)$ is the Heaviside function.

Note that the small scale of variation of the initial condition $\overline{\xi_0} \ll 1$ cannot emerge formally in the solution of a purely phase problem with Lagrangian (5) since the latter corresponds to the long-wave approximation $|\varphi'| \ll \xi_0^{-1}$.[2] It was mentioned above (see Ref. 7 also) that such an initial condition is the result of joining of the instanton solution[6] formed during the time τ_Δ with a long-wave description valid for $\tau \geqslant \tau_\varphi$.

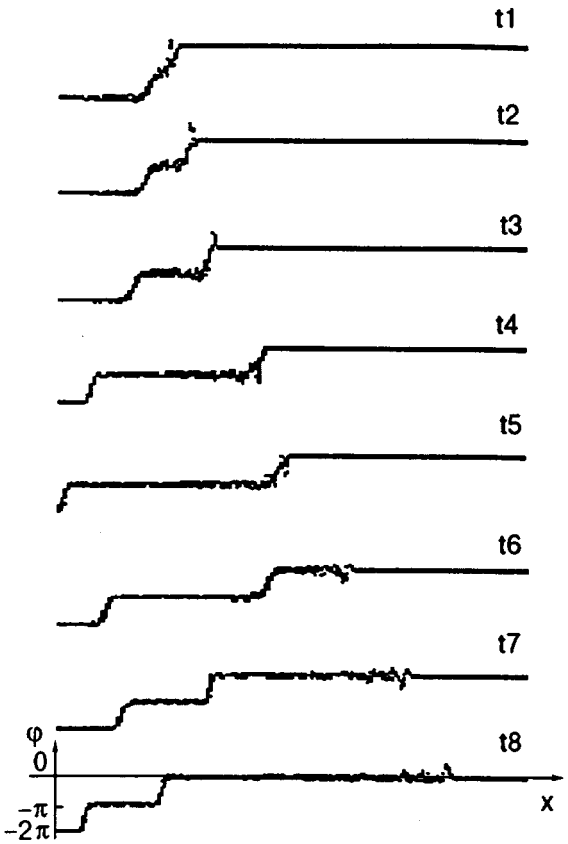

FIG. 1. Evolution of the initial condition in a retarding field $\varepsilon=-0.05$, $M=2$: $t1<t2<t3<t4<t5<t6<t7<t8$.

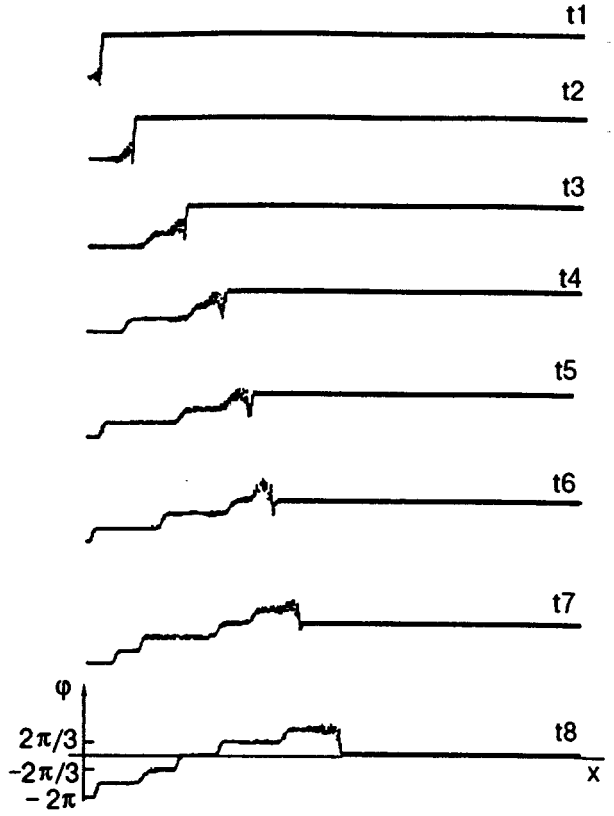

FIG. 2. Evolution of the initial condition in a retarding field $\varepsilon=-0.3$, $M=3$. CDW solitons with an asymptotic form $2\pi/3$ are produced from the initial condition $(t1)$ with increasing time: $t1<t2<t3<t4<t5<t6<t7<t8$.

Equation (7) with the boundary conditions (9) was solved numerically by the method of finite differences. The difference equation corresponding to Eq. (7) has the form

$$\frac{\chi_{i+1,k}+\chi_{i-1,k}-2\chi_{i,k}}{(\Delta\tau)^2}-\frac{\chi_{i,k+1}+\chi_{i,k-1}-2\chi_{i,k}}{(\Delta y)^2}+\sin M(\chi+\varphi_0)=\varepsilon, \tag{10}$$

where $\Delta\tau$ is the time step, Δy is the coordinate step, and $\chi_{i,k}=\chi(\Delta\tau i,\Delta y k)$. Equation (10) was solved for different values of $\Delta\tau$, Δy, and M, and under different initial conditions (9). Typical solutions have been constructed in Figs. 1, 2, and 3. The number of sites (k) is 10000. It was found that a change in the initial conditions (9) has no significant effect on the solution of Eq. (7).

In a weakly retarding field $|\varepsilon|\ll 0.1$ (Fig. 1), the initial profile moving against the field loses stability after some time and simply splits into commensurability solitons. The latter are retarded, reverse their direction, and eventually gather near $x=0$. Radiation propagating with the maximum speed is observed. With increasing field, charge creation by the field is observed additionally (Fig. 2).

In an accelerating field, the initial condition trivially decomposes into topological solitons with time for $\varepsilon<0.1$, while the field merely affects the time of formation of solitons and their velocity. Movement of radiation at the highest velocity was observed in front of the profile. For $\varepsilon>0.1$, charge creation by the field is observed (Fig. 3). A similar effect was also observed in Ref. 9 during a numerical analysis of the motion of Josephson vortices in a system with dissipation. However, the difference lies in that, instead of an infinite number, we are looking at a finite number of created charges, this number depending on the field (Fig. 4). The dependence of the charge creation time on the field is shown in Fig. 5 and is approximated well by the law $\overline{\tau}=A+B/\sqrt{\varepsilon-\varepsilon_T}$.

A reversal of the sign of created charges upon a change in the direction of the field unambiguously indicates that the mechanism of their formation is polarization: for $\varepsilon>0$, the soliton moves along the field, and the antisoliton moves against the field; for $\varepsilon<0$, s and $\overline{s}$ interchange their places.

The time of formation of free charge carriers is estimated as follows.

Suppose that, in a CDW profile moving with a practically limiting velocity, nonlinear fluctuations produce a deformation of the front with $\delta\varphi=0$ over a time τ_0. In the absence of a field, such a process does not lead to charge creation since such a deformation moves with the front and is not polarized.

We shall assume that, in the presence of a field $\varepsilon>0$, the leading front of the created deformation continues to move with the CDW front with a limiting velocity, while the trailing front gets retarded by the field and is ultimately transformed into a soliton with $\delta\varphi_S=2\pi/M$, which subsequently reverses its direction. The equations of motion for the lead-

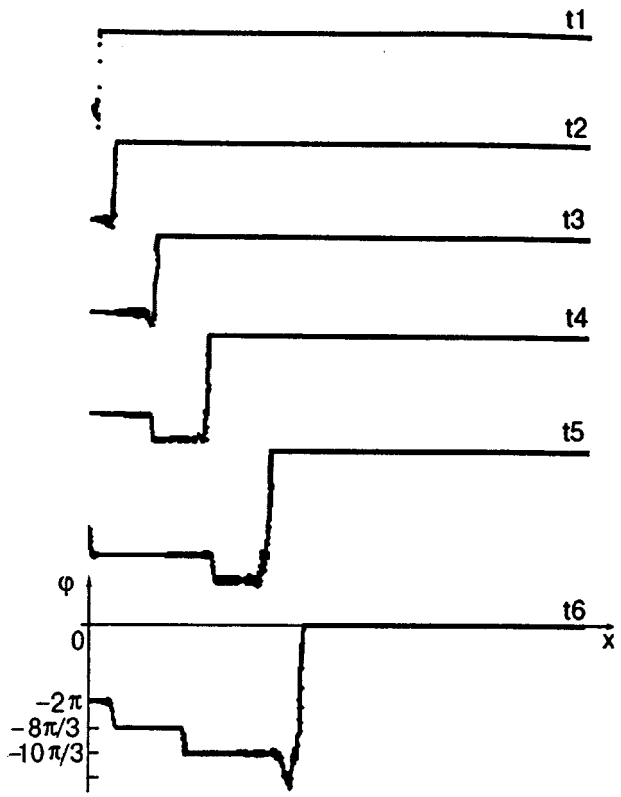

FIG. 3. Evolution of the initial condition in an accelerating field $\varepsilon=0.3$, $M=3$. CDW solitons with an asymptotic form $2\pi/3$ are produced from the initial condition ($t1$) with increasing time. $t1<t2<t3<t4<t5<t6$.

ing front x_+ and the trailing front x_- of deformation have the form

$$(+): x_+ = C_0(\tau-\tau_0)+x_0,$$

$$(-): x_- = \frac{(\varepsilon-\varepsilon_T)\tau^2}{2}+\lambda\tau+C, \tag{11}$$

where C_0 is the maximum velocity in the system, ε_T is the threshold field, while the constants λ and C are determined from the conditions

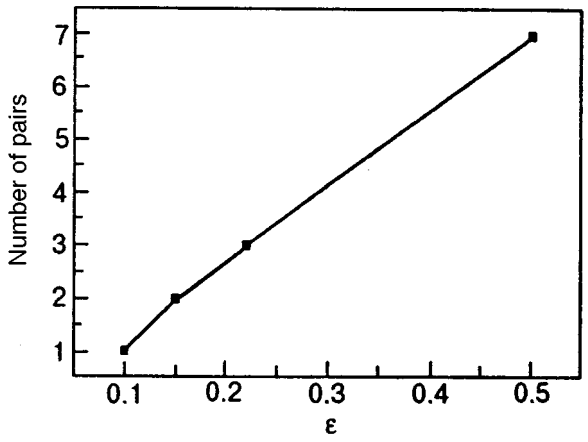

FIG. 4. Field dependence of the number of topological solitons created, $\varepsilon>0$, $M=3$.

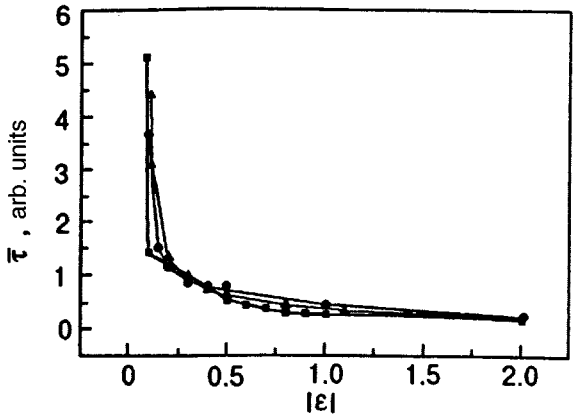

FIG. 5. Dependence of the topological charge creation time on field $|\varepsilon|$. Numerical method for $\varepsilon>0$ (■); numerical method for $\varepsilon<0$ (●), results obtained by using formula (14) (dark triangles).

$$x_+(\tau_0)=x_0, \quad \left.\frac{\partial x_-}{\partial\tau}\right|_{\tau=\tau_0}=C_0. \tag{12}$$

As soon as the field $\varepsilon-\varepsilon_T$ separates the centers x_+ and x_- by a distance of the order of the kink width d over a time $\overline{\tau}$, we can see that the trailing profile of the created deformation moves like a free charge, i.e.,

$$d=x_+-x_-=\left\{-\frac{\overline{\tau}^2}{2}+\tau_0\overline{\tau}-\frac{\tau_0^2}{2}\right\}(\varepsilon-\varepsilon_T). \tag{13}$$

From the last equation, we obtain

$$\overline{\tau}=\tau_0+\sqrt{2d/(\varepsilon-\varepsilon_T)}, \tag{14}$$

as is indeed observed in the numerical experiment (Fig. 5). The quantity $\overline{\tau}^{-1}(\varepsilon)$ defines the intensity of free charge creation, i.e., the current (4).

Thus, we have discovered and explained a new mechanism of formation of the nonlinear CDW current near the interface with a normal conductor. This mechanism supplements the known mechanisms studied for an infinite CDW.

*E-mail: rozhavsky@ilt.kharkov.ua

[1] P. Manceau (Ed.), *Electronic Properties of Inorganic Quasi-One-Dimensional Compounds*, Riedel Co., Dordrecht (1985), parts 1 and 2; G. Grüner (Ed.), *Density Waves in Solids*, Addison-Wesley, Reading, Mass. (1994).
[2] I. V. Krive, A. S. Rozhavsky, and I. O. Kulik, Fiz. Nizk. Temp. **12**, 635 (1986) [Sov. J. Low Temp. Phys. **12**, 360 (1986)].
[3] S. A. Brazovskii, Zh. Éksp. Teor. Fiz. **51**, 342 (1980) [*sic*].
[4] S. Brazovskii and S. Matveenko. J. Plasma Phys. **2**, 725 (1992).
[5] B. Rejaei and G. E. Bauer, Phys. Rev. B **54**, 8487 (1996).
[6] I. V. Krive, A. S. Rozhavsky, and V. A. Rubakov, Pis'ma Zh. Éksp. Teor. Fiz. **46**, 99 (1987) [JETP Lett. **46**, 121 (1987)].
[7] A. S. Kovalev, Yu. V. Pershin, and A. S. Rozhavsky, Phys. Rev. B **53**, 16227 (1996); Fiz. Nizk. Temp. **22**, 322 (1996) [Low Temp. Phys. **22**, 253 (1996)].
[8] V. G. Bar'yakhtar, B. I. Ivanov, and M. V. Chetkin, Usp. Fiz. Nauk, **146**, 417 (1985) [Sov. Phys. Usp. **28**, 563 (1985)].
[9] K. Nakagama, Y. Onodera, T. Nakamura, and R. Sato, J. Appl. Phys. **45**, 4095 (1974).

Translated by R. S. Wadhwa